

Swarthmore College

## Works

---

Senior Theses, Projects, and Awards

Student Scholarship


---

Spring 2021

# Synthesis and Characterization of $\alpha$ -diimine Complexes of Aluminum

Judah B. Raab , '21

Follow this and additional works at: <https://works.swarthmore.edu/theses>

 Part of the [Chemistry Commons](#)

---

### Recommended Citation

Raab, Judah B. , '21, "Synthesis and Characterization of  $\alpha$ -diimine Complexes of Aluminum" (2021). *Senior Theses, Projects, and Awards*. 255.

<https://works.swarthmore.edu/theses/255>



This work is licensed under a [Creative Commons Attribution-Share Alike 4.0 International License](#).

This work is brought to you for free by Swarthmore College Libraries' Works. It has been accepted for inclusion in Senior Theses, Projects, and Awards by an authorized administrator of Works. For more information, please contact [myworks@swarthmore.edu](mailto:myworks@swarthmore.edu).

**SYNTHESIS AND CHARACTERIZATION  
OF  $\alpha$ -DIIMINE COMPLEXES OF  
ALUMINUM**

Judah B. Raab  
Senior Honors Thesis  
Advised by Christopher R. Graves  
Department of Chemistry and Biochemistry  
Swarthmore College  
April 19<sup>th</sup>, 2021

# Table of Contents

ACKNOWLEDGEMENTS .....	I
TABLE OF FIGURES .....	II
<b>0. ABSTRACT .....</b>	<b>III</b>
<b>1. INTRODUCTION .....</b>	<b>1</b>
1.1 SUSTAINABLE CATALYSIS WITH ALUMINUM .....	1
1.2 NON-INNOCENT LIGANDS EQUIP COMPLEXES OF AL WITH REDOX ACTIVITY .....	2
1.3 A-DIIMINE COMPLEXES OF AL ARE VERSATILE .....	3
1.3.1 THE REDOX CHEMISTRY OF A-DIIMINE COMPLEXES OF AL IS LIGAND-DEPENDENT .....	3
1.3.2 NEUTRAL-LIGAND A-DIIMINE COMPLEXES OF AL CATALYZE EPOXIDATION .....	5
1.3.3 REDUCED-LIGAND A-DIIMINE COMPLEXES OF AL DO DIVERSE AND INTERESTING CHEMISTRY .....	6
1.3.4 A-DIIMINE COMPLEXES CONTAINING AL-AL BONDS POSSESS POWERFUL REACTIVITY .....	10
1.4 CURRENT WORK .....	12
<b>2. RESULTS AND DISCUSSION .....</b>	<b>13</b>
2.1 NEUTRAL-LIGAND A-DIIMINE COMPLEXES OF AL .....	13
2.1.1 <sup>1</sup> H AND <sup>13</sup> C NMR CHARACTERIZATION OF THE [AL(L <sub>AR</sub> ) <sub>2</sub> I <sub>2</sub> ] <sup>•</sup> I AND [AL(L <sub>AR</sub> ) <sub>2</sub> (NCME) <sub>2</sub> ] <sup>•</sup> 3I SERIES .....	14
2.1.2 SOLID-STATE STRUCTURAL ANALYSIS OF THE [AL(L <sub>AR</sub> ) <sub>2</sub> I <sub>2</sub> ] <sup>•</sup> I AND [AL(L <sub>AR</sub> ) <sub>2</sub> (NCME) <sub>2</sub> ] <sup>•</sup> 3I SERIES .....	18
2.1.3 DFT INVESTIGATION OF THE [AL(L <sub>AR</sub> ) <sub>2</sub> I <sub>2</sub> ] <sup>•</sup> I AND [AL(L <sub>AR</sub> ) <sub>2</sub> (NCME) <sub>2</sub> ] <sup>•</sup> 3I SERIES .....	22
2.1.4 CYCLIC VOLTAMMETRY OF THE [AL(L <sub>AR</sub> ) <sub>2</sub> I <sub>2</sub> ] <sup>•</sup> I AND [AL(L <sub>AR</sub> ) <sub>2</sub> (NCME) <sub>2</sub> ] <sup>•</sup> 3I SERIES .....	26
2.1.5 EPOXIDATION AIDED BY [AL(L <sub>AR</sub> ) <sub>2</sub> I <sub>2</sub> ] <sup>•</sup> I AND [AL(L <sub>AR</sub> ) <sub>2</sub> (NCME) <sub>2</sub> ] <sup>•</sup> 3I CATALYSTS .....	28
2.1.6 FURTHER DERIVATIZATION OF THE NEUTRAL-LIGAND SERIES .....	30
2.2 REDUCED-LIGAND A-DIIMINE COMPLEXES OF AL .....	32
2.2.1 SYNTHESIS AND XRD, EPR, & CV CHARACTERIZATION OF AL(L <sub>MES</sub> <sup>-</sup> )ME <sub>2</sub> .....	32
2.2.2 SYNTHESIS AND XRD & DFT CHARACTERIZATION OF [ALME <sub>2</sub> ] <sub>2</sub> (M-L <sub>HMES</sub> -L <sub>HMES</sub> ) .....	38
2.2.3 SYNTHESIS AND XRD, DFT, & CV CHARACTERIZATION OF [(L <sub>MES</sub> <sup>2+</sup> )(THF)AL-AL(THF)(L <sub>MES</sub> <sup>2+</sup> )] .....	43
<b>3. CONCLUSIONS AND FUTURE WORK .....</b>	<b>49</b>
<b>4. REFERENCES .....</b>	<b>50</b>
<b>5. SUPPLEMENTARY INFORMATION .....</b>	<b>S1</b>
5.1 METHODS .....	S1
5.1.1 PHYSICAL MEASUREMENTS .....	S1
5.1.2 COMPUTATIONAL DETAILS .....	S2
5.1.3 PREPARATION OF COMPOUNDS .....	S2
5.2 SPECTRA .....	S9
5.3 X-RAY STRUCTURE DETERMINATION .....	S26
5.4 COMPUTATIONAL DATA .....	S38

## Acknowledgements

I have been incredibly lucky in my time at Swarthmore: to meet so many wonderful people, to learn from brilliant classmates and professors, to grow as a person. First, I want to thank Chris Graves, whose mentorship in the lab and during my thesis writing has been second to none. He has been instrumental in my commitment to chemistry—I'm so grateful for his consistent guidance and expectations.

I'm infinitely thankful for my glovebox buddy and best friend Claire Heinzerling, whose humor and camaraderie were a cornerstone of my time in Graves lab. I'm also so grateful for my memories in lab (and over Zoom) with Mika Maenaga, Scout Clark, Audra Woodside, Omar Saleh, Mackinsey Smith, Alec Ferry, and Joe Scott. I must also thank Ben Hejna, my dear friend and former neighbor of the Graves lab, for his guidance and support in and out of chemistry. Many thanks also to Dr. Rablen, who taught me density functional theory—allowing me to continue with my project during the pandemic.

I'm deeply indebted to Henry Wilson, the previous driving force behind the  $\alpha$ -diimine project, for his ideas, notebooks, and data. To my many collaborators who I one day hope to meet—Christian Goldsmith, Alexander Saunders, Bren Cole, Justin Bogart, Thibault Cheisson, Brian Manor, Michael Gau, and Pat Carrol—many, many thanks for the help.

My thesis would not be possible without the professors of the Department of Chemistry & Biochemistry: Liliya Yatsunyk, Dr. Paley, Dr. Riley, Dr. Howard, Dr. Stephenson, and others. I'm particularly thankful for Dr. Stephenson's help during thesis workshops—in which Mika, Hyun Kyung Lee, and Dana Beseiso were also a source of indispensable advice and support.

I must thank my parents, Mom and Bub, who have never shown me anything short of unconditional love. I would not be the person I am today without their tireless support and the years we've spent together.

I also want to thank Greta Studier, who is a boundless source of happiness and support. I continue to be inspired by her kindness, her intelligence, and her work as a scientist. This thesis couldn't have been written without her love and encouragement.

My friends have played a huge role in my thesis too—listening to me complain, grabbing me meals, taking breaks with me, making me write, making me laugh, staying up late with me—I can't thank them enough for their love and support during this spring semester.



## Table of Figures

<b>FIGURE 1.</b> COMMONLY USED A-DIIMINE LIGANDS.....	3
<b>FIGURE 2.</b> L <sub>AR</sub> ACROSS THREE OXIDATION STATES .....	3
<b>FIGURE 3.</b> OVERLAID CV DATA FOR [AL(L <sub>AR</sub> ) <sub>2</sub> CL <sub>2</sub> ][ALCL <sub>4</sub> ] COMPLEXES.....	5
<b>FIGURE 4.</b> A SERIES OF [( <sup>DPP</sup> BIAN <sup>-</sup> )ALR <sub>2</sub> ] COMPLEXES .....	7
<b>FIGURE 5.</b> VISUALIZATION OF THE H---I INTERACTION IN <b>1</b> .....	15
<b>FIGURE 6.</b> EXPERIMENTAL AND SIMULATED <sup>1</sup> H NMR SPECTRA OF <b>1</b> .....	17
<b>FIGURE 7.</b> SOLID-STATE STRUCTURES OF THE CATIONS OF <b>1–3, 5, AND 6</b> .....	19
<b>FIGURE 8.</b> HOMO OF THE CATION OF <b>1</b> , ITS DICHLORO ANALOG, AND <b>4</b> .....	24
<b>FIGURE 9.</b> LUMO AND LUMO+1 OF <b>1, 4</b> , AND THE [(L <sub>PH</sub> ) <sub>2</sub> ALCL <sub>2</sub> ] <sup>+</sup> CATION. ....	25
<b>FIGURE 10.</b> CYCLIC VOLTAMMOGRAMS OF [AL(L <sub>PH</sub> ) <sub>2</sub> X <sub>2</sub> ][R] COMPLEXES .....	26
<b>FIGURE 11.</b> CYCLIC VOLTAMMOGRAMS OF COMPLEXES <b>2, 3, 5 AND 6</b> .....	28
<b>FIGURE 12.</b> SOLID-STATE STRUCTURE OF COMPLEX <b>8</b> .....	32
<b>FIGURE 13.</b> SOLID-STATE STRUCTURE OF COMPLEX <b>9</b> .....	34
<b>FIGURE 14.</b> X-BAND EPR SPECTRUM OF <b>9</b> .....	35
<b>FIGURE 15.</b> SOMO OF COMPLEX <b>9</b> .....	37
<b>FIGURE 16.</b> CYCLIC VOLTAMMOGRAM OF COMPLEX <b>9</b> .....	38
<b>FIGURE 17.</b> SOLID-STATE STRUCTURES OF COMPLEX <b>10</b> .....	40
<b>FIGURE 18.</b> FRONTIER ORBITALS FOR COMPLEX <b>10</b> .....	42
<b>FIGURE 19.</b> SOLID-STATE STRUCTURES OF COMPLEX <b>11</b> .....	45
<b>FIGURE 20.</b> NOTABLE MOLECULAR ORBITALS FOR COMPLEX <b>11</b> .....	47
<b>FIGURE 21.</b> CYCLIC VOLTAMMOGRAM OF COMPLEX <b>11</b> .....	48

## 0. Abstract

Conventional aluminum complexes are incapable of one- and two-electron redox chemistry. As a result, despite being the most abundant metal on Earth, aluminum is seldom used in redox catalysis—one of chemistry's most impactful fields. We are motivated to break this barrier to provide a green alternative to the countless redox catalysts built around the toxic, mining-intensive platinum-group metals. To create aluminum complexes that do desirable redox chemistry, we coordinate redox-active  $\alpha$ -diimine ligands to the metal center. These ligands are stable across multiple oxidation states, allowing for multi-electron redox chemistry for their aluminum complexes.

This thesis will report the synthesis of several  $\alpha$ -diimine complexes of aluminum, across various ligand substitution patterns and oxidation states. These complexes have been characterized by combinations of X-ray diffraction, multinuclear NMR spectroscopy, cyclic voltammetry, electron paramagnetic resonance spectroscopy, and density functional theory. For our neutral-ligand compounds, we will report their catalytic activity for the epoxidation of cyclohexene by peracetic acid.

# 1. Introduction

## 1.1 Sustainable catalysis with aluminum

In the pursuit of greener chemistry, sustainable catalyst development is a crucial step forward. In the United States alone, revenue from the industrial use of catalysis rivals the gross national product of nations like Brazil and Canada.<sup>1</sup> Many of chemistry's most prolific catalysts rely upon the platinum-group metals (PGMs; Pt, Pd, Rh, Ir, Os, and Ru). These catalysts are capable of countless transformations (hydrogenation, oxidation, carbonylation, dehydrogenation, carbon-carbon and carbon-heteroatom coupling, hydroxylation, and more<sup>2-4</sup>) and are essential to industrial processes<sup>5</sup> as well as fine chemistry<sup>6</sup>. However, PGMs require exhaustive mining operations for acquisition, intensive efforts for purification, and they are often toxic when spent.<sup>6-8</sup> Increasing PGM concentrations in both air and soil are raising concern about potential mutagenic and carcinogenic consequences.<sup>9,10</sup>

We hope to develop a redox catalyst capable of similar transformations as PGM-based catalysts without the negative impacts on environment and public health. Aluminum (Al) is a sensible framework within these guidelines, as it is the most abundant metal in the Earth's crust<sup>11</sup> and is relatively low in toxicity.<sup>12,13</sup> Al (~\$2/kg<sup>14</sup>) is also many orders of magnitude less expensive than all PGMs (from \$8,400/kg for Ru to \$300,000/kg for Rh<sup>14</sup>), adding a major financial incentive to the development of Al-based catalysts. For both environmental and financial reasons,

the implementation of Al-based catalysts in the industrial and fine chemistry sectors would have a profoundly positive impact.

## 1.2 Non-innocent ligands equip complexes of Al with redox activity

Al coordination complexes are well-represented in the literature, most commonly as Lewis acid activators.<sup>15,16</sup> Historically, such complexes have rarely been implemented in redox catalysis—for a clear reason: the tripositive oxidation state of Al is too stable to facilitate desirable one- and two-electron redox chemistry. This thesis will investigate a niche area of Al-based coordination chemistry and reactivity aimed to overcome this limitation: redox-active Al complexes. Since the metal center of a redox-active complex of Al will provide minimal assistance with the flow of electrons, one approach is the utilization of non-innocent, redox-active ligands. Such ligands allow the Al complex to carry electrons with no change to the Al(III) oxidation state.

One class of redox-active ligands are  $\alpha$ -diimines, which are easily prepared and can be extensively derivatized along the N–C–C–N backbone (Figure 1). The redox ability of  $\alpha$ -diimines is a result of their stability across three oxidation states: 0, -1, and -2 (Figure 2). With judicious manipulation of the  $\alpha$ -diimine framework, we aim to synthesize a series of aluminum complexes with tunable redox activity.

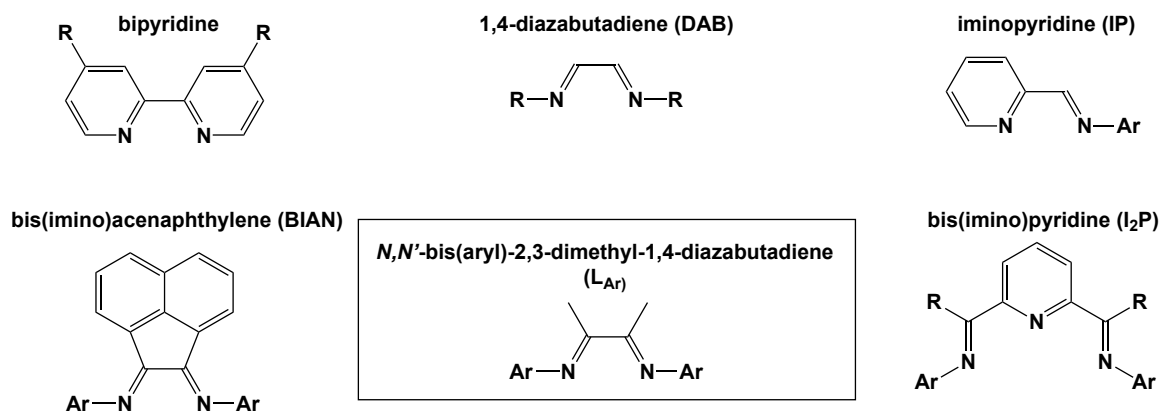


**Figure 1.** Commonly used  $\alpha$ -diimine ligands.  $N,N'$ -bis(aryl)-2,3-dimethyl-1,4-diazabutadiene ( $L_{Ar}$ , boxed) is the primary  $\alpha$ -diimine studied in this work.

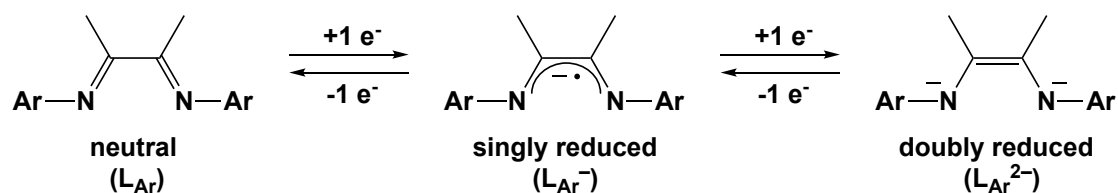


**Figure 2.**  $L_{Ar}$  across three oxidation states.

In the following sections, the aforementioned tunability of these  $\alpha$ -diimine complexes of Al will be discussed. This topic leads naturally into a discussion of the chemistry of these complexes, which we segregate into those bearing neutral ligands and those bearing reduced ligands. This distinction results from the difference in transformations observed in the literature upon altering ligand oxidation state.

### 1.3 $\alpha$ -diimine complexes of Al are versatile

#### **1.3.1 The redox chemistry of $\alpha$ -diimine complexes of Al is ligand-dependent**

For a redox-active catalyst, the ability to tune the electronic potential(s) at which redox events occur is extremely desirable. This tunability allows for a versatile catalyst, as different reactions require different electrochemical

conditions. For  $\alpha$ -diimine complexes of Al, fine electronic adjustments have been shown to occur with facile manipulation of the Al coordination environment. There are two predominant manipulations to this end: addition/substitution of other (non- $\alpha$ -diimine) ligands at the Al center and tuning of the  $\alpha$ -diimine's electronic profile through ligand derivatization. A study by Myers and coworkers demonstrates ligand control over the potentials of redox events for aluminum complexes of iminopyridine (IP).<sup>17</sup> Myers and coworkers prepared IP complexes across all ligand oxidation states—(IP)AlCl<sub>3</sub> (neutral), (IP<sup>-</sup>)<sub>2</sub>AlCl (singly reduced), [(IP<sup>2-</sup>)<sub>2</sub>Al]<sup>-</sup> (doubly reduced)—by reacting IP, AlCl<sub>3</sub> and varying equivalents of sodium metal in DME. Cyclic voltammetry (CV) experiments show vastly different voltammograms for (IP<sup>-</sup>)<sub>2</sub>AlCl and [(IP<sup>2-</sup>)<sub>2</sub>Al]<sup>-</sup>. Notably, the potentials corresponding to the IP<sup>1-</sup>/IP<sup>2-</sup> and IP<sup>0</sup>/IP<sup>1-</sup> redox couples are both shifted by nearly 1 V between the two complexes, which Myers et. al. concluded was due to differing electronic effects in the Al coordination environment resulting from the presence (or absence) of a chloride ligand.

Previous Graves group member Henry Wilson ran CV experiments for a series of [Al(L<sub>Ar</sub>)<sub>2</sub>Cl<sub>2</sub>][AlCl<sub>4</sub>] complexes.<sup>18</sup> The electrochemical potential at which the L<sub>Ar</sub><sup>0</sup>/L<sub>Ar</sub><sup>-</sup> redox event occurred was monitored for eight complexes, with various electron-donating and electron-withdrawing groups (EDGs and EWGs, respectively) substituted in the para position of the phenyl ring. It was found that EWGs shifted the L<sub>Ar</sub><sup>0</sup>/L<sub>Ar</sub><sup>1-</sup> redox process to more positive potentials, while EDGs resulted in a shift of the L<sub>Ar</sub><sup>0</sup>/L<sub>Ar</sub><sup>1-</sup> redox event to more negative potentials (Figure 3).

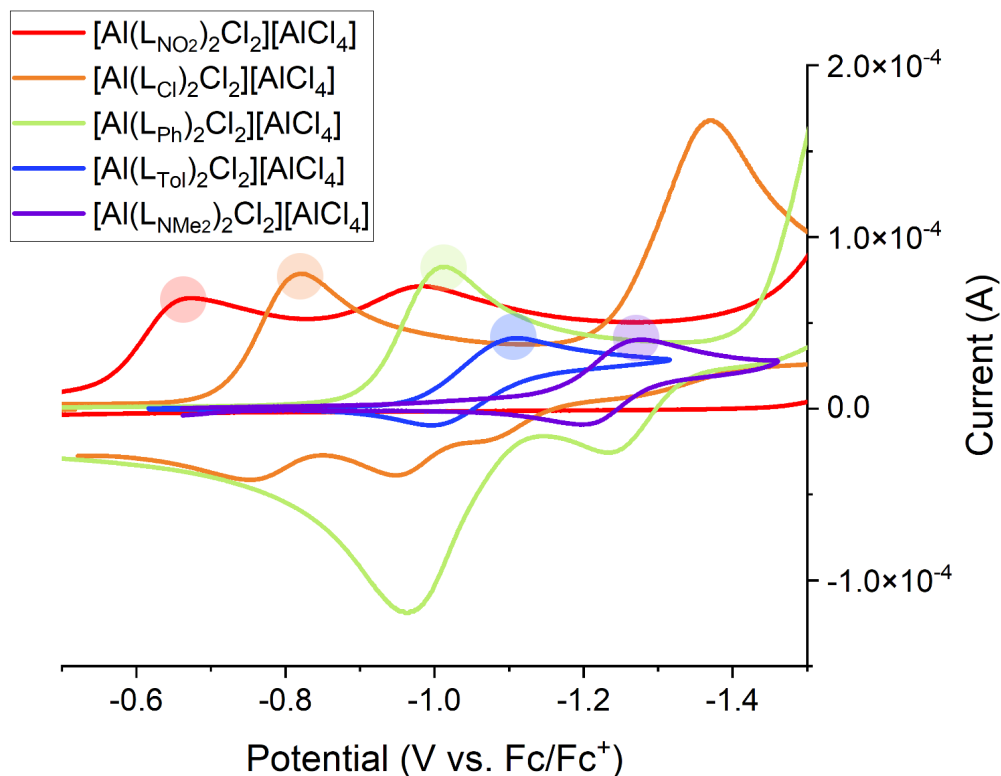


**Figure 3.** Overlaid CV data for  $[\text{Al}(\text{L}_{\text{Ar}})_2\text{Cl}_2][\text{AlCl}_4]$  complexes of varying aryl substitution. Each complex's first reduction event is highlighted for clarity. Experimental data were collected by Henry Wilson.

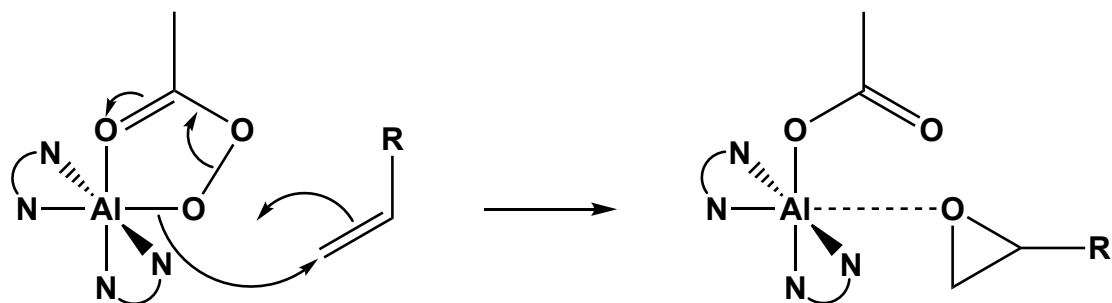
From these examples, it is clear that the redox potentials of  $\alpha$ -diimine complexes of Al have an explicit dependence on other ligands around the Al center, as well as substituents on the  $\alpha$ -diimine ligands. Such effects influence the choices of aryl substitution and inner-sphere manipulation of the complexes reported herein.

### 1.3.2 Neutral-ligand $\alpha$ -diimine complexes of Al catalyze epoxidation

Previous members of our group, Koellner et. al., demonstrated the ability of the  $[\text{Al}(\text{L}_{\text{Ph}})_2\text{Cl}_2][\text{AlCl}_4]$  complex to catalyze the epoxidation of various alkenes by

peracetic acid.<sup>19</sup> It was found that the epoxidation of alkenes by this complex proceeded with unusually high selectivity. High conversions and yields were obtained after short reaction times for most alkenes at ambient temperature and pressure in air. These findings are extremely encouraging, particularly considering that typical epoxidations of such substrates are run at elevated temperature (~80 °C), over long time intervals (24 h), or both.<sup>20–22</sup>

A review paper from Goldsmith<sup>23</sup> discusses these findings from Koellner et. al., drawing upon the observation that *trans*-4-octene is converted to a single epoxide to conclude that the reaction proceeds via a Sharpless-like concerted O atom transfer (Scheme 1). Goldsmith therefore expects that the more efficiently the peracetic acid can coordinate to the Al center, the more efficiently the epoxidation will proceed.



**Scheme 1.** Concerted epoxidation of a generic alkene by peracetic acid, catalyzed by a neutral  $\alpha$ -diimine complex of aluminum. Only coordinating atoms are shown for clarity. Adapted from Goldsmith<sup>23</sup> (2018).

### **1.3.3 Reduced-ligand $\alpha$ -diimine complexes of Al do diverse and interesting chemistry**

The majority of  $\alpha$ -diimine complexes of Al in the literature contain ligands in the -1 or -2 oxidation state. These oxidation states are more conducive for proton-



transfer and dehydrogenation chemistry, as explained by Berben<sup>24</sup> in a concept paper. Berben discusses the application for reduced ligand complexes of IP and bis(imino)pyridine (I<sub>2</sub>P) in proton transfer chemistry and dehydrogenation catalysis. Drawing upon the observed redox chemistry of these complexes, Berben suggests a pathway in which a catalyst assists in electron transfer when its ligands are more oxidized, and proton transfer when its ligands are more reduced, a notion corroborated by Goldsmith<sup>23</sup>. Such complexes have been demonstrated to selectively dehydrogenate formic acid<sup>25</sup> as well as activate O–H and N–H bonds<sup>26</sup>—demonstrating extreme promise towards Berben’s goal.

Aluminum complexes of reduced bis(imino)acenaphthylene (BIAN) ligands are also extensively reported to perform interesting redox chemistry.<sup>27–37</sup> A 2005 study from Schumann et. al.<sup>27</sup> investigates the solid-state and electronic structure of a series of novel [(<sup>dpp</sup>BIAN<sup>-</sup>)AlR<sub>2</sub>] complexes (dpp = 2,6-diisopropylphenyl; Figure 4). At the time, these were the first paramagnetic alkylaluminum complexes bearing a radical-anionic ligand in the literature.

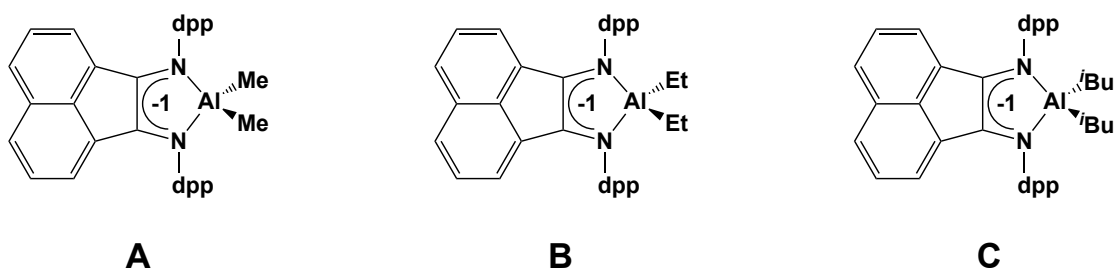


**Figure 4.** A series of [(<sup>dpp</sup>BIAN<sup>-</sup>)AlR<sub>2</sub>] complexes. Adapted from Schumann et. al.<sup>27</sup> (2005).

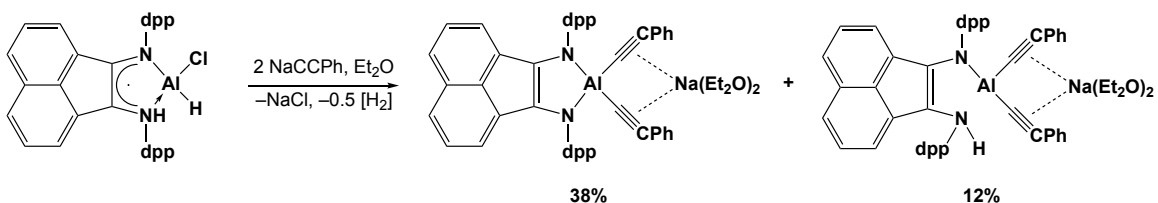
Table 1 summarizes the bonding parameters for **A–C**. Interestingly, increasing the steric bulk of the alkyl groups on the Al center has at most a weak effect on the bonding within the –Al–N–C–C–N– metallacycle. Based upon

literature comparisons<sup>38–40</sup> for C–C<sub>backbone</sub> and C–N<sub>imine</sub> bond distances in similar complexes, Schumann et. al. assigned the <sup>dpp</sup>BIAN ligand as singly reduced, as expected.

**Table 1.** Selected bond lengths (Å) and angles (°) for **A–C**. Adapted from Schumann et. al.<sup>27</sup> (2005).

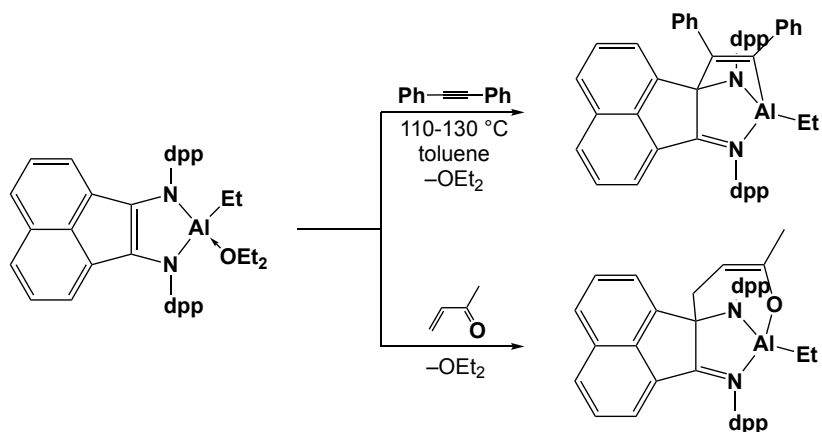
	<b>A</b>	<b>B</b>	<b>C</b>
Al–N <sub>imine</sub>	1.949(2) 1.950(2)	1.958(4) 1.967(4)	1.968(3) 1.965(4)
Al–C	1.972(3) 1.965(3)	1.945(3) 1.968(3)	1.956(2) 1.974(2)
C–C <sub>backbone</sub>	1.441(3)	1.439(4)	1.424(4)
C–N <sub>imine</sub>	1.330(3) 1.331(3)	1.339(4) 1.323(4)	1.340(3) 1.345(3)
N <sub>imine</sub> –Al–N <sub>imine</sub>	86.25(8)	85.31(12)	85.46(9)
R–Al–R	117.07(13)	110.21(18)	119.48(16)

A later study from Sokolov et. al.<sup>28</sup> investigates the reactivity of a singly reduced [(<sup>dpp</sup>BIAN<sup>-</sup>)Al(H)Cl] complex (dpp = 2,6-diisopropylphenyl). Aluminum hydrides are commonly used reagents in  $\alpha$ -olefin polymerization, or as reducing agents in well-known organic transformations. However, incorporation of the redox-active BIAN ligand dramatically affects the reaction profile of the [(<sup>dpp</sup>BIAN<sup>-</sup>)Al(H)Cl] complex, yielding it inert towards alkenes. Instead the [(<sup>dpp</sup>BIAN<sup>-</sup>)Al(H)Cl] complex is observed to undergo an intramolecular electron transfer when treated with nucleophilic phenylacetylide, ejecting H<sub>2</sub> gas and reducing the BIAN<sup>1-</sup> ligand to BIAN<sup>2-</sup> (Scheme 2).



**Scheme 2.** Intramolecular electron transfer upon reaction of  $[(^{\text{dpp}}\text{BIAN}^-)\text{Al}(\text{H})\text{Cl}]$  with phenylacetylide. Adapted from Sokolov et. al.<sup>28</sup> (2018).

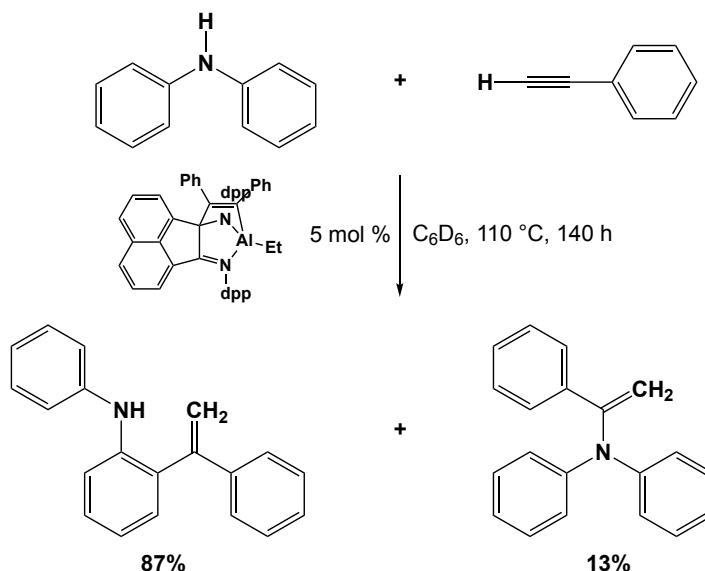
Another study from Fedushkin and coworkers<sup>29</sup> examines the reactivity of a doubly reduced  $[(^{\text{dpp}}\text{BIAN}^{2-})\text{AlEt}(\text{Et}_2\text{O})]$  complex towards diphenylacetylene and methylvinylketone (Scheme 3). As in the previous case, the BIAN ligand changes the reactivity of the alkylaluminum component, which would typically be expected to react with the diphenylacetylene in a carbometallation reaction. Instead, the reaction proceeds via cycloaddition across the metal and  $\alpha$ -diimine. Notably, the addition of methylvinylketone across a metal-ligand system is first of its kind.



**Scheme 3.** Cycloaddition of diphenylacetylene and methylvinylketone to a  $[(^{\text{dpp}}\text{BIAN}^{2-})\text{AlEt}(\text{Et}_2\text{O})]$  complex. Adapted from Fedushkin et. al.<sup>29</sup> (2013).

Fedushkin and coworkers then examined the viability of the diphenylacetylene cycloaddition product as a catalyst for the hydroamination of alkynes, with promising results (Scheme 4). Full conversion to products was

observed, though a long period of heating was required. Notably, the same reaction run with 10 mol%  $\text{AlCl}_3$  in place of the cycloaddition product gave exclusively the minor product of Scheme 4, indicating that the cycloaddition product plays an important role in directing the hydroamination.

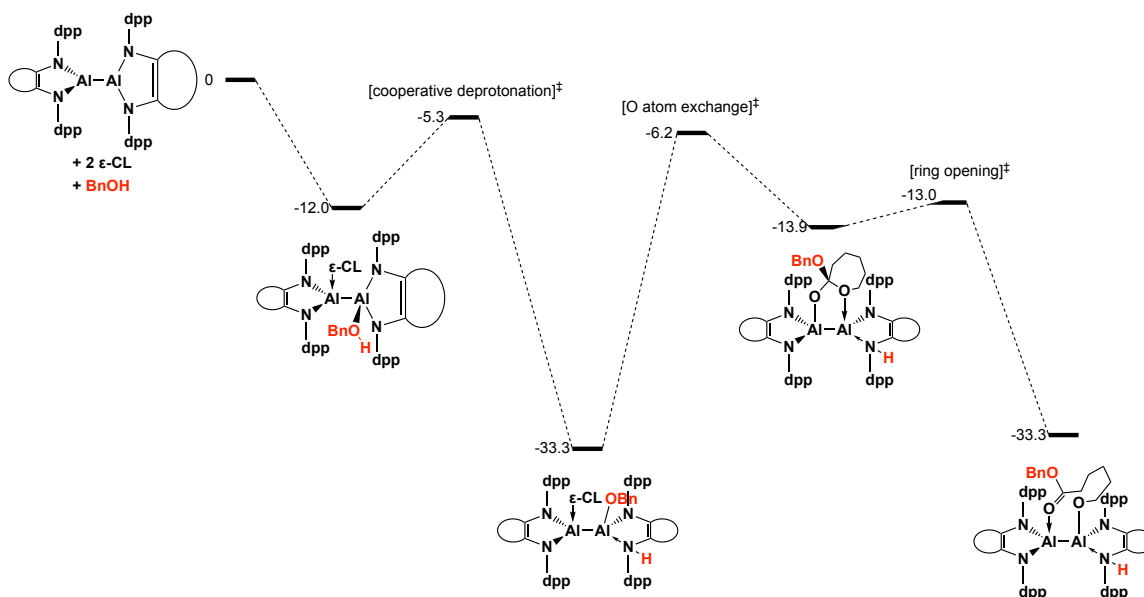


**Scheme 4.** Catalysis of the hydroamination of phenylacetylene by diphenylamine by Al complex. Adapted from Fedushkin et. al.<sup>29</sup> (2013).

### 1.3.4 $\alpha$ -diimine complexes containing Al–Al bonds possess powerful reactivity

A rapidly evolving area of main group chemistry is the study of complexes with metal–metal bonds. To our knowledge, the first  $\alpha$ -diimine complex containing an Al–Al bond was synthesized by Fedushkin and coworkers in 2012.<sup>37</sup> The complex—of the form  $[(^{\text{dpp}}\text{BIAN}^{2-})\text{Al}-\text{Al}(^{\text{dpp}}\text{BIAN}^{2-})]$ —displays analogous reactivity towards acetylene and phenylacetylene as the  $[(^{\text{dpp}}\text{BIAN}^{2-})\text{AlEt}(\text{Et}_2\text{O})]$  complex (Scheme 3) discussed in Section 1.3.3. This observation implies the potential of the dialane as a catalyst for the transformation of alkynes, in which each Al center

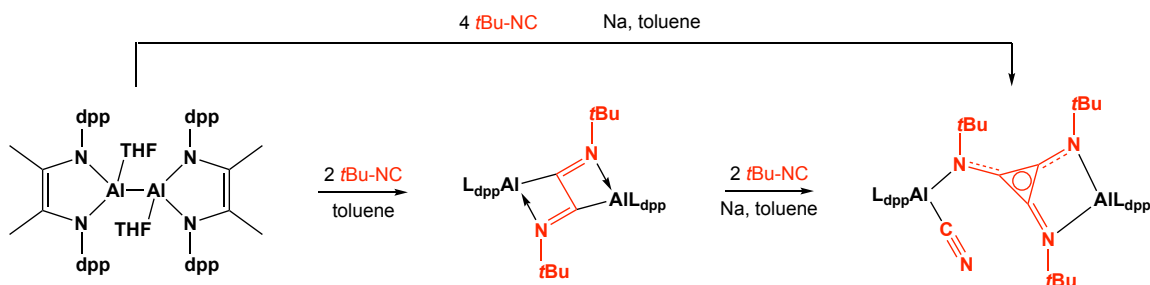
possesses independent reactivity. Interestingly, further work from Kazarina and coworkers has demonstrated the ability of the neighboring Al atoms to cooperate.<sup>41</sup> In the presence of benzyl alcohol, the same  $[(\text{dppBIAN}^{2-})\text{Al}-\text{Al}(\text{dppBIAN}^{2-})]$  complex catalyzes the ring-opening polymerization of  $\epsilon$ -caprolactone ( $\epsilon$ -CL) with >90% conversion in just 15 minutes. Kazarina et. al. modelled the system computationally, finding that the Al centers work in tandem to achieve the ROP (Scheme 5).



**Scheme 5.** Proposed mechanism for the ROP of  $\epsilon$ -CL by  $[(\text{dppBIAN})\text{Al}-\text{Al}(\text{dppBIAN})]$ . Calculations were performed at the B3LYP/6-31+G\*\* level of theory. Energies are given in kcal/mol relative to the starting materials. Adapted from Kazarina et. al.<sup>35</sup> (2018).

A 2019 study from Chen et. al.<sup>42</sup> investigated the behavior of a  $[(\text{L}_{\text{dpp}}^{2-})(\text{THF})\text{Al}-\text{Al}(\text{THF})(\text{L}_{\text{dpp}}^{2-})]$  complex in the presence of tert-butyl isocyanide and sodium metal. It was observed that reaction proceeds with sequential oligomerization of isocyanide, generating an aromatic  $[\text{C}_3\text{N}_3(\text{tBu})_3]^{2-}$  ring (Scheme

6). This aromatic  $[C_3N_3]$  moiety is cutting-edge chemistry—the only literature example of such a fragment requires multiple steps under harsh conditions.<sup>43</sup> Using the  $[(L_{dpp}^{2-})(THF)Al-Al(THF)(L_{dpp}^{2-})]$  complex, this transformation can be achieved in a single step under mild conditions.



**Scheme 6.** Reactivity of  $[(L_{dpp}^{2-})(THF)Al-Al(THF)(L_{dpp}^{2-})]$  towards  $tBuCN$  and sodium metal in toluene. Adapted from Chen et. al.<sup>36</sup> (2019).

## 1.4 Current work

Motivated by the tenets of green chemistry and an interest in the structure and reactivity of literature  $\alpha$ -diimine complexes of Al, we chose to study Al complexes bearing  $L_{Ar}$  across all ligand oxidation states. For our neutral-ligand complexes, we took inspiration from Graves group alum Henry Wilson's observation that the inner-sphere iodides of  $[Al(L_{Ph})_2I_2] \cdot I$  are easily displaced by acetonitrile (NCMe) molecules to give  $[Al(L_{Ph})_2(NCMe)_2] \cdot 3I$ .<sup>18</sup> Thus, we have characterized  $[Al(L_{Ar})_2I_2] \cdot I$  and  $[Al(L_{Ar})_2(NCMe)_2] \cdot 3I$  series by multinuclear NMR spectroscopy, X-ray diffraction (XRD), and cyclic voltammetry. Computational methods will be utilized to corroborate structure, provide insight into NMR data, and perform a frontier orbital analysis. The ability of these complexes to catalyze the epoxidation of cyclohexene by peracetic acid will be interrogated.

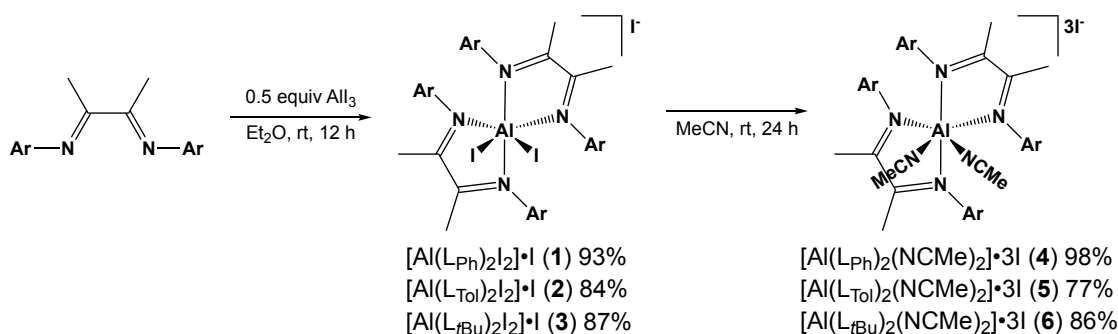
We will also describe the synthesis and characterization of several reduced-ligand  $\alpha$ -diimine complexes of Al. These complexes have been characterized by combinations of XRD,  $^1\text{H}$  NMR, EPR, and CV. Computational methods will also be used in this section to evaluate structural findings, visualize frontier orbitals, and simulate EPR spectra.

## 2. Results and Discussion

### 2.1 Neutral-ligand $\alpha$ -diimine complexes of Al

The  $[\text{Al}(\text{L}_{\text{Ar}})_2\text{I}_2]\cdot\text{I}$  complexes **1–3** [ $\text{L}_{\text{Ar}}$  = *N,N'*-bis(phenyl)-2,3-dimethyl-1,4-diazabutadiene ( $\text{L}_{\text{Ph}}$ ), *N,N'*-bis(4-methylphenyl)-2,3-dimethyl-1,4-diazabutadiene ( $\text{L}_{\text{Tol}}$ ), and *N,N'*-bis(4-*tert*-butylphenyl)-2,3-dimethyl-1,4-diazabutadiene ( $\text{L}_{\text{tBu}}$ )] were prepared via the 2:1 reaction of  $\text{L}_{\text{Ar}}$  and  $\text{AlI}_3$  in diethyl ether at room temperature (Scheme 7). In all cases, product precipitates from the reaction medium and is collected by filtration as an analytically pure, orange powder in 84–93% yield. Compounds **1–3** are stable for several months at room temperature under a dinitrogen atmosphere.

Following dissolution in acetonitrile, complexes **1–3** underwent immediate color change from vibrant orange to dark purple. Upon concentrating acetonitrile solutions of **1–3**, we were able to isolate the  $[\text{Al}(\text{L}_{\text{Ar}})_2(\text{NCMe})_2]\cdot 3\text{I}$  complexes **4–6** in 77–98% yield. These purple crystals were washed with cold acetonitrile and dried under vacuum.



**Scheme 7.** Synthesis of the  $[Al(L_{Ar})_2I_2] \cdot I$  and  $[Al(L_{Ar})_2(NCMe)_2] \cdot 3I$  series.

### 2.1.1 $^1H$ and $^{13}C$ NMR characterization of the $[Al(L_{Ar})_2I_2] \cdot I$ and $[Al(L_{Ar})_2(NCMe)_2] \cdot 3I$ series

Complexes **1–6** were characterized by  $^1H$  and  $^{13}C$  NMR spectroscopy. For both sets of compounds, two resonances corresponding to the methyl groups along the N–C–N backbone were observed. In complexes containing aryl substitutions (**2**, **3**, **5**, and **6**), two resonances corresponding to the NMR active signatures of the R group of the aryl ring were also observed. These results support a  $C_2$  symmetric complex in solution. In complexes containing iodo ligands (**1–3**), it was observed that an aromatic proton was shifted upfield to the ~5 ppm range. This shift occurred concomitant with a broadening of all aromatic signals in the  $^1H$  NMR spectra, suggesting the presence of H---I interactions in complexes **1–3**. An analogous H---Cl interaction was observed for the  $[Al(L_{Ph})_2Cl_2]^+$  cation by Wilson et. al.<sup>18</sup> Analysis of single crystals of **1–3** reveals that these H---I interactions are also present in the solid-state structures of the complexes (Figure 5). The average H---I distance was found to be 3.17 Å for **1–3**, which comports with the H---Cl distance observed by Wilson et. al. (2.96 Å) considering iodine's larger radius.<sup>18</sup> This phenomenon was also interrogated computationally using density functional



theory (DFT). The NMR spectrum for the  $[\text{Al}(\text{L}_{\text{Ph}})_2\text{I}_2]^+$  cation of **1** in  $\text{CDCl}_3$  was modelled using a modified (to account for the large iodide atoms) version of Jain and coworkers' 2009 recommendation.<sup>44</sup> The results corroborated the empirical observation that the ortho proton is shifted upfield, with  $< 0.5$  ppm agreement (Figure 6).

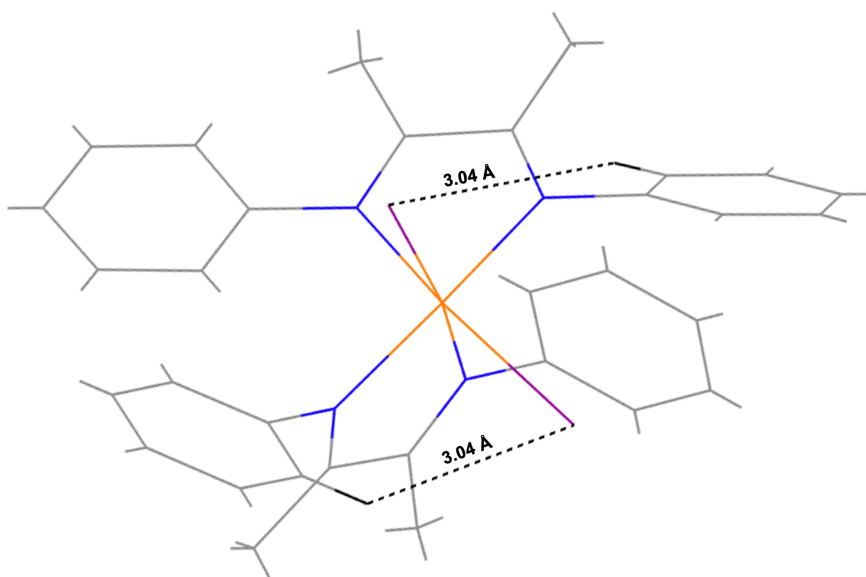


**Figure 5.** Visualization of the H---I interaction rendered from the X-ray structure of the  $[\text{Al}(\text{L}_{\text{Ph}})_2\text{I}_2]^+$  cation of **1**.

The  $^1\text{H}$  NMR spectra for complexes **4–6** also feature an aromatic resonance in the  $\sim 5$  ppm range, indicating that an analogous N---H interaction occurs. The average distance of this interaction is 2.98 Å, which (as expected) is significantly longer than a typical N---H hydrogen bond, but comparable to the distance observed by Wilson and coworkers.<sup>45</sup> Jain et. al.'s method again succeeds in predicting this upfield shift within 0.5 ppm (Figure S7).

$^{13}\text{C}$  NMR spectra of **1–6** further corroborate the  $C_2$  symmetry of the complexes (Section 5.2). All compounds feature two resonances corresponding to both the  $\text{CH}_3\text{C}=\text{N}_{\text{imine}}$  and  $\text{CH}_3\text{C}=\text{N}_{\text{imine}}$  nuclei. Inspection of the aromatic region for **1–6** reveals 12 different environments, consistent with Wilson et. al.'s observation for alkyl-substituted  $[\text{Al}(\text{L}_{\text{Ar}})_2\text{Cl}_2][\text{AlCl}_4]$  complexes.<sup>18</sup> As suggested by Wilson et. al., this phenomenon is likely due to hindered rotation about the  $\text{N}_{\text{imine}}-\text{C}_{\text{Ar}}$  bond. For complexes **2**, **3**, **5**, and **6**, two sets of resonances corresponding to the respective alkyl substituents of the aryl ring were observed.

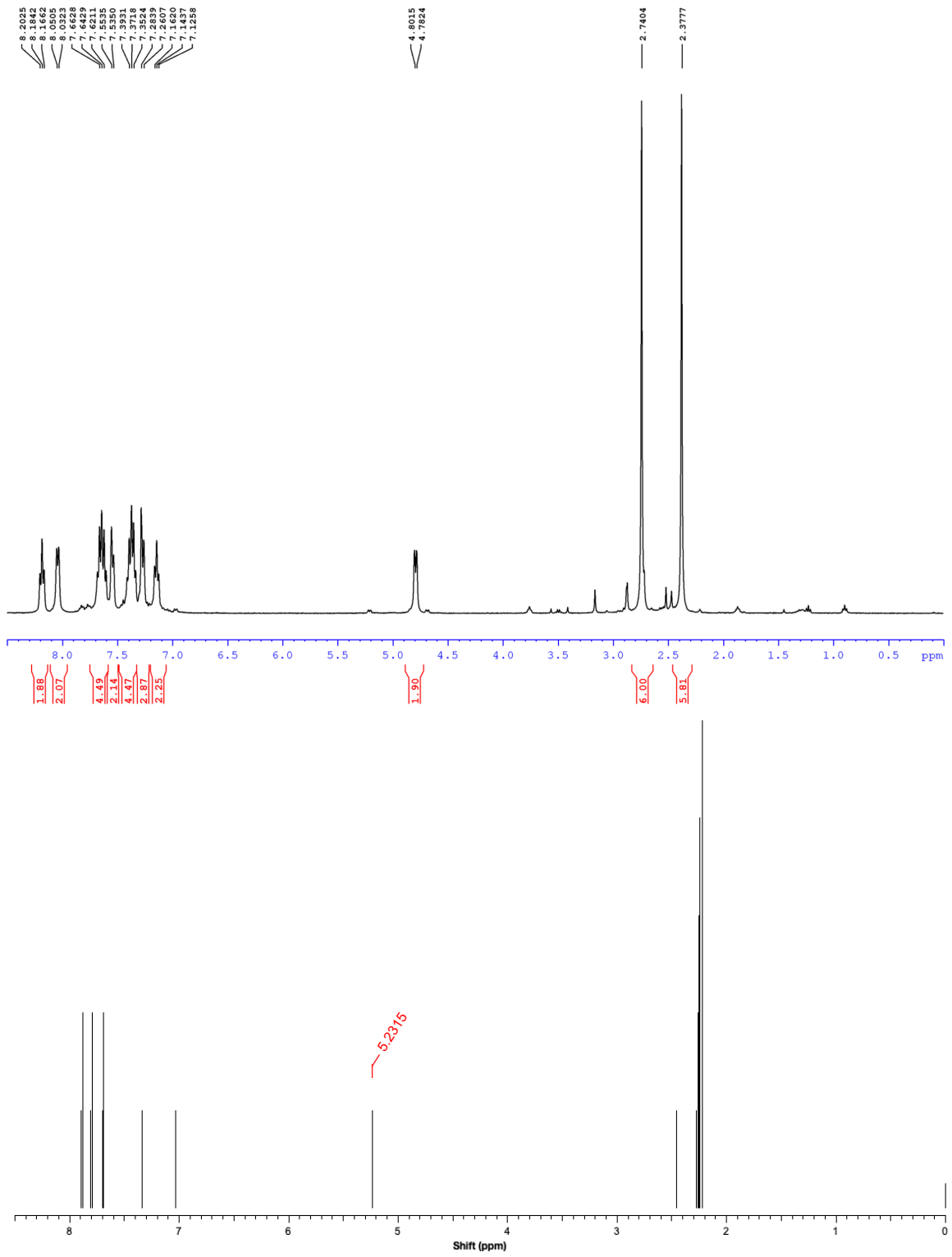


Figure 6. Experimental (top) and simulated (bottom) <sup>1</sup>H NMR spectra of 1.

## 2.1.2 Solid-state structural analysis of the $[Al(L_{Ar})_2I]$ and $[Al(L_{Ar})_2(NCMe)_2] \cdot 3I$ series

Complexes **1–6** were further characterized via XRD, allowing for robust solid-state structural analysis. Selected structural parameters are provided for the cations of **1–6** in Table 2, and their representations are shown in Figure 7.

**Table 2.** Selected bond distances (Å) and angles (°) for **1–6**.

	<b>1</b>	<b>1</b> <sub>theory</sub> <sup>a</sup>	<b>2</b>	<b>3</b>	<b>4</b> <sup>b</sup>	<b>4</b> <sub>theory</sub> <sup>a</sup>	<b>5</b>	<b>6</b>
Al–N <sub>imine</sub>	2.032(7)	2.0918	2.051(4)	2.063(9)	2.020(8)	2.0465	1.997(4)	2.002(6)
	2.062(7)		2.032(4)	2.047(9)	1.993(8)		2.023(4)	1.997(6)
	2.033(7)	2.0909	2.053(4)	2.041(9)	2.006(8)	2.0558	2.000(4)	2.001(6)
	2.053(7)		2.041(4)	2.060(8)	2.007(8)		2.023(4)	2.006(6)
Al–R	2.646(2)	2.7768	2.6633(14)	2.648(3)	1.94(3)	2.0257	1.953(4)	1.984(6)
	2.676(2)		2.6932(14)	2.659(3)	1.97(2)		1.958(4)	1.965(6)
C–C <sub>backbone</sub>	1.504(10)	1.4993	1.496(7)	1.495(15)	1.507(13)	1.5192	1.507(6)	1.521(9)
	1.485(11)		1.507(6)	1.499(14)	1.494(13)		1.515(6)	1.508(9)
C–N <sub>imine</sub>	1.285(10)	1.3141	1.296(6)	1.280(13)	1.291(11)	1.3139	1.290(5)	1.281(9)
	1.286(10)		1.299(6)	1.292(14)	1.270(12)		1.291(6)	1.289(9)
	1.282(10)	1.3122	1.289(6)	1.268(13)	1.289(12)	1.3140	1.291(6)	1.289(9)
	1.289(10)		1.292(6)	1.297(13)	1.277(13)		1.287(6)	1.297(9)
N <sub>imine</sub> –Al– N <sub>imine</sub>	77.8(3)	77.97	78.88(16)	77.6(3)	79.6(3)	79.76	79.56(14)	79.7(2)
	166.9(3)	169.65	167.26(17)	166.8(4)	175.2(4)	178.28	175.97(16)	174.8(3)
	93.4(3)	94.37	93.35(16)	92.4(3)	96.1(3)	99.03	98.29(15)	95.5(2)
	91.4(3)	94.37	91.11(16)	92.7(3)	97.8(3)	99.03	97.11(15)	97.4(2)
	86.1(3)	85.80	88.41(16)	87.0(3)	89.1(3)	92.11	91.21(15)	92.1(2)
	78.4(3)	77.97	78.49(16)	78.0(3)	79.8(3)	79.76	79.44(15)	80.2(2)
N <sub>imine</sub> –Al–R	97.2(2)	98.62	88.79(12)	92.2(2)	95.1(9)	89.52	91.38(15)	91.3(2)
	172.9(2)	171.76	174.95(13)	173.3(3)	169.1(7)	171.29	170.32(16)	172.9(3)
	92.9(2)	88.03	92.46(11)	96.7(3)	90.5(11)	89.68	90.88(15)	93.1(3)
	89.3(2)	86.99	97.49(12)	89.2(2)	90.5(8)	91.54	89.92(15)	91.0(3)
	91.4(2)	88.03	89.05(11)	97.2(2)	93.5(8)	89.68	91.01(15)	91.4(3)
	87.60(18)	86.99	98.17(12)	87.9(3)	87.7(6)	89.52	89.21(16)	91.0(3)
	95.6(2)	98.62	88.87(12)	91.5(3)	92.1(11)	91.54	92.28(15)	91.6(2)
	171.1(2)	171.76	175.94(13)	172.6(3)	171.3(11)	171.29	170.52(16)	170.8(3)
R–Al–R	97.56(8)	100.46	94.15(4)	96.38(10)	89.6(9)	90.16	91.26(15)	86.8(3)

<sup>a</sup> Values were calculated in Gaussian 16 at the B3LYP/LANL2DZ level of theory.

<sup>b</sup> Solid-state structural data for **4** was previously reported by Wilson et. al.<sup>18</sup>

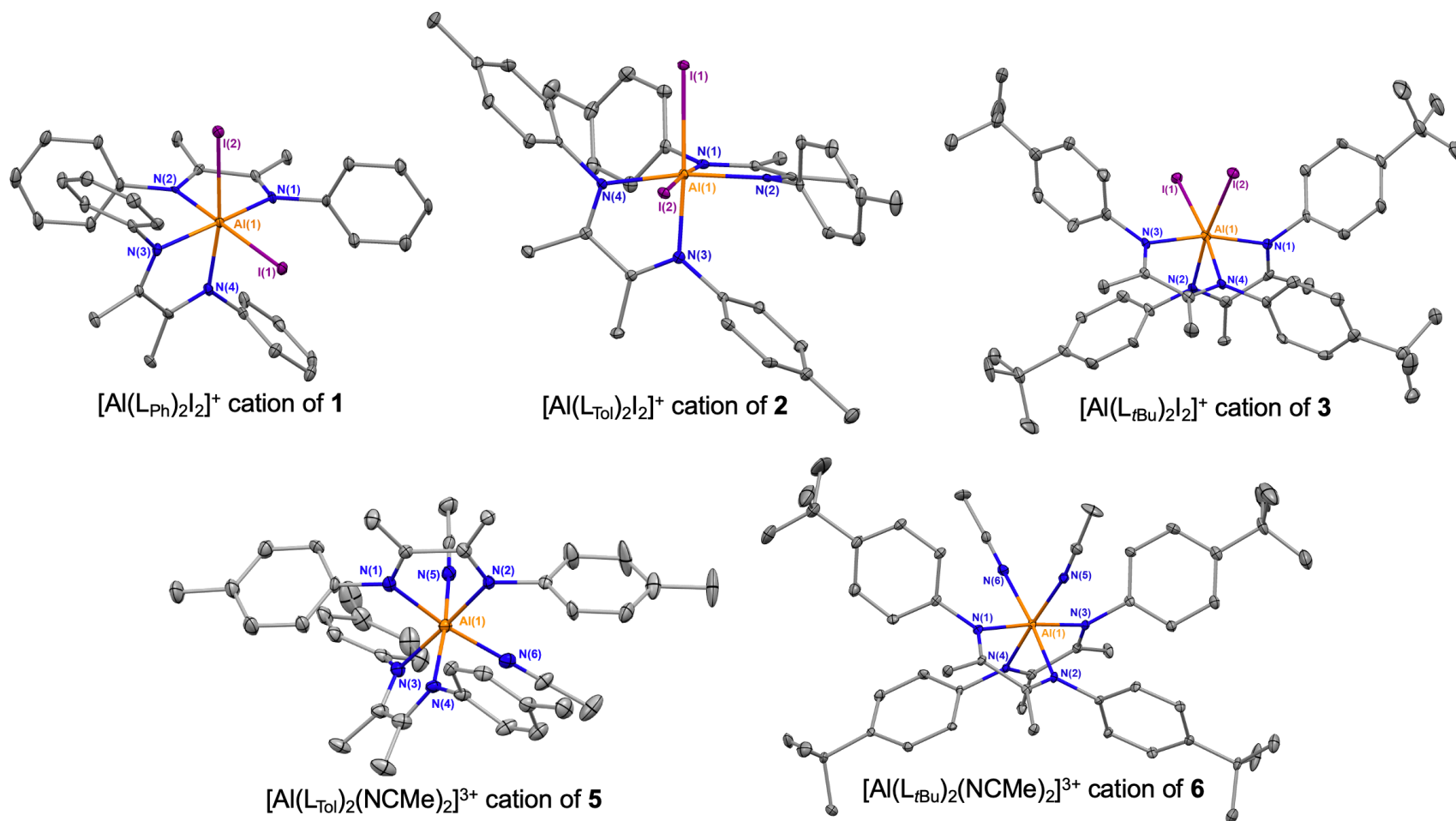


**Figure 7.** Solid-state structures of the cations of complexes **1–3**, **5**, and **6**. Ellipsoids are projected at 30% probability. Hydrogen atoms and interstitial dichloromethane molecules are omitted for clarity. The solid-state structure of compound **4** was previously reported by Wilson et. al.<sup>18</sup>

Crystals of **1–3** were grown from slow diffusion of hexane or pentane into a concentrated dichloromethane solution of the complexes at -25 °C. **1–3** crystallize as  $[\text{Al}(\text{L}_{\text{Ar}})_2\text{I}_2]^+$  cations with one outer-sphere iodide anion. Analogous to the dichloro series, the  $[\text{Al}(\text{L}_{\text{Ar}})_2\text{I}_2]^+$  cation consists of an  $\text{Al}^{3+}$  ion coordinated by two  $\alpha$ -diimine and two iodo ligands in a slightly distorted octahedral geometry.<sup>18</sup> Complexes **4–6** were crystallized from concentrated solutions of acetonitrile at room temperature. They crystallize as  $[\text{Al}(\text{L}_{\text{Ar}})_2(\text{NCMe})_2]^{3+}$  cations with three outer-sphere iodide anions, and are structurally similar to complexes **1–3**. For each of **1–6**, the  $[\text{Al}(\text{L}_{\text{Ar}})_2\text{R}_2]^{n+}$  cations exhibit near- $\text{C}_2$  symmetry, with the iodo or acetonitrile ligands occupying *cis* coordination sites.

The average Al–I bond distance for complexes **1–3** (2.664(1) Å) agrees with literature Al complexes bearing nitrogen-donor ligands.<sup>35,46–52</sup> As expected, this distance is longer than both the Al–Cl and Al–Br distances of the  $[\text{Al}(\text{L}_{\text{Ph}})_2\text{X}_2]^+$  cations (Table 3). However, an interesting trend in Al–N<sub>imine</sub> bond distance emerges across the  $[\text{Al}(\text{L}_{\text{Ph}})_2\text{X}_2]^+$  halide series. From X = Cl to X = Br, a lengthening of the Al–N<sub>imine</sub> bond is observed, but this distance is shortest for X = I (Table 3).

**Table 3.** Selected bond lengths across the halide series of  $[\text{Al}(\text{L}_{\text{Ph}})_2\text{X}_2]^+$  cations.

	Al–N <sub>imine</sub> (Å)	Al–X (Å)
X = Cl <sup>a</sup>	2.052(1)	2.227(1)
X = Br <sup>a</sup>	2.072(1)	2.386(1)
X = I	2.047(2)	2.664(1)

<sup>a</sup> Previously reported by Wilson et. al.<sup>18</sup>

We offer that competing Lewis acidity and steric effects may account for this unclear trend. Though the order of Lewis acidity across the molecular aluminum

halides has been debated<sup>53,54</sup>, recent calculations (which agree better with experimental data than those previous) indicate the order:  $\text{AlF}_3 < \text{AlCl}_3 < \text{AlBr}_3 \approx \text{AlI}_3$ .<sup>55</sup> Employing hard-soft acid-base theory, we therefore expect the  $[\text{Al}(\text{L}_{\text{Ph}})_2\text{Cl}_2]^+$  cation to form the weakest (and thus longest)  $\text{Al}-\text{N}_{\text{imine}}$  bond of the halide series. However, we must also consider the steric implications of the inner-sphere halogens, which favor a shorter  $\text{Al}-\text{N}_{\text{imine}}$  bond for the  $[\text{Al}(\text{L}_{\text{Ph}})_2\text{Cl}_2]^+$  cation. We cautiously attribute the inconsistencies in  $\text{Al}-\text{N}_{\text{imine}}$  distance for different inner-sphere halogens to the balance of these effects. In comparing steric effects between the dibromo and diiodo complexes, we must be careful to consider both ionic radius and bond length—the latter grows faster than the former for the  $[\text{Al}(\text{L}_{\text{Ph}})_2\text{X}_2]^+$  series (Table 3). Therefore, despite iodide being a larger ion than bromide, the  $\text{AlI}_2^+$  fragment may indeed be sterically unencumbered relative to  $\text{AlBr}_2^+$ . The same trend in  $\text{Al}-\text{N}$  distance is observed across a series of four-coordinate  $[\{\text{HC}(\text{Ph}_2\text{PNC}_6\text{H}_2\text{Me}_{3-2,4,6})_2\}\text{AlX}_2]$  ( $\text{X} = \text{Cl}, \text{Br}, \text{I}$ ) complexes reported by Hill et. al.<sup>56</sup> However, we are cautious to make conclusions about this behavior, particularly because the differences in  $\text{Al}-\text{N}_{\text{imine}}$  length are only slight ( $< 0.03 \text{ \AA}$ ).

The average  $\text{Al}-\text{N}_{\text{MeCN}}$  bond distance in complexes **4–6** ( $1.962(6) \text{ \AA}$ ) agrees well with literature examples of aluminum-acetonitrile adducts.<sup>57,58</sup> The  $\text{Al}-\text{N}_{\text{imine}}$  distance is notably shorter in complexes **4–6** ( $2.006(2) \text{ \AA}$ ) than in **1–3** ( $2.047(2) \text{ \AA}$ ), which follows intuitively from a rudimentary charge analysis. The Al center of complexes **4–6**, in which neutral acetonitrile molecules have displaced negatively-charged iodo ligands to the outer-sphere, will be significantly more Lewis acidic than the Al center of complexes **1–3**. The average  $\text{R}-\text{Al}-\text{R}$  angle for complexes **4–**

**6** (89.2(3) Å) also notably differs from that of complexes **1–3** (96.03(5) Å). This likely contributes to a slightly larger bite angle of the  $\alpha$ -diimine (78.2(2) for complexes **1–3** vs. 79.7(2) for complexes **4–6**), but more importantly may facilitate the coordination of larger substrates in catalysis.

Bonding parameters along  $L_{Ar}$  in **1–6** provide insight into the oxidation state of the ligand. The average C–C<sub>backbone</sub> (1.503(3) Å) and C–N<sub>imine</sub> (1.287(4) Å) bond lengths agree with literature examples of neutral- $\alpha$ -diimine complexes of Al.<sup>51,59,60</sup> Indeed, upon inspection of typical C( $sp^2$ )–C( $sp^2$ ) and C( $sp^2$ )=N bond lengths, we are confident that the  $\alpha$ -diimine ligands in complexes **1–6** are fully oxidized.<sup>61</sup>

### **2.1.3 DFT investigation of the $[Al(L_{Ar})_2I_2]^+$ and $[Al(L_{Ar})_2(NCMe)_2]^+3I^-$ series**

The geometry of the  $[Al(L_{Ph})_2I_2]^+$  cation of compound **1** was optimized using DFT, with no symmetry constraints. Along the N–C–C–N backbone, computed bond distances are within 0.03 Å of those found in the XRD analysis (Table 2). Around the Al center, calculated bond lengths were found to be longer than those in the solid-state structure for both the Al–N<sub>imine</sub> bonds (by ~0.04–0.06 Å) and the Al–I bonds (~0.10–0.13 Å). Computed bond angles for the complex agree closely with experimental results, with no differences exceeding 5°. The optimized structure for the  $[Al(L_{Ph})_2(NCMe)_2]^+$  cation of **4** was also calculated using DFT, with no symmetry constraints. Like the cation of complex **1**, computed bond lengths along the N–C–C–N backbone were in strong agreement with the X-ray analysis (all bonds agree within 0.03 Å). There is greater discrepancy around the Al center; bonds around aluminum are systematically longer in the DFT optimization (Al–



$N_{\text{imine}}$  by  $\sim 0.04\text{-}0.06$  Å and  $\text{Al-N}_{\text{MeCN}}$  by  $\sim 0.05\text{-}0.08$  Å). Charges within the optimized structures were calculated using the natural bonding orbital (NBO) method (Table 4). Atomic charges calculated via the NBO method show a significantly higher charge on the Al center in complex **4** than complex **1**, consistent with the trend in  $\text{Al-N}_{\text{imine}}$  bond distance.

**Table 4.** NBO charge distribution for the cations of **1** and **4**.

	$[\text{Al}(\text{L}_{\text{Ph}})_2\text{I}_2]^+$	$[\text{Al}(\text{L}_{\text{Ph}})_2(\text{NCMe})_2]^{3+}$
Al	1.467	2.022
I or $\text{N}_{\text{MeCN}}$	-0.391	-0.600
$N_{\text{imine}}$	-0.640 -0.653	-0.667 -0.662

The molecular orbitals of the  $[\text{Al}(\text{L}_{\text{Ph}})_2\text{I}_2]^+$  cation were also modeled. The highest occupied molecular orbital (HOMO) and HOMO-1 are similar in structure and are nearly degenerate ( $\Delta E = 0.07$  eV). Both are located almost entirely on the iodo ligands, whereas the same set of orbitals of the  $[\text{Al}(\text{L}_{\text{Ph}})_2\text{Cl}_2]^+$  cation were found to have a significant amount of electron density located on the phenyl rings of the  $\alpha$ -diimine ligand in addition to the halide ligands (Figure 8).<sup>18</sup>

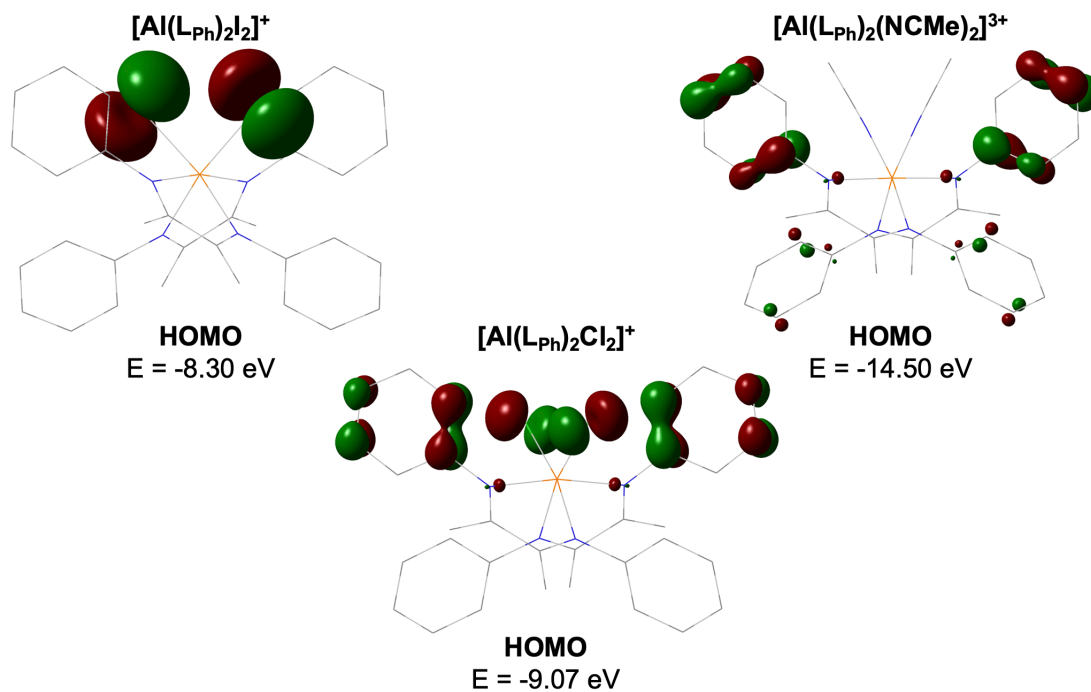


**Figure 8.** HOMO of the cation of complex **1**, its dichloro analog, and the cation of complex **4**. Hydrogen atoms are omitted for clarity.

In contrast to the HOMO and HOMO-1, the lowest occupied molecular orbital (LUMO) and LUMO+1 for the cation of **1** were found to be almost entirely  $\alpha$ -diimine-based. They are localized along the N–C–C–N backbone, with a bonding interaction along the C–C bond and antibonding interactions along the two C–N bonds (Figure 9). The orbitals are extremely similar in structure, and relatively close in energy ( $\Delta E = 0.17$  eV). The location of the LUMO and LUMO+1 orbital density agrees with our intuition for these complexes: reduction events will be  $\alpha$ -diimine-based.

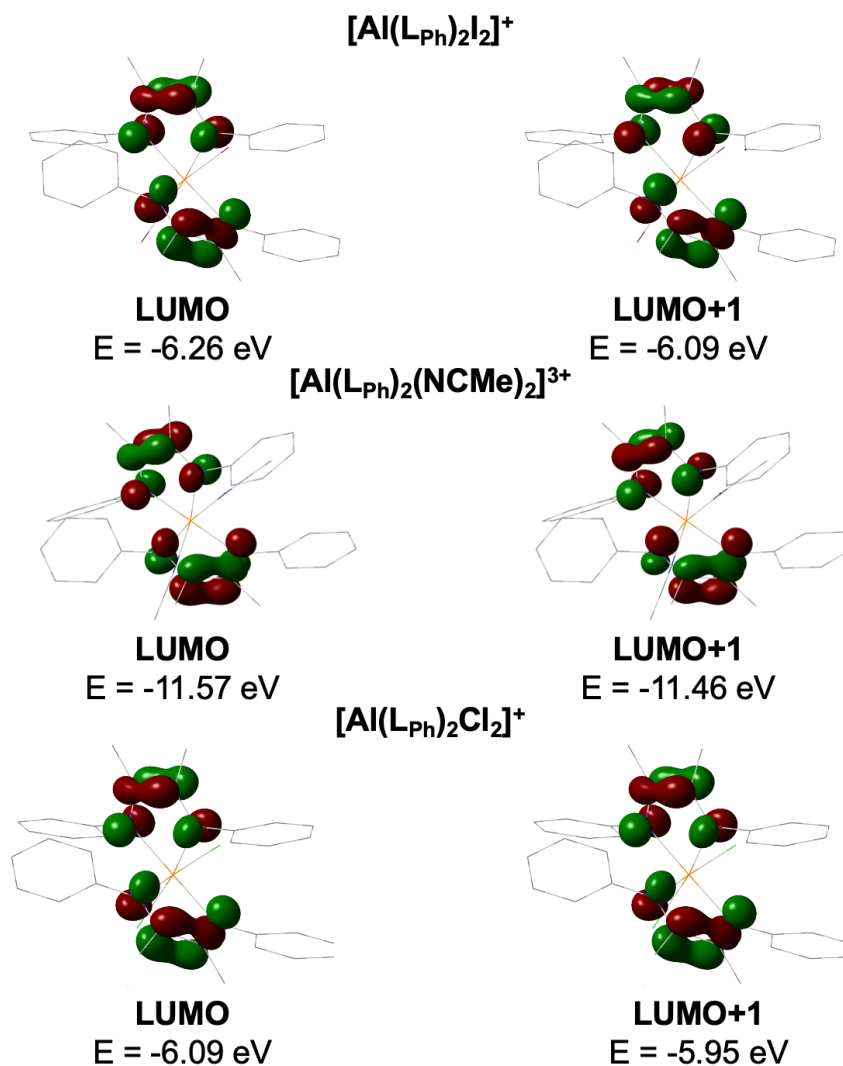


**Figure 9.** LUMO and LUMO+1 of the  $[(\text{L}_{\text{Ph}})_2\text{AlI}_2]^+$  cation of **1**, the  $[(\text{L}_{\text{Ph}})_2\text{Al}(\text{NCMe})_2]^{3+}$  cation of **4**, and the  $[(\text{L}_{\text{Ph}})_2\text{AlCl}_2]^+$  cation.

The frontier orbitals of the  $[(\text{L}_{\text{Ph}})_2\text{Al}(\text{NCMe})_2]^{3+}$  cation of **4** were also modelled. The LUMO and LUMO+1 are located along the N–C–C–N backbone and are close to degenerate ( $\Delta E = 0.11$  eV). They have identical features as the LUMO and LUMO+1 for the  $[(\text{L}_{\text{Ph}})_2\text{AlX}_2]^+$  cations. Conversely, the electron density of the HOMO and HOMO-1 for the cation of **4** is located almost entirely on one phenyl ring of each  $\alpha$ -diimine ligand (Figure 8).

### 2.1.4 Cyclic voltammetry of the $[Al(L_{Ar})_2I_2] \cdot I$ and $[Al(L_{Ar})_2(NCMe)_2] \cdot 3I$ series

The cyclic voltammograms of **1–3**, **5**, and **6** were collected in DCM. In all cases, multiple ligand-based, reversible redox events are observed. Figure 10 juxtaposes the voltammograms of complex **1** and Wilson et. al.'s previously reported  $[Al(L_{Ph})_2Cl_2][AlCl_4]$  complex. Wilson et. al. assigned the two events for the complex as the  $L_{Ar}^0/L_{Ar}^-$  redox couple of each  $\alpha$ -diimine ligand, citing DFT visualization of the SOMO and HOMO of the singly reduced and doubly reduced  $[Al(L_{Ph})_2Cl_2][AlCl_4]$  complexes (respectively).<sup>18</sup>

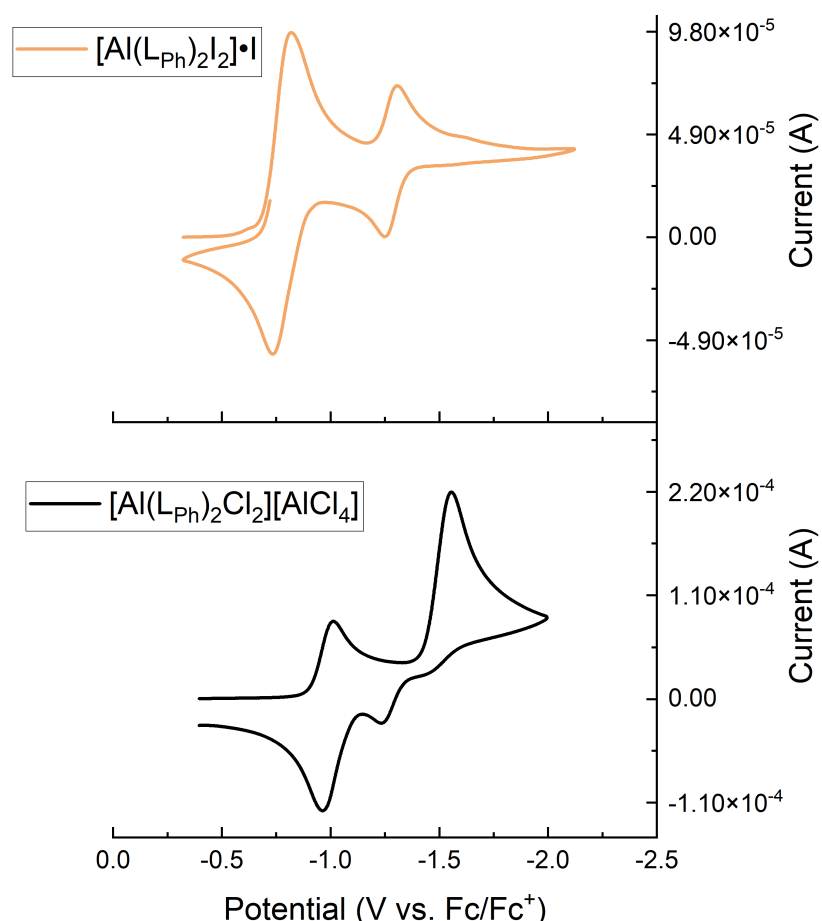


**Figure 10.** Cyclic voltammograms of  $[Al(L_{Ph})_2X_2][R]$  complexes recorded in 0.1 M  $[n\text{-Pr}_4\text{N}][\text{BAR}^F]$  DCM solution. Top: **1**, CV recorded at  $100 \text{ mV s}^{-1}$ . Bottom:  $[Al(L_{Ar})_2Cl_2][AlCl_4]$ , CV collected by Wilson et. al.<sup>18</sup> at  $500 \text{ mV s}^{-1}$ .

For complex **1**, the first redox event qualitatively indicates the movement of two electrons (based upon its height compared to the second redox event). Though a more rigorous quantitative analysis of the CV would be necessary to make a certain assignment, we suggest that the first redox event of **1** corresponds to the  $L_{Ar}^0/L_{Ar}^-$  redox couple of both  $\alpha$ -diimine ligands and the second corresponds to the  $L_{Ar}^-/L_{Ar}^{2-}$  redox couple of one  $\alpha$ -diimine ligand. In both cases, the couples exhibit excellent reversibility.

Figure 11 presents CV data for complexes **2**, **3**, **5**, and **6**. The data for all complexes are summarized in Table 5. The overlapping  $L_{Ar}^0/L_{Ar}^-$  redox couples in the CV of **1** appear to resolve slightly into two processes for complexes **2** and **3**, supporting our assignment of a multi-electron event. As expected, the redox events for **2** and **3** are shifted to be more negative than for **1** due to the electron-donating groups on  $L_{Ar}$  (Section 1.3.2). Voltammograms of complexes **5** and **6** also contain two distinct redox events, with **5** exhibiting slight resolution of the first event (analogous to **2** and **3**). The CV of **6** contains more features than expected, but the same two events are still observed.

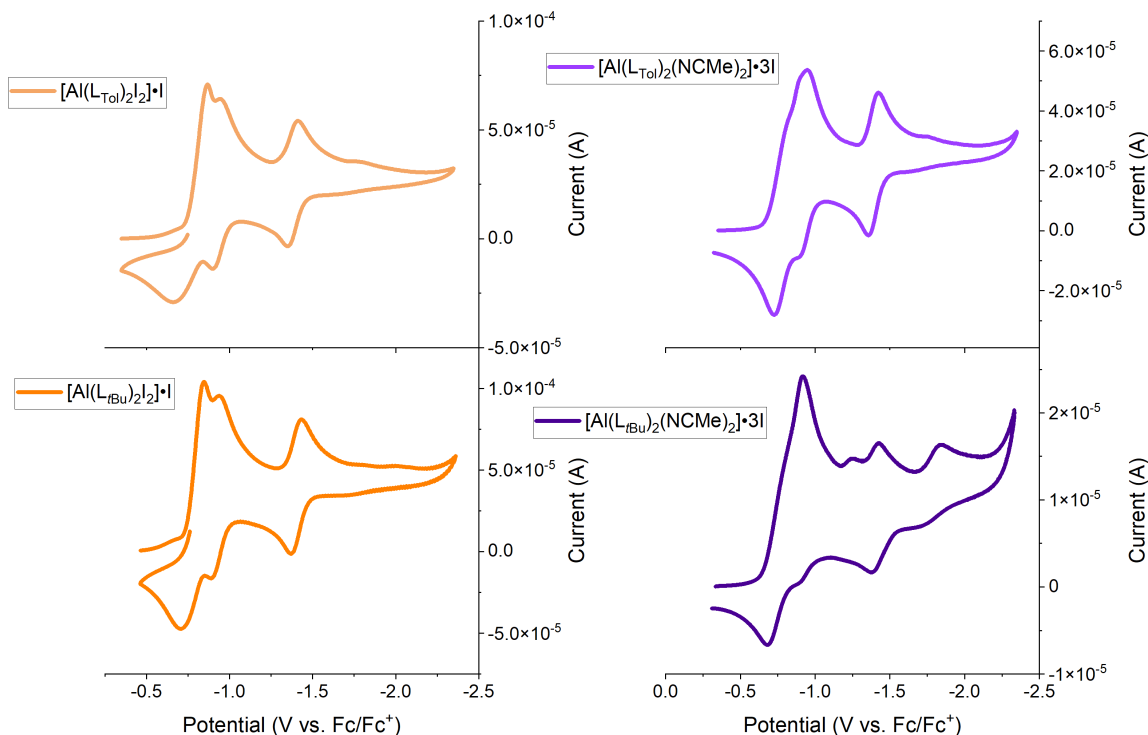


**Figure 11.** Cyclic voltammograms of complexes **2**, **3**, **5** and **6** recorded in 0.1 M  $[n\text{-Pr}_4\text{N}][\text{BAr}^{\text{F}}]$  DCM solution at 100  $\text{mV s}^{-1}$ .

**Table 5.** Electrochemical potentials (V vs.  $\text{Fc}/\text{Fc}^+$ ) for **1–3**, **5**, and **6**.

	$[\text{Al}(\text{L}_{\text{Ar}}^0)_2\text{I}_2]^+ / [\text{Al}(\text{L}_{\text{Ar}}^0)(\text{L}_{\text{Ar}}^-)\text{I}_2]$	$[\text{Al}(\text{L}_{\text{Ar}}^0)(\text{L}_{\text{Ar}}^-)\text{I}_2] / [\text{Al}(\text{L}_{\text{Ar}}^-)_2\text{I}_2]^-$	$[\text{Al}(\text{L}_{\text{Ar}}^-)_2\text{I}_2]^- / [\text{Al}(\text{L}_{\text{Ar}}^-)(\text{L}_{\text{Ar}}^{2-})\text{I}_2]^{2-}$
<b>1</b>	-0.78	-0.78	-1.28
<b>2</b>	-0.76	-0.92	-1.38
<b>3</b>	-0.78	-0.91	-1.40
<b>5</b>	-0.84	-0.84	-1.39
<b>6</b>	-0.80	-0.80	-1.40

### 2.1.5 Epoxidation aided by $[\text{Al}(\text{L}_{\text{Ar}})_2\text{I}_2]\cdot\text{I}$ and $[\text{Al}(\text{L}_{\text{Ar}})_2(\text{NCMe})_2]\cdot 3\text{I}$ catalysts

The efficacy of **1** and **4** towards the epoxidation of cyclohexene was investigated in collaboration with the Goldsmith Group at Auburn University. Koellner et. al. previously demonstrated the ability of the  $[\text{Al}(\text{L}_{\text{Ph}})_2\text{Cl}_2][\text{AlCl}_4]$

complex to catalyze the epoxidation of various alkenes using peracetic acid in high selectivity under relatively mild conditions.<sup>19</sup> We were therefore interested in the impact of the different coordination environments of **1** and **4** on this catalytic process. Data for the epoxidation of cyclohexene by commercially available peracetic acid (PA) catalyzed by **1**, **4**, and  $[\text{Al}(\text{L}^{\text{Ph}})_2\text{Cl}_2][\text{AlCl}_4]$  are presented in Table 6.

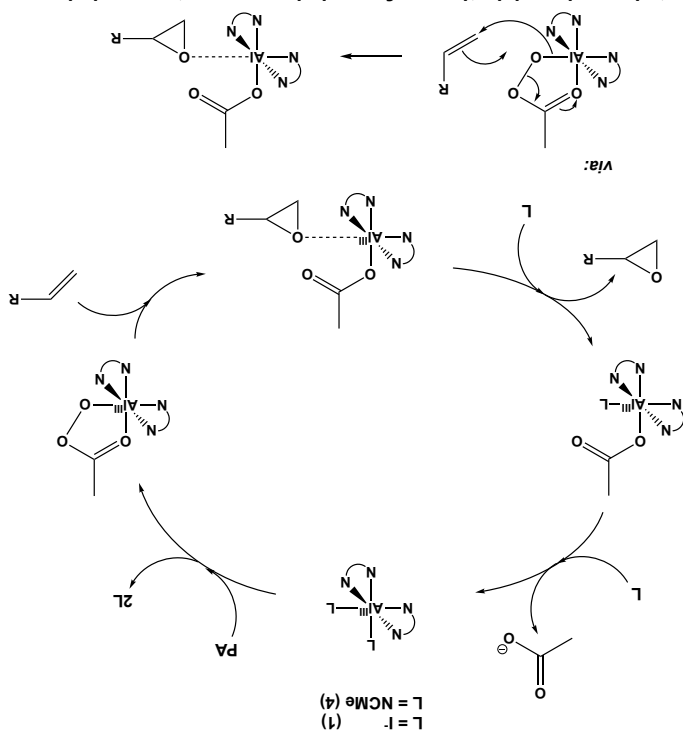
**Table 6.** Al(III)-catalyzed oxidation of cyclohexene to cyclohexene oxide by PA. Reactions were run in acetonitrile at 295 K under  $\text{N}_2$ . Initial concentrations of reagents:  $[\text{catalyst}] = 5.0 \text{ mM}$ ,  $[\text{cyclohexene}] = 500 \text{ mM}$ ,  $[\text{PA}] = 1.0 \text{ M}$ .

	Yield (%) <sup>a,b</sup>	Turn-Over-Number (TON) <sup>b,c</sup>
<b>1</b>	50 ± 16	50 ± 16
<b>4</b>	33 ± 13	50 ± 12
$[\text{Al}(\text{L}^{\text{Ph}})_2\text{Cl}_2][\text{AlCl}_4]$	38 ± 7	37 ± 7

<sup>a</sup> All yields were measured by GC at 60 min.

<sup>b</sup> All reported values and errors are averages of results from three independent measurements. Errors represent one standard deviation.

<sup>c</sup> TON defined as the number of equiv. of cyclohexene oxide produced per equiv. of catalyst.



In all cases, cyclohexene is converted exclusively to cyclohexene oxide—no allylic oxidation or epoxide ring-opening is observed. Koellner et. al. previously reported 68 turnovers for the  $[\text{Al}(\text{L}_{\text{Ph}})_2\text{Cl}_2][\text{AlCl}_4]$  complex, which is substantially higher than the  $37 \pm 7$  found here.<sup>19</sup> This discrepancy is attributable to the purity of PA used in the respective experiments. Previously, PA was prepared following a technique that eliminates a sulfuric acid impurity found in commercial PA sources. In the current experiment, unmodified commercial PA was used—suggesting that sulfuric acid impurities reduce the epoxidation activity of our Al complexes. This observation is corroborated by Jiang et. al., who previously found treated PA promoted more epoxidation than commercially available PA for a Ga(III) catalyst.<sup>62</sup>

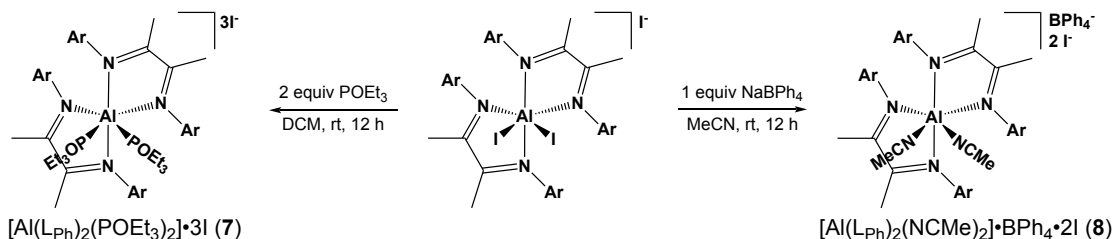
We observe a statistically significant enhancement in TON for **1** and **4** relative to  $[\text{Al}(\text{L}_{\text{Ar}})_2\text{Cl}_2][\text{AlCl}_4]$ . The activities of **1** and **4** are nearly identical, consistent with rapid displacement of their inner-sphere ligands. The lesser activity of the dichloro complex is likely a result of the increased strength of the Al–Cl bond relative to the Al–I or Al–NCMe bonds, which inhibits the coordination of PA necessary for epoxidation (Scheme 1).

### **2.1.6 Further derivatization of the neutral-ligand series**

Further derivatization of the  $[\text{Al}(\text{L}_{\text{Ph}})_2\text{I}_2]\cdot\text{I}$  complex was also investigated. Via an analogous inner-sphere displacement to the synthesis of **4**–**6**, a  $[\text{Al}(\text{L}_{\text{Ph}})_2(\text{POEt}_3)_2]\cdot 3\text{I}$  complex was synthesized. This compound was characterized by <sup>1</sup>H and <sup>31</sup>P NMR spectroscopy (Figure S13 and Figure S14). It



was additionally observed that introduction of NaBPh<sub>4</sub> into the reaction matrix during the second step of Scheme 7 resulted in the displacement of an outer-sphere iodide counterion. (Scheme 8). This exchange proceeds via salt metathesis, evidenced by the precipitation of NaI as the reaction progresses. This product was characterized by XRD (Figure 12).



**Scheme 8.** Further derivatization pathways of the  $[Al(L_{Ar})_2I_2] \cdot I$  series.

The potential influence of the triethylphosphine oxide ligands is straightforward: as in complexes **4–6**, the inner-sphere flexibility of complex **7** may lend itself to favorable reactivity. Displacement of the iodide counterions by tetraphenylborate in complexes **1–6** would remove the non-redox-innocent iodo ligand from the complex. Two events corresponding to the oxidation of iodide are observed at more positive potentials in the CVs of complexes **1–3**.

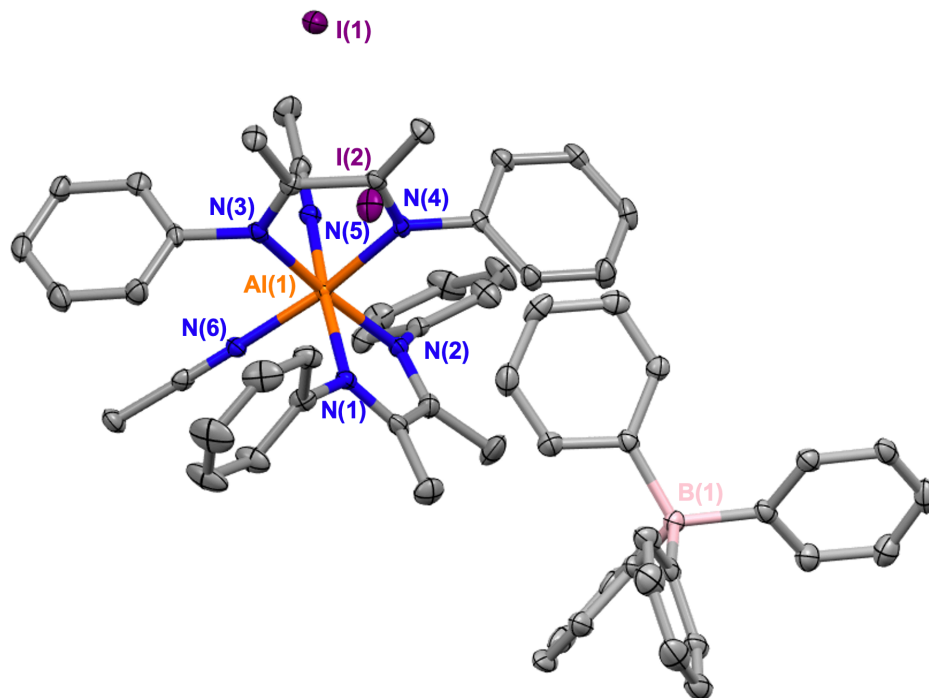


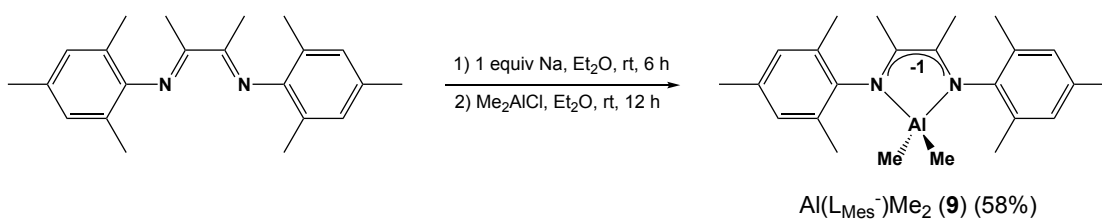
**Figure 12.** Solid-state structure of complex **8**. Ellipsoids are projected at 30% probability. Hydrogen atoms are omitted for clarity.

## 2.2 Reduced-ligand $\alpha$ -diimine complexes of Al

### **2.2.1 Synthesis and XRD, EPR, & CV characterization of $Al(L_{Mes}^-)Me_2$**

Organoaluminum complexes exhibit broad, useful reactivity (Section 1.3.3 provides applications within the context of this thesis). However, the same properties of the Al–C bond that impart this desirable chemistry (specifically, the high nucleophilicity of the C atom), plague the reaction between alkylaluminum species and fully oxidized  $L_{Ar}$  with side-alkylation. The reduced-ligand framework provides an opportunity to incorporate organoaluminum fragments in our  $\alpha$ -diimine complexes, since increasing electron density on the ligand will reduce unwanted byproducts.

Previously, Graves group alum Bren Cole synthesized a singly reduced  $\text{Al}(\text{L}_{\text{Mes}}^-)\text{Cl}_2$  complex.<sup>63</sup> We took this complex as the framework for our organoaluminum goals, synthesizing the analogous singly reduced  $\text{Al}(\text{L}_{\text{Mes}}^-)\text{Me}_2$  (**9**). Complex **9** is prepared via single-electron reduction of  $\text{L}_{\text{Mes}}$  (*N,N'*-bis(mesityl)-2,3-dimethyl-1,4-diazabutadiene) with sodium metal followed by complexation with  $\text{Me}_2\text{AlCl}$  in diethyl ether. Upon vacuum filtration over celite and removal of solvents, **9** is isolated in 58% yield as a light-orange powder (Scheme 9).



**Scheme 9.** Synthesis of complex **9**.

The  $^1\text{H}$  NMR of a concentrated sample of complex **9** is almost completely silent, suggesting the presence of a paramagnetic species (Figure S15). We therefore rely upon XRD, EPR, and CV as our characterization methods.

*Solid-state structure.* Single crystals of **9** were grown from a saturated hexane solution at  $-25\text{ }^\circ\text{C}$ . Selected bonding parameters for complex **9** are reported in Table 7, and its representation is given in Figure 13.

**Table 7.** Selected bond distances ( $\text{\AA}$ ) and angles ( $^\circ$ ) for **9**.

	<b>9</b>	<b>9</b> <sub>theory</sub> <sup>a</sup>
Al–N <sub>imine</sub>	1.9088(15)	1.9088
	1.9364(15)	1.9365
Al–Me	2.0035(14)	2.0035
	2.0036(14)	
C–C <sub>backbone</sub>	1.438(2)	1.4383
C–N <sub>imine</sub>	1.360(2)	1.3594
	1.335(2)	1.3355

N <sub>imine</sub> –Al–N <sub>imine</sub>	84.43(6)	84.42
N <sub>imine</sub> –Al–Me	114.60(5)	114.61
	113.12(4)	
	114.60(5)	113.12
	113.12(4)	
Me–Al–Me	113.76(9)	113.76

<sup>a</sup> Values were calculated in Gaussian 16 at the B3LYP/LANL2DZ level of theory.

The geometry of **9** resembles Cole et. al.'s Al(L<sub>Mes</sub><sup>-</sup>)Cl<sub>2</sub> complex almost exactly, particularly along the  $\alpha$ -diimine backbone. Bond distance agreements for C–C<sub>backbone</sub> (1.438(2) Å for **9** and 1.438(2) Å for Al(L<sub>Mes</sub><sup>-</sup>)Cl<sub>2</sub>) and C–N<sub>imine</sub> (1.348(1) Å for **9** and 1.352(1) Å for Al(L<sub>Mes</sub><sup>-</sup>)Cl<sub>2</sub>) are particularly outstanding. Ligand bonding parameters are also in good agreement with other singly reduced  $\alpha$ -diimine complexes of Al in the literature, corroborating that **9** is in fact singly reduced.<sup>27,59,64–67</sup> The average Al–Me bond distance observed for complex **9** (2.0036(10) Å) is consistent with literature values for N-donor alkylaluminum complexes.<sup>27,68–71</sup>

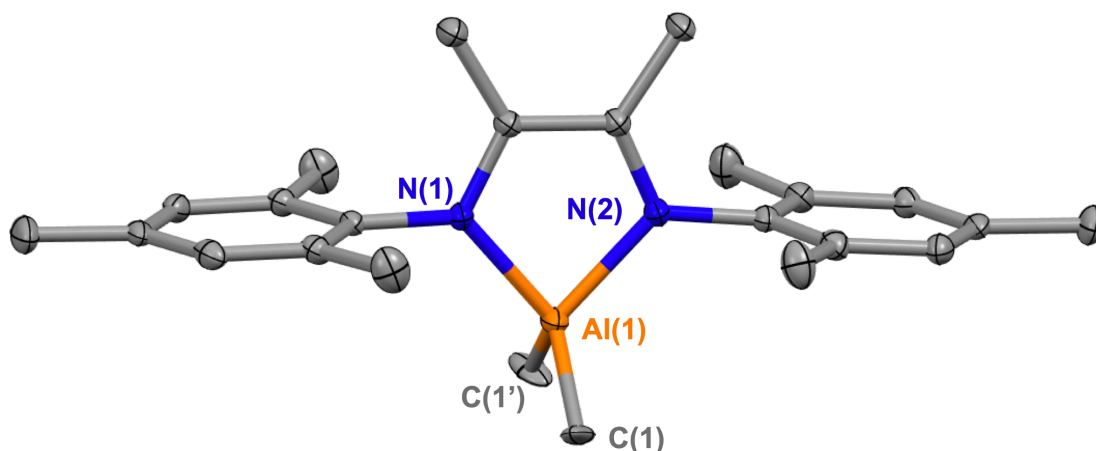


**Figure 13.** Solid-state structure of complex **9**. Ellipsoids are projected at 30% probability. Hydrogen atoms are omitted for clarity.  $\tau_4 = 0.93$ .

The structure of complex **9** differs from complexes **1–6** in predictable ways. Along the N–C–C–N backbone, the C–N<sub>imine</sub> distance is 0.061(5) Å longer for **9** than **1–6**, and the C–C<sub>backbone</sub> distance is 0.065(5) Å shorter. Interestingly, the Al–N<sub>imine</sub> bond is 0.1044(12) Å shorter for **9** than **1–6**, which we attribute to a stronger interaction between the Al center and the increasingly electron-rich N atom.

*EPR Spectroscopy.* Room temperature X-band continuous wave EPR spectroscopy was used to probe the location of the unpaired electron on complex **9**. The EPR spectrum appears noisy, but this is a result of the hyperfine coupling to several of the compound's nuclei (Figure 14). In fact, the EPR spectrum of complex **9** resembles other literature examples of singly reduced  $\alpha$ -diimine complexes of Al.<sup>64,65</sup>

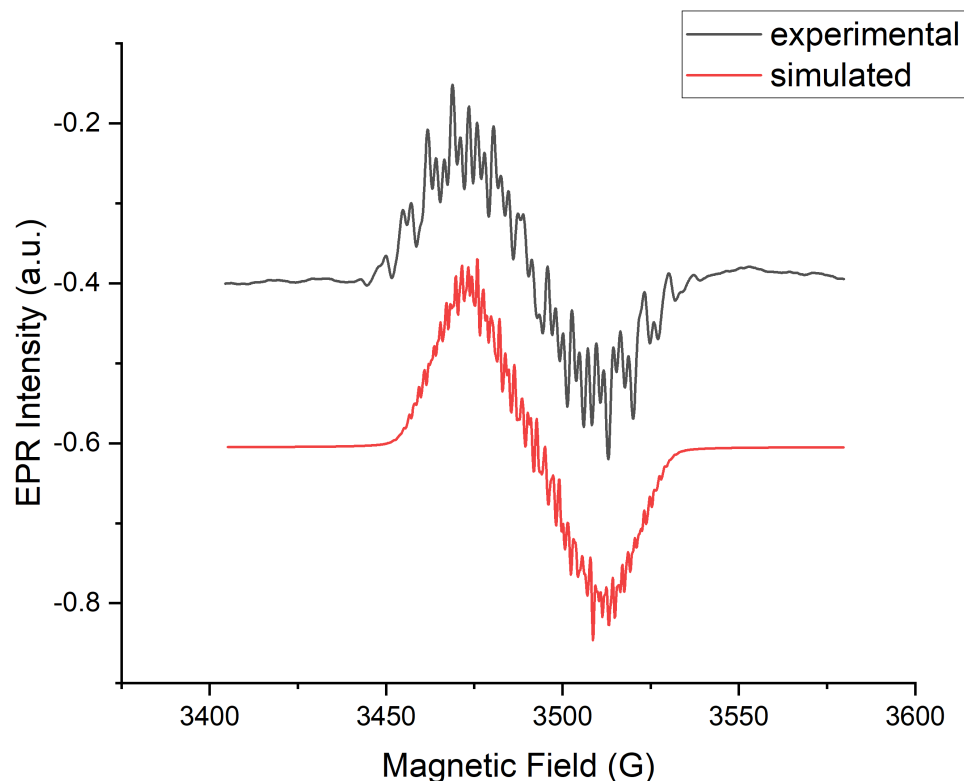


**Figure 14.** X-band EPR spectrum of **9** recorded in 50:50 toluene:dichloromethane at 298 K. The simulated spectrum is vertically offset for clarity. The root-mean-square deviation for the simulation is 1.83.

A simulated EPR spectrum of **9** was computed using EasySpin<sup>72</sup>, a MATLAB-based software. The radical was assumed to be in isotropic fast-motion, in accordance with the symmetry about the center of the resonance. Radical density was assumed to be delocalized over several nuclei. Initial parameters were either calculated from experimental data (in the case of the isotropic  $g$ -tensor,  $g_{\text{iso}}$ ) or extrapolated from literature values<sup>27,64,65</sup> (in the case of the  $A$ -tensor). A Nelder/Mead simplex method was used to target the integral of the experimental spectrum. Optimized parameters are given in Table 8.

**Table 8.** Isotropic  $g$  and hyperfine coupling constants (mT) for EasySpin EPR fitting of **9**

$g_{\text{iso}}$	<sup>27</sup> Al	<sup>14</sup> N <sup>a</sup>	<sup>1</sup> H <sup>b</sup>	<sup>1</sup> H <sup>c</sup>
2.0061	0.66	0.63	0.27	0.17

<sup>a</sup> <sup>14</sup>N refers to two equivalent nitrogen nuclei

<sup>b</sup> <sup>1</sup>H refers to the six equivalent protons of the methyl groups bound to the Al center

<sup>c</sup> <sup>1</sup>H refers to the six equivalent protons of the methyl groups of the N–C–N backbone

These parameters agree reasonably well with the SOMO density of complex **9** as calculated by DFT (Figure 15). Orbital density is primarily located on the N–C–N backbone, with nearly zero contribution from the Al center. This observation agrees exactly with the SOMO of Scott et. al.'s singly reduced (<sup>dpp</sup>I<sub>2</sub>P<sup>-</sup>)AlMe<sub>2</sub> complex.<sup>65</sup>

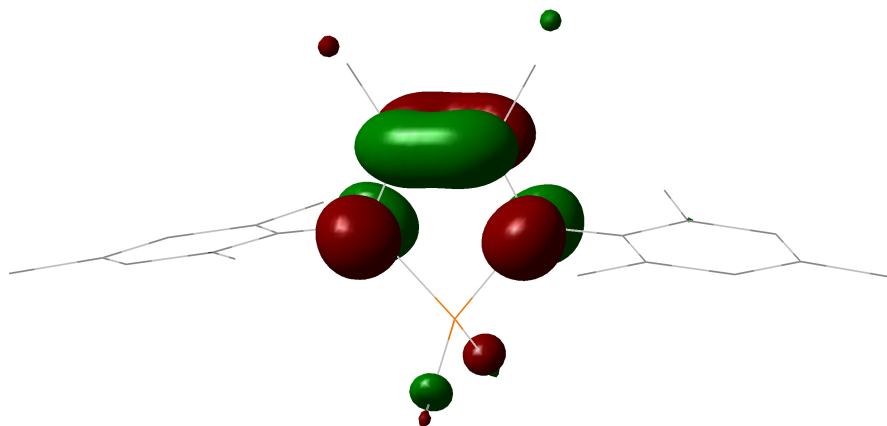


**Figure 15.** SOMO of complex **9**.

*Electrochemistry.* The cyclic voltammogram of complex **9** is presented in Figure 16. We observe a highly reversible redox event ( $E_{1/2} = -1.88$  V vs. Fc/Fc<sup>+</sup>), presumably corresponding to the  $\text{Al}(\text{L}_{\text{Mes}}^-)\text{Me}_2/[\text{Al}(\text{L}_{\text{Mes}}^{2-})\text{Me}_2]^-$  redox couple. There is also a significantly less reversible redox event at a more positive potential ( $E_{1/2} = -0.97$  V vs. Fc/Fc<sup>+</sup>) corresponding to the  $[\text{Al}(\text{L}_{\text{Mes}}^0)\text{Me}_2]^+/\text{Al}(\text{L}_{\text{Mes}}^-)\text{Me}_2$  couple.

The two redox couples observed in the voltammogram of **9** are shifted to more negative potentials than those recorded by Cole et. al. for the  $\text{Al}(\text{L}_{\text{Mes}}^-)\text{Cl}_2$  complex ( $-1.34$  V vs. Fc/Fc<sup>+</sup> for  $\text{Al}(\text{L}_{\text{Mes}}^-)\text{Me}_2/[\text{Al}(\text{L}_{\text{Mes}}^{2-})\text{Me}_2]^-$  and  $-0.73$  V vs. Fc/Fc<sup>+</sup> for  $[\text{Al}(\text{L}_{\text{Mes}}^0)\text{Cl}_2]^+/\text{Al}(\text{L}_{\text{Mes}}^-)\text{Cl}_2$ ).<sup>63</sup> This difference is particularly pronounced for the  $\text{Al}(\text{L}_{\text{Mes}}^-)\text{R}_2/[\text{Al}(\text{L}_{\text{Mes}}^{2-})\text{R}_2]^-$  couple, which is nearly 0.5 V more negative for complex **9** than  $\text{Al}(\text{L}_{\text{Mes}}^-)\text{Cl}_2$ . That difference is larger than what Cole et. al. found between  $\text{Al}(\text{L}_{\text{Mes}}^-)\text{Cl}_2$  and  $\text{Al}(\text{L}_{\text{Mes}}^{2-})\text{Cl}(\text{THF})$ —complexes that start at different oxidation states.<sup>63</sup>

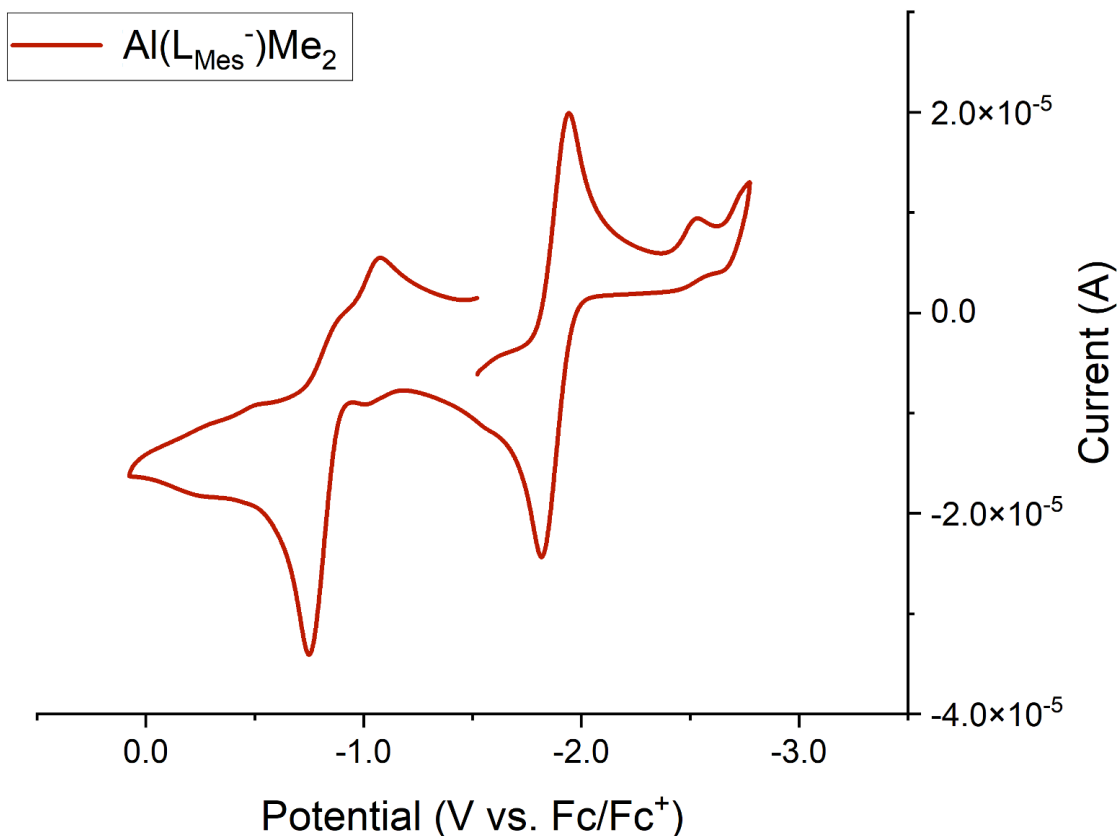
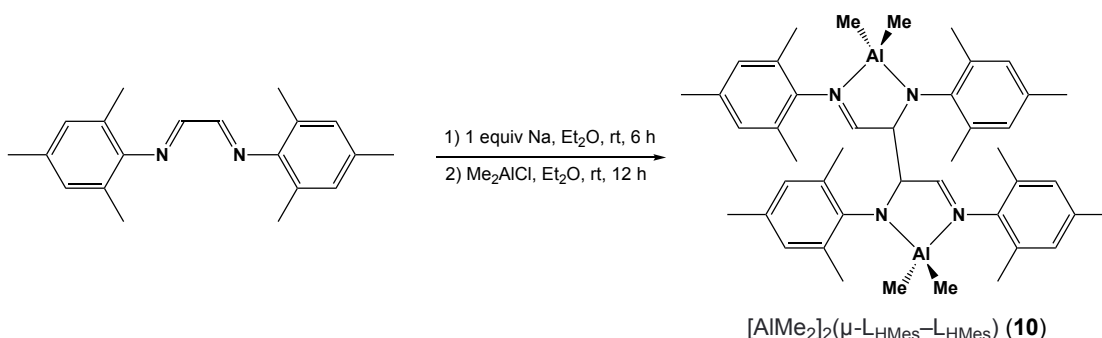


**Figure 16.** Cyclic voltammogram of complex **9** recorded in 0.1 M [*n*-Pr<sub>4</sub>N][BAR<sup>F</sup>] THF solution at 100 mV s<sup>-1</sup>.

### 2.2.2 Synthesis and XRD & DFT characterization of [AlMe<sub>2</sub>]<sub>2</sub>(μ-L<sub>HMes</sub>-L<sub>HMes</sub>)

Interested in tweaking the properties of the α-diimine in complex **9**, we pursued an analogous reaction to Scheme 9 for L<sub>HMes</sub> (*N,N'*-bis(mesityl)-1,4-diazabutadiene). In a preliminary reaction, we observed backbone-based radicals coupling to give the [AlMe<sub>2</sub>]<sub>2</sub>(μ-L<sub>HMes</sub>-L<sub>HMes</sub>) complex **10** (Scheme 10). Following vacuum filtration over celite, solvents were removed from the reaction matrix to give **10** as a “gunky” brown solid that did not respond well to trituration. This solid was concentrated in hexane, and from this solution single crystals of **10** were grown at 25 °C.





**Scheme 10.** Synthesis of complex **10**.

The backbone-coupling behavior shown in Scheme 10 has precedent: Myers et. al.<sup>17</sup> observed the same radical coupling following single reduction of an [(IP<sup>-</sup>)<sub>2</sub>AlCl] complex (yielding [(IP<sup>2-</sup>)<sub>2</sub>Al]<sub>2</sub>(μ-IP-IP<sup>2-</sup>)), and Hinchliffe et. al.<sup>73</sup> observed an analogous coupling to give a complex of the form [AlCl<sub>2</sub>]<sub>2</sub>(μ-dppDAB-dppDAB).

*Solid-state structure.* Table 9 contains selected structural data for complex **10**, and Figure 17 gives its XRD-derived representation.

**Table 9.** Selected bond distances (Å) and angles (°) for **10**.

	<b>10</b>	<b>10</b> <sub>theory</sub> <sup>a</sup>
Al-N <sub>imine</sub>	2.0025(12) 1.8620(12)	2.0484 1.9113
Al-Me	1.9644(16) 1.9915(15)	1.9933 1.9974
C-C <sub>backbone</sub>	1.5044(19)	1.5079
C-C <sub>bridge</sub>	1.590(3)	1.6390
C-N <sub>imine</sub>	1.4475(17)	1.4596
C-N <sub>amine</sub>	1.2780(18)	1.3026
N <sub>imine</sub> -Al-N <sub>amine</sub>	84.11(5)	83.12
N <sub>ligand</sub> -Al-Me	114.93(6) 105.66(6)	112.72 108.06

	113.05(6)	114.94
	119.42(6)	118.91
Me–Al–Me	115.33(7)	114.52

<sup>a</sup> Values were calculated in Gaussian 16 at the B3LYP/LANL2DZ level of theory.

There is a rather large difference in the two Al–N<sub>ligand</sub> bond distances for complex **10**, consistent with the more electron-rich amine of the now-asymmetrical ligand interacting more strongly with the Lewis acidic Al center. Analogous differences in Al–N<sub>ligand</sub> bond distances are present in the Myers. et. al. and Hinchliffe et. al. complexes resembling **10**.<sup>17,73</sup> The C–C<sub>bridge</sub> bond distance in complex **10** (1.590(3) Å) agrees excellently with the value found by Hinchliffe et. al.<sup>73</sup> for the analogous [AlCl<sub>2</sub>]<sub>2</sub>(μ-dppDAB–dppDAB) complex (1.585(9) Å). The average Al–Me bond distance observed for complex **10** (1.9780(11) Å) is consistent with literature values for N-donor alkylaluminum complexes.<sup>27,68–71</sup>

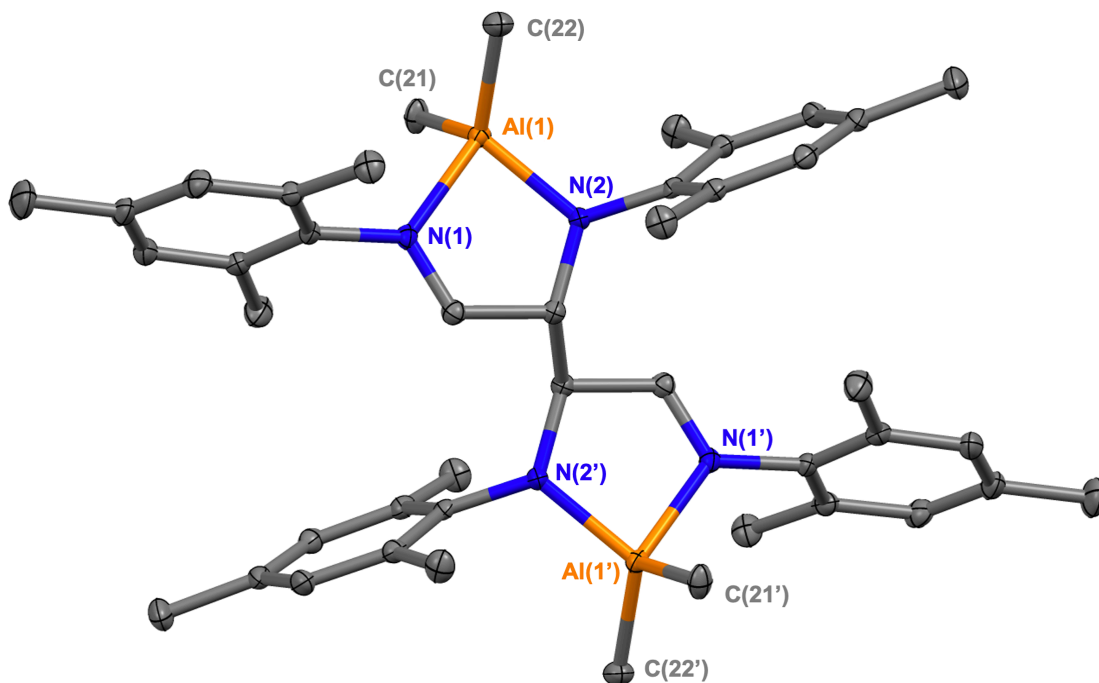


**Figure 17.** Solid-state structures of complex **10**. Ellipsoids are projected at 30% probability. Hydrogen atoms are omitted for clarity.  $\tau_4 = 0.89$ .

*DFT Studies.* Figure 18 shows the frontier orbitals for complex **10**. Intuitively, the LUMO and LUMO+1 of complex **10** have orbital density along the portion of the N–C–C–N backbone that is fully oxidized (i.e., further reduction will place electrons in the fully oxidized portion of the backbone). Likewise, the HOMO and HOMO-1 for **10** are predominantly located on the fully reduced portion of the  $\alpha$ -diimine backbone. The HOMO has significant orbital density along the C–C<sub>bridge</sub> bond that is absent in the HOMO-1, suggesting that single-electron oxidation will assist in the breakage of the C–C<sub>bridge</sub> bond (Figure 18).

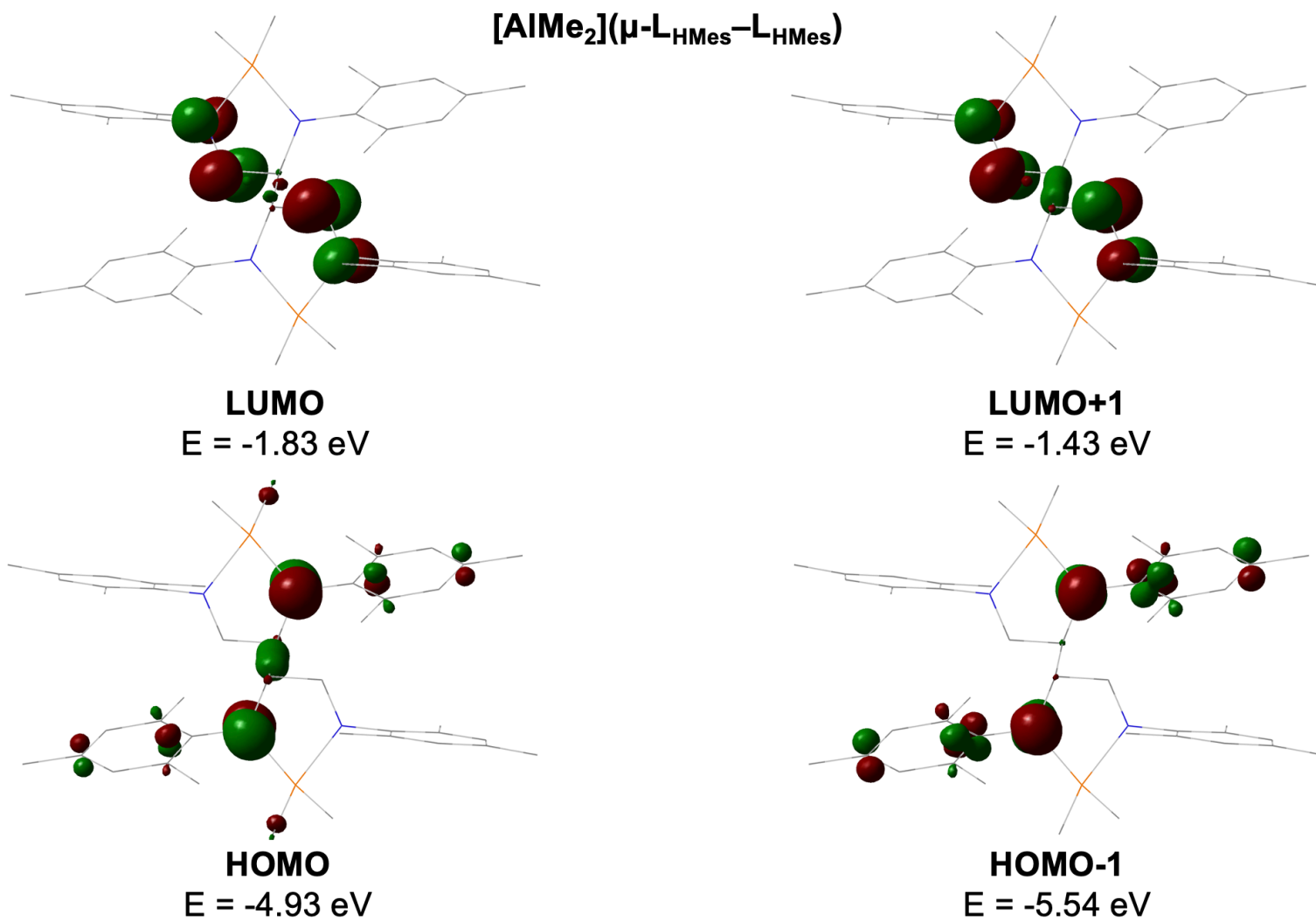
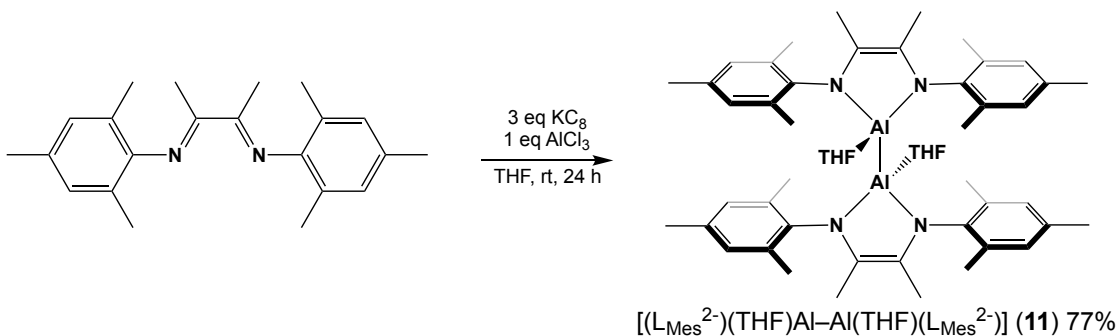


Figure 18. Frontier orbitals for complex 10.

### 2.2.3 Synthesis and XRD, DFT, & CV characterization of $[(L_{Mes}^{2-})(THF)Al-Al(THF)(L_{Mes}^{2-})]$

A different area of reduced-ligand chemistry that we are interested in exploring is the synthesis of Al–Al bonded complexes bearing  $\alpha$ -diimines. Such complexes are relatively uncommon in the literature but are shown to possess interesting reactivity and promising catalytic potential (Section 1.3.4). We are happy to report that we have successfully synthesized a novel complex containing an Al–Al bond.

The  $[(L_{Mes}^{2-})(THF)Al-Al(THF)(L_{Mes}^{2-})]$  complex **11** is synthesized in a one-pot reduction of  $L_{Mes}$  in the presence of  $AlCl_3$  (Scheme 11). Following addition of  $KC_8$  to a stirring matrix of  $AlCl_3$  and  $L_{Mes}$ , there is a rapid color change from yellow to green. Upon filtration over Celite, the reaction mixture again appears yellow. Removal of volatiles gives **11** as a light-yellow powder. This protocol compares favorably to the Zhao et. al. protocol to prepare the similar  $[(L_{dpp}^{2-})(THF)Al-Al(THF)(L_{dpp}^{2-})]$  complex, which requires a week of stirring and many excess equivalents of sodium metal.<sup>74</sup>  $^1H$  NMR of **11** suggests a low-symmetry complex (Figure S16).



**Scheme 11.** Synthesis of complex **11**.

*Solid-state structure.* Single crystals of **11** were grown from slow evaporation from a concentrated THF solution into toluene. Selected bonding parameters are given in Table 10, and an XRD-derived representation of **11** is given in Figure 19.

**Table 10.** Selected bond distances (Å) and angles (°) for **11**.

	<b>11</b>	<b>11</b> <sub>theory</sub> <sup>a</sup>
Al–N <sub>imine</sub>	1.8464(13)	1.8887
	1.8474(13)	1.8827
		1.8900
		1.8800
Al–O <sub>THF</sub>	1.9341(11)	2.0109
		2.0119
Al–Al	2.5998(9)	2.6227
C–C <sub>backbone</sub>	1.354(2)	1.3766
C–N <sub>imine</sub>		1.4477
	1.4275(18)	1.4474
	1.4328(18)	1.4461
		1.4491
N <sub>imine</sub> –Al–N <sub>imine</sub>	89.57(6)	88.88
		88.91
N <sub>imine</sub> –Al–O <sub>THF</sub>		100.84
	101.38(5)	100.95
	101.31(5)	101.84
		100.52
Al–Al–O <sub>THF</sub>	106.23(4)	104.92
		104.35

<sup>a</sup> Values were calculated in Gaussian 16 at the B3LYP/LANL2DZ level of theory.

The Al–O<sub>THF</sub> bond distance in complex **11** (1.9341(11) Å) agrees fairly well with literature bond distances for Al–THF adducts.<sup>75–81</sup> Similarly, the Al–Al bond distance in complex **11** (2.5998(9) Å) is comfortably within the range of comparable literature dialanes (2.52 Å – 2.68 Å).<sup>37,50,74,81–86</sup>

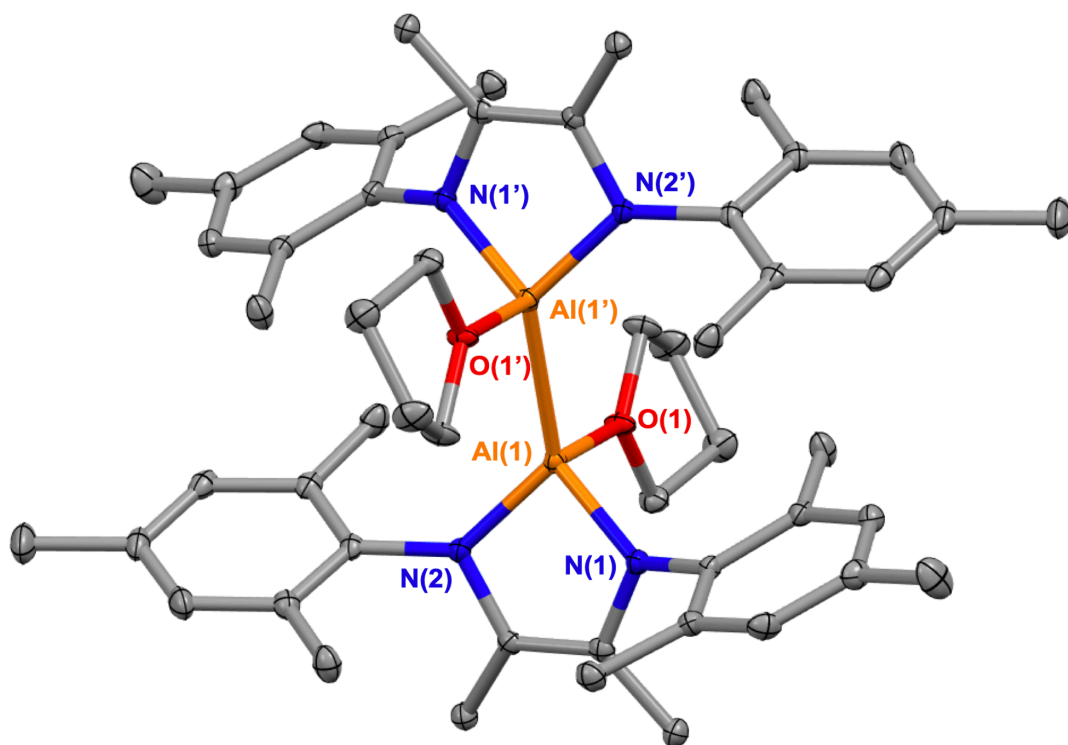


**Figure 19.** Solid-state structures of complex **11**. Ellipsoids are projected at 30% probability. Hydrogen atoms are omitted for clarity.  $\tau_4 = 1.08$ .

$C-C_{\text{backbone}}$  and  $C-N_{\text{imine}}$  bond distances for complex **11** (1.354(2) Å and 1.4302(13) Å, respectively) are consistent with other doubly reduced  $\alpha$ -diimine complexes of Al in the literature.<sup>28,33,36,42,87,88</sup> Taking a step back, we notice consistent, intuitive changes in the bonding parameters along the  $-Al-N-C-C-N-$  metallacycle for our complexes of varying oxidation state. Table 11 summarizes these ligand oxidation state-dependent bonding parameters.

**Table 11.** Selected average bond distances (Å) for complexes of differing ligand oxidation state.

Complexes	Ligand ox. state	Al–N <sub>imine</sub>	C–C <sub>backbone</sub>	C–N <sub>imine</sub>
<b>1–6</b>	0	2.027(1)	1.503(3)	1.287(4)
<b>9</b>	-1	1.9226(11)	1.438(2)	1.348(1)
<b>11</b>	-2	1.8469(9)	1.354(2)	1.4302(13)

As  $L_{Ar}$  becomes doubly reduced,  $C-C_{backbone}$  shortens from 1.503(3) Å to 1.354(2) Å—exactly consistent with an increase in bond order from 1 to 2. For the same change in ligand oxidation state,  $C-N_{imine}$  increases from 1.287(4) Å to 1.4302(13) Å, suggesting a decrease in bond order from 2 to 1.<sup>61</sup> These structural changes were expected (Figure 2), but the dependence of  $Al-N_{imine}$  is slightly more subtle. As the  $\alpha$ -diimine is reduced, electron density increases on the N atoms of the ligand. We therefore expect stronger interactions between the electron-rich N atoms and the Lewis acidic Al—leading to shorter  $Al-N_{imine}$  bonds—consistent with the trend seen in Table 11.

*DFT Studies.* The calculated frontier orbitals and Al–Al bonding MOs for complex **11** are presented in Figure 20. As expected for the doubly reduced **11**, orbital densities of the HOMO and HOMO-1 are located on the  $\alpha$ -diimine backbone. Interestingly, orbital densities of the LUMO and LUMO+1 resemble a  $\pi^*$  orbital of the mesityl group. These orbitals are also significantly higher in energy than the HOMO and HOMO-1 ( $\Delta E_{avg} = 0.396$  eV). This observation is consistent with our intuition that complex **11** is likely to engage in reducing behavior.

The Al–Al bonding MOs for **11** are low-lying relative to the HOMO and HOMO-1 (8 electrons would need to be oxidized before electrons were removed from an MO contributing to the Al–Al bond). This observation has favorable implications for Al–Al cooperative reactivity, allowing for simultaneous contribution from both metals (Scheme 5).



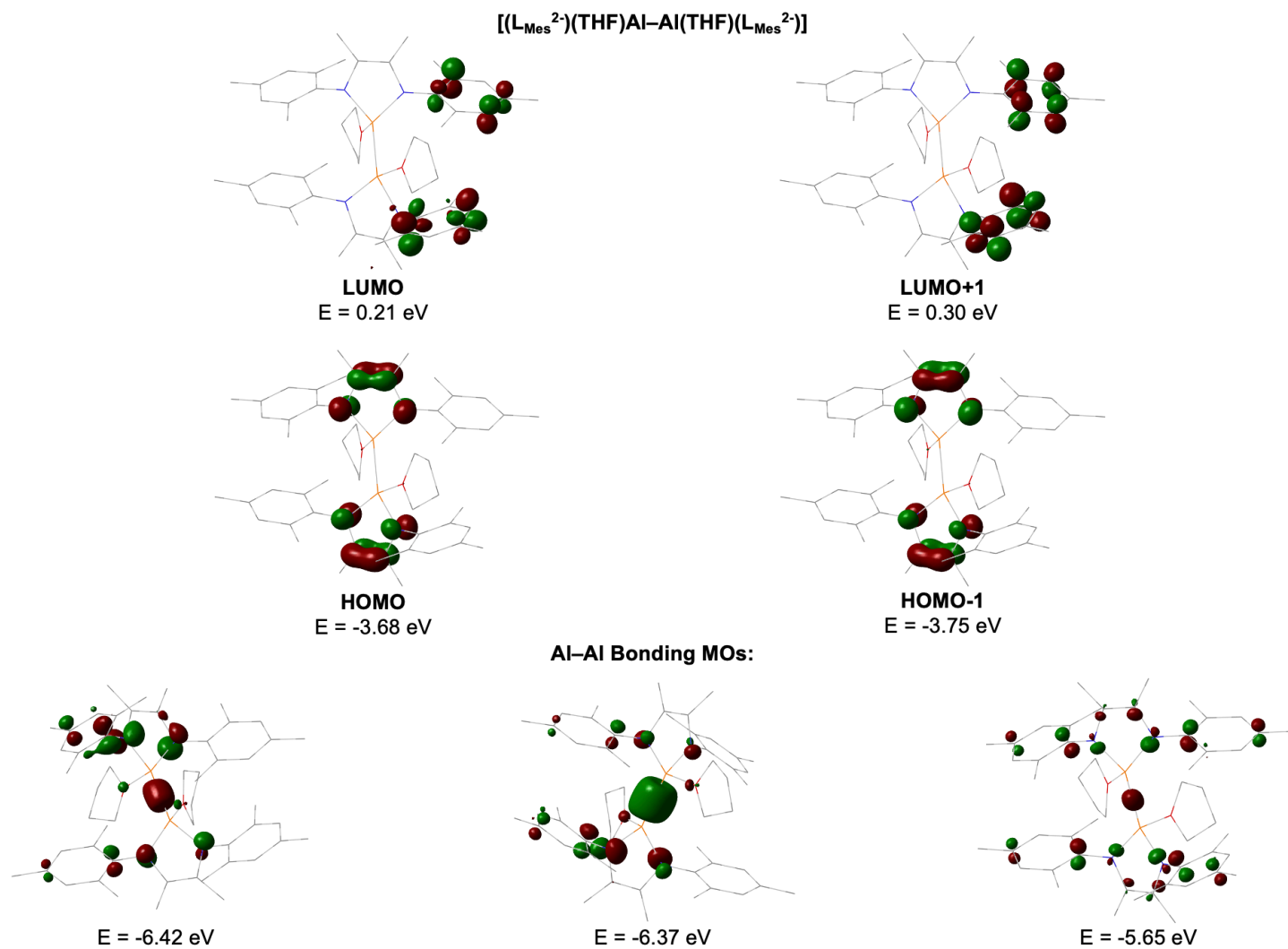


**Figure 20.** Notable molecular orbitals for complex **11**.

*Electrochemistry.* The cyclic voltammogram for complex **11** is given in Figure 21. Notably, no reduction events are observed during the initial cathodic sweep, corroborating the reducing behavior of **11**. The voltammogram has several features, but two reversible redox events are discernible at  $E_{1/2} = -1.05$  V vs. Fc/Fc<sup>+</sup> and  $E_{1/2} = -0.73$  V vs. Fc/Fc<sup>+</sup>. Our initial assessment is that these features correspond to the  $[(L_{Mes}^{2-})(THF)Al-Al(THF)(L_{Mes}^{2-})]/[(L_{Mes}^{-})(THF)Al-Al(THF)(L_{Mes}^{2-})]$  and  $[(L_{Mes}^{-})(THF)Al-Al(THF)(L_{Mes}^{2-})]/[(L_{Mes}^{-})(THF)Al-Al(THF)(L_{Mes}^{-})]$  redox couples, respectively. To our knowledge, this is the first cyclic voltammogram collected for an  $\alpha$ -diimine complex containing an Al–Al bond.

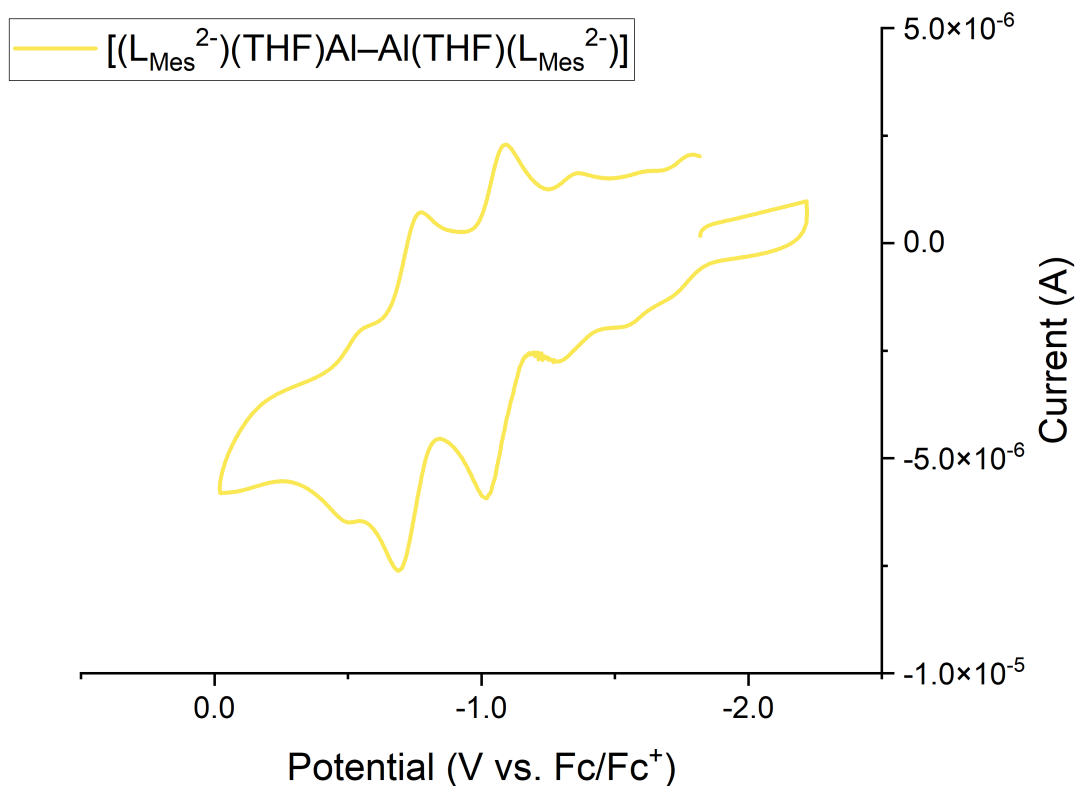


**Figure 21.** Cyclic voltammogram of complex **11** recorded in 0.1 M [*n*-Pr<sub>4</sub>N][BAR<sup>F</sup>] THF solution at 100 mV s<sup>-1</sup>.

### 3. Conclusions and Future Work

We have synthesized and characterized many  $\alpha$ -diimine complexes of aluminum. The two neutral-ligand series,  $[\text{Al}(\text{L}_{\text{Ar}})_2\text{I}_2]\cdot\text{I}$  (**1–3**) and  $[\text{Al}(\text{L}_{\text{Ar}})_2(\text{NCMe})_2]\cdot 3\text{I}$  (**4–6**), have been compared favorably to the previous  $[\text{Al}(\text{L}_{\text{Ar}})\text{Cl}_2][\text{AlCl}_4]$  series: they possess a more reversible electrochemical profile and catalyze epoxidation more extensively. We hope to continue exploring the derivatization of these complexes via inner-sphere iodo exchange, aryl substitution, and counterion displacement, but we will also want to explore the catalytic activity of these complexes further. Goldsmith speculates that a chiral  $\alpha$ -diimine complex may synthesize epoxides asymmetrically, a sensible and promising notion.<sup>23</sup> We will certainly pursue enantioselective epoxidation catalysis with a chiral analog of our  $\alpha$ -diimine complexes of Al.

We have also reported the synthesis and preliminary characterization of three reduced-ligand  $\alpha$ -diimine complexes of Al. Our work with these complexes remains limited due to the pandemic, though we are encouraged by DFT calculations and CV data. Once we complete our characterization of **9–11**, we will investigate their reaction profiles. We are specifically interested in the chemistry of complex **11** towards imides and other heteroatom substituents, motivated by Al=E adducts which have been shown to reduce  $\text{CO}_2$ .<sup>89</sup>

## 4. References

- (1) Godwin, H.; Hoffman, B.; Bowman-James, K. *The Frontiers of Inorganic Chemistry* 2002, 2001.
- (2) Parshall, G. W.; Iltel, S. D. *Homogeneous Catalysis*, 2nd ed.; Wiley–Interscience: New York, 1992.
- (3) *Catalytic Asymmetric Synthesis*, 2nd ed.; Ojima, I., Ed.; Wiley–VCH, 2000.
- (4) *Applied Homogeneous Catalysis with Organometallic Compounds*, 2nd ed.; Cornils, B., Herrmann, W., Eds.; Wiley, 2002.
- (5) Hartley, F. R. *Chemistry of the Platinum Group Metals: Recent Developments*; Elsevier, 2013.
- (6) Kettler, P. B. Platinum Group Metals in Catalysis: Fabrication of Catalysts and Catalyst Precursors. *Org. Process Res. Dev.* **2003**, 7 (3), 342–354. <https://doi.org/10.1021/op034017o>.
- (7) Wilburn, D. R.; Bleiwas, D. I. *Platinum–Group Metals—World Supply and Demand*; Open-File Report; Open-File Report 2004–1224; U.S. Geological Survey, 2004.
- (8) Kielhorn, J.; Melber, C.; Keller, D.; Mangelsdorf, I. Palladium – A Review of Exposure and Effects to Human Health. *International Journal of Hygiene and Environmental Health* **2002**, 205 (6), 417–432. <https://doi.org/10.1078/1438-4639-00180>.
- (9) Ravindra, K.; Bencs, L.; Van Grieken, R. Platinum Group Elements in the Environment and Their Health Risk. *Science of The Total Environment* **2004**, 318 (1–3), 1–43. [https://doi.org/10.1016/S0048-9697\(03\)00372-3](https://doi.org/10.1016/S0048-9697(03)00372-3).
- (10) Suchá, V.; Mihaljevič, M.; Ettl, V.; Strnad, L. The PH-Dependent Release of Platinum Group Elements (PGEs) from Gasoline and Diesel Fuel Catalysts: Implication for Weathering in Soils. *Journal of Environmental Management* **2016**, 171, 52–59. <https://doi.org/10.1016/j.jenvman.2016.01.034>.
- (11) Rabinovich, D. The Allure of Aluminium. *Nature Chem* **2013**, 5 (1), 76–76. <https://doi.org/10.1038/nchem.1535>.
- (12) Krewski, D.; Yokel, R. A.; Nieboer, E.; Borchelt, D.; Cohen, J.; Harry, J.; Kacew, S.; Lindsay, J.; Mahfouz, A. M.; Rondeau, V. HUMAN HEALTH RISK ASSESSMENT FOR ALUMINIUM, ALUMINIUM OXIDE, AND ALUMINIUM HYDROXIDE. *J Toxicol Environ Health B Crit Rev* **2007**, 10 (Suppl 1), 1–269. <https://doi.org/10.1080/10937400701597766>.
- (13) Sorenson, J. R. J.; Campbell, I. R.; Tepper, L. B.; Lingg, R. D. Aluminum in the Environment and Human Health. *Environ Health Perspect* **1974**, 8, 3–95.
- (14) Mineral Commodity Summaries 2021. **2021**, 204.
- (15) Ooi, T.; Maruoka, K. Achiral Al(III) Lewis Acids. In *Lewis Acids in Organic Synthesis*; Yamamoto, H., Ed.; Wiley-VCH Verlag GmbH: Weinheim, Germany, 2000; pp 191–281. <https://doi.org/10.1002/9783527618309.ch6>.
- (16) Taguchi, T.; Yamamoto, H. Al(III) Lewis Acids. *Acid Catalysis in Modern Organic Synthesis* **2008**, 1, 241–345.

- (17) Myers, T. W.; Kazem, N.; Stoll, S.; Britt, R. D.; Shanmugam, M.; Berben, L. A. A Redox Series of Aluminum Complexes: Characterization of Four Oxidation States Including a Ligand Biradical State Stabilized via Exchange Coupling. *J. Am. Chem. Soc.* **2011**, *133* (22), 8662–8672. <https://doi.org/10.1021/ja2015718>.
- (18) Wilson, H. H.; Koellner, C. A.; Hannan, Z. M.; Endy, C. B.; Bezpalko, M. W.; Piro, N. A.; Kassel, W. S.; Sonntag, M. D.; Graves, C. R. Synthesis and Characterization of Neutral Ligand  $\alpha$ -Diimine Complexes of Aluminum with Tunable Redox Energetics. *Inorg. Chem.* **2018**, *57* (16), 9622–9633. <https://doi.org/10.1021/acs.inorgchem.8b00045>.
- (19) Koellner, C. A.; Piro, N. A.; Kassel, W. S.; Goldsmith, C. R.; Graves, C. R. Synthesis and Characterization of  $\alpha$ -Diimine Complexes of Group 13 Metals and Their Catalytic Activity toward the Epoxidation of Alkenes. *Inorg. Chem.* **2015**, *54* (15), 7139–7141. <https://doi.org/10.1021/acs.inorgchem.5b01136>.
- (20) Rinaldi, R.; de Oliveira, H. F. N.; Schumann, H.; Schuchardt, U. Homogeneously Catalyzed Epoxidation of  $\alpha,\beta$ -Unsaturated Ketones Using Simple Aluminum Salts and Aqueous H<sub>2</sub>O<sub>2</sub>—Is It Possible? *Journal of Molecular Catalysis A: Chemical* **2009**, *307* (1), 1–8. <https://doi.org/10.1016/j.molcata.2009.04.005>.
- (21) Kuznetsov, M. L.; Kozlov, Y. N.; Mandelli, D.; Pombeiro, A. J. L.; Shul'pin, G. B. Mechanism of Al<sup>3+</sup>-Catalyzed Oxidations of Hydrocarbons: Dramatic Activation of H<sub>2</sub>O<sub>2</sub> toward O–O Homolysis in Complex [Al(H<sub>2</sub>O)<sub>4</sub>(OOH)(H<sub>2</sub>O<sub>2</sub>)]<sup>2+</sup> Explains the Formation of HO• Radicals. *Inorg. Chem.* **2011**, *50* (9), 3996–4005. <https://doi.org/10.1021/ic102476x>.
- (22) Pescarmona, P. P.; Janssen, K. P. F.; Jacobs, P. A. Novel Transition-Metal-Free Heterogeneous Epoxidation Catalysts Discovered by Means of High-Throughput Experimentation. *Chemistry – A European Journal* **2007**, *13* (23), 6562–6572. <https://doi.org/10.1002/chem.200700074>.
- (23) Goldsmith, C. R. Aluminum and Gallium Complexes as Homogeneous Catalysts for Reduction/Oxidation Reactions. *Coordination Chemistry Reviews* **2018**, *377*, 209–224. <https://doi.org/10.1016/j.ccr.2018.08.025>.
- (24) Berben, L. A. Catalysis by Aluminum(III) Complexes of Non-Innocent Ligands. *Chem. Eur. J.* **2015**, *21* (7), 2734–2742. <https://doi.org/10.1002/chem.201405400>.
- (25) Myers, T. W.; Berben, L. A. Aluminium–Ligand Cooperation Promotes Selective Dehydrogenation of Formic Acid to H<sub>2</sub> and CO<sub>2</sub>. *Chem. Sci.* **2014**, *5* (7), 2771–2777. <https://doi.org/10.1039/C4SC01035C>.
- (26) Sherbow, T. J.; Carr, C. R.; Saisu, T.; Fettingner, J. C.; Berben, L. A. Insight into Varied Reaction Pathways for O–H and N–H Bond Activation by Bis(Imino)Pyridine Complexes of Al(III). *Organometallics* **2016**, *35* (1), 9–14. <https://doi.org/10.1021/acs.organomet.5b00743>.
- (27) Schumann, H.; Hummert, M.; Lukoyanov, A. N.; Fedushkin, I. L. Monomeric Alkylaluminum Complexes (Dpp-BIAN)AlR<sub>2</sub> (R = Me, Et, <sup>*i*</sup>Bu) Supported by the Rigid Chelating Radical-Anionic 1,2-Bis[(2,6-Diisopropylphenyl)Imino]Acenaphthene Ligand (Dpp-BIAN).

- Organometallics* **2005**, *24* (16), 3891–3896.  
<https://doi.org/10.1021/om0491037>.
- (28) Sokolov, V. G.; Koptseva, T. S.; Dodonov, V. A.; Rummyantsev, R. V.; Fedushkin, I. L. Reactivity of an Aluminum Hydride Complex with a Redox-Active Diimine Ligand. *Russ Chem Bull* **2018**, *67* (12), 2164–2171.  
<https://doi.org/10.1007/s11172-018-2349-3>.
- (29) Fedushkin, I. L.; Moskalev, M. V.; Baranov, E. V.; Abakumov, G. A. Addition of Diphenylacetylene and Methylvinylketone to Aluminum Complex of Redox-Active Diimine Ligand. *Journal of Organometallic Chemistry* **2013**, *747*, 235–240.  
<https://doi.org/10.1016/j.jorganchem.2013.06.032>.
- (30) Lukoyanov, A. N.; Fedushkin, I. L.; Hummert, M.; Schumann, H. Aluminum Complexes with Mono- and Dianionic Diimine Ligands. *Russ Chem Bull* **2006**, *55* (3), 422–428. <https://doi.org/10.1007/s11172-006-0273-4>.
- (31) Sokolov, V. G.; Koptseva, T. S.; Moskalev, M. V.; Piskunov, A. V.; Samsonov, M. A.; Fedushkin, I. L. Aluminum Hydrides with Radical-Anionic and Dianionic Acenaphthene-1,2-Diimine Ligands. *Russ Chem Bull* **2017**, *66* (9), 1569–1579. <https://doi.org/10.1007/s11172-017-1926-1>.
- (32) Kazarina, O. V.; Moskalev, M. V.; Fedushkin, I. L. Complexes of Group 13 Metals with Redox-Active Ligands as Catalysts for the Hydroamination of Carbodiimides. *Russ Chem Bull* **2015**, *64* (1), 32–37.  
<https://doi.org/10.1007/s11172-015-0816-7>.
- (33) Fedushkin, I. L.; Moskalev, M. V.; Skatova, A. A.; Fukin, G. K.; Abakumov, G. A. Formation of Carbon-Carbon Bonds between Activated Alkynes and Diimine Ligands in the Aluminum Complexes. *Russ Chem Bull* **2013**, *62* (3), 731–744. <https://doi.org/10.1007/s11172-013-0100-7>.
- (34) Fedushkin, I. L.; Lukoyanov, A. N.; Fukin, G. K.; Hummert, M.; Schumann, H. Reduction of Aromatic Ketones with the (Dpp-BIAN)Al(Et<sub>2</sub>O) Complex. *Russ Chem Bull* **2006**, *55* (7), 1177–1183. <https://doi.org/10.1007/s11172-006-0396-7>.
- (35) Tishkina, A. N.; Lukoyanov, A. N.; Morozov, A. G.; Fukin, G. K.; Lyssenko, K. A.; Fedushkin, I. L. Synthesis and Structure of Novel Chiral Amido-Imine Complexes of Aluminum, Gallium, and Indium. *Russ Chem Bull* **2009**, *58* (11), 2250–2257. <https://doi.org/10.1007/s11172-009-0314-x>.
- (36) Moskalev, M. V.; Lukoyanov, A. N.; Baranov, E. V.; Fedushkin, I. L. Unexpected Reactivity of an Alkylaluminum Complex of a Non-Innocent 1,2-Bis[(2,6-Diisopropylphenyl)imino]Acenaphthene Ligand (Dpp-Bian). *Dalton Trans.* **2016**, *45* (40), 15872–15878.  
<https://doi.org/10.1039/C6DT01750A>.
- (37) Fedushkin, I. L.; Moskalev, M. V.; Lukoyanov, A. N.; Tishkina, A. N.; Baranov, E. V.; Abakumov, G. A. Dialane with a Redox-Active Bis-Amido Ligand: Unique Reactivity towards Alkynes. *Chem. Eur. J.* **2012**, *18* (36), 11264–11276. <https://doi.org/10.1002/chem.201201364>.
- (38) Fedushkin, I. L.; Khvoynova, N. M.; Baurin, A. Yu.; Fukin, G. K.; Cherkasov, V. K.; Bubnov, M. P. Divalent Germanium Compound with a Radical-Anionic Ligand: Molecular Structures of (Dpp-BIAN)<sup>•-</sup>GeCl and Its

- Hydrochloration Products [(Dpp-BIAN)(H)<sub>2</sub>]<sup>•+</sup>[GeCl<sub>3</sub>]<sup>-</sup> and [{"(Dpp-BIAN)(H)<sub>2</sub>•+}<sub>2</sub>(Cl<sup>-</sup>)<sub>2</sub>]+[GeCl<sub>3</sub>]<sup>-</sup> (Dpp-BIAN = 1,2-Bis{(2,6-Diisopropylphenyl)Imino}acenaphthene). *Inorg. Chem.* **2004**, *43* (24), 7807–7815. <https://doi.org/10.1021/ic048801g>.
- (39) Fedushkin, I. L.; Chudakova, V. A.; Fukin, G. K.; Dechert, S.; Hummert, M.; Schumann, H. Protonation of Magnesium and Sodium Complexes Containing Dianionic Diimine Ligands. Molecular Structures of 1,2-Bis{(2,6-Diisopropylphenyl)Imino}acenaphthene (Dpp-BIAN), [(Dpp-BIAN)H<sub>2</sub>(Et<sub>2</sub>O)], and [(Dpp-BIAN)HNa(Et<sub>2</sub>O)]. *Russ Chem Bull* **2004**, *53* (12), 2744–2750. <https://doi.org/10.1007/s11172-005-0185-8>.
- (40) Fedushkin, I. L.; Skatova, A. A.; Chudakova, V. A.; Fukin, G. K.; Dechert, S.; Schumann, H. Monomeric Magnesium and Calcium Complexes Containing the Bidentate, Dianionic 1,2-Bis[(2,6-Diisopropylphenyl)Imino]Acenaphthene Ligand. *European Journal of Inorganic Chemistry* **2003**, *2003* (18), 3336–3346. <https://doi.org/10.1002/ejic.200300181>.
- (41) Kazarina, O. V.; Gourlaouen, C.; Karmazin, L.; Morozov, A. G.; Fedushkin, I. L.; Dagonne, S. Low Valent Al(II)–Al(II) Catalysts as Highly Active ε-Caprolactone Polymerization Catalysts: Indication of Metal Cooperativity through DFT Studies. *Dalton Trans.* **2018**, *47* (39), 13800–13808. <https://doi.org/10.1039/C8DT02614A>.
- (42) Chen, W.; Zhao, Y.; Xu, W.; Su, J.-H.; Shen, L.; Liu, L.; Wu, B.; Yang, X.-J. Reductive Linear- and Cyclo-Trimerization of Isocyanides by an Al–Al-Bonded Compound. *Chem. Commun.* **2019**, *55* (1), 9452–9455. <https://doi.org/10.1039/C9CC04344F>.
- (43) Gerecht, B.; Offermann, G.; Seitz, G. Tris[cyanoimino]-deltat, das erste Stickstoff-Analogon des Dreiecksäure-Dianions. *Synthesis* **1982**, *1982* (09), 726–728. <https://doi.org/10.1055/s-1982-29915>.
- (44) Jain, R.; Bally, T.; Rablen, P. R. Calculating Accurate Proton Chemical Shifts of Organic Molecules with Density Functional Methods and Modest Basis Sets. *J. Org. Chem.* **2009**, *74* (11), 4017–4023. <https://doi.org/10.1021/jo900482q>.
- (45) Jeffrey, G. A. *An Introduction to Hydrogen Bonding*; Oxford University Press, 1997.
- (46) Gianopoulos, C. G.; Kumar, N.; Zhao, Y.; Jia, L.; Kirschbaum, K.; Mason, M. R. Aluminum Alkoxide, Amide and Halide Complexes Supported by a Bulky Dipyrromethene Ligand: Synthesis, Characterization, and Preliminary ε-Caprolactone Polymerization Activity. *Dalton Trans.* **2016**, *45* (35), 13787–13797. <https://doi.org/10.1039/C6DT02449A>.
- (47) Trinh, C.; Bodensteiner, M.; Virovets, A. V.; Peresyphkina, E. V.; Scheer, M.; Matveev, S. M.; Timoshkin, A. Y. Chelating Ionic versus Bridged Molecular Structures of Group 13 Metal Complexes with Bidentate Ligands. *Polyhedron* **2010**, *29* (1), 414–424. <https://doi.org/10.1016/j.poly.2009.06.020>.
- (48) Paparo, A.; Smith, C. D.; Jones, C. Diagonally Related S- and P-Block Metals Join Forces: Synthesis and Characterization of Complexes with

- Covalent Beryllium–Aluminum Bonds. *Angew. Chem. Int. Ed.* **2019**, *58* (33), 11459–11463. <https://doi.org/10.1002/anie.201906609>.
- (49) Masuda, J. D.; Stephan, D. W. Neutral and Cationic Aluminium Complexes of a Sterically Demanding N-Imidoylamidine Ligand. *Dalton Trans.* **2006**, No. 17, 2089. <https://doi.org/10.1039/b513531a>.
- (50) Bonyhady, S. J.; Collis, D.; Frenking, G.; Holzmann, N.; Jones, C.; Stasch, A. Synthesis of a Stable Adduct of Dialane(4) (Al<sub>2</sub>H<sub>4</sub>) via Hydrogenation of a Magnesium(I) Dimer. *Nature Chem* **2010**, *2* (10), 865–869. <https://doi.org/10.1038/nchem.762>.
- (51) Baker, R. J.; Farley, R. D.; Jones, C.; Kloth, M.; Murphy, D. M. The Reactivity of Diazabutadienes toward Low Oxidation State Group 13 Iodides and the Synthesis of a New Gallium(I) Carbene Analogue. *J. Chem. Soc., Dalton Trans.* **2002**, No. 20, 3844–3850. <https://doi.org/10.1039/B206605J>.
- (52) Altman, A. B.; Pemmaraju, C. D.; Camp, C.; Arnold, J.; Minasian, S. G.; Prendergast, D.; Shuh, D. K.; Tyliszczak, T. Theory and X-Ray Absorption Spectroscopy for Aluminum Coordination Complexes – Al K-Edge Studies of Charge and Bonding in (BDI)Al, (BDI)AlR<sub>2</sub>, and (BDI)AlX<sub>2</sub> Complexes. *J. Am. Chem. Soc.* **2015**, *137* (32), 10304–10316. <https://doi.org/10.1021/jacs.5b05854>.
- (53) Christe, K. O.; Dixon, D. A.; McLemore, D.; Wilson, W. W.; Sheehy, J. A.; Boatz, J. A. On a Quantitative Scale for Lewis Acidity and Recent Progress in Polynitrogen Chemistry. *Journal of Fluorine Chemistry* **2000**, *3*.
- (54) Beste, A.; Krämer, O.; Gerhard, A.; Frenking, G. The Lewis Basicity of Diaminocarbene – A Theoretical Study of Donor–Acceptor Complexes of C(NH<sub>2</sub>)<sub>2</sub>, NH<sub>3</sub> and CO with the Lewis Acids EF<sub>3</sub>, ECl<sub>3</sub> (E = B, Al, Ga, In), TiF<sub>4</sub> and TiCl<sub>4</sub>. *European Journal of Inorganic Chemistry* **1999**, *1999* (11), 2037–2045. [https://doi.org/10.1002/\(SICI\)1099-0682\(199911\)1999:11<2037::AID-EJIC2037>3.0.CO;2-T](https://doi.org/10.1002/(SICI)1099-0682(199911)1999:11<2037::AID-EJIC2037>3.0.CO;2-T).
- (55) Krahl, T.; Kemnitz, E. The Very Strong Solid Lewis Acids Aluminium Chlorofluoride (ACF) and Bromofluoride (ABF)—Synthesis, Structure, and Lewis Acidity. *Journal of Fluorine Chemistry* **2006**, *127* (6), 663–678. <https://doi.org/10.1016/j.jfluchem.2006.02.015>.
- (56) Hill, M. S.; Hitchcock, P. B.; Karagouni, S. M. A. Group 1 and 13 Complexes of Aryl-Substituted Bis(Phosphinimino)Methyls. *Journal of Organometallic Chemistry* **2004**, *689* (4), 722–730. <https://doi.org/10.1016/j.jorganchem.2003.11.030>.
- (57) Korolev, A. V.; Ihara, E.; Guzei, I. A.; Young, V. G.; Jordan, R. F. Cationic Aluminum Alkyl Complexes Incorporating Aminotroponimate Ligands. *J. Am. Chem. Soc.* **2001**, *123* (34), 8291–8309. <https://doi.org/10.1021/ja010242e>.
- (58) Stennett, T. E.; Pahl, J.; Zijlstra, H. S.; Seidel, F. W.; Harder, S. A Frustrated Lewis Pair Based on a Cationic Aluminum Complex and Triphenylphosphine. *Organometallics* **2016**, *35* (2), 207–217. <https://doi.org/10.1021/acs.organomet.5b00927>.



- (59) Zarkesh, R. A.; Ichimura, A. S.; Monson, T. C.; Tomson, N. C.; Anstey, M. R. Voltage Clustering in Redox-Active Ligand Complexes: Mitigating Electronic Communication through Choice of Metal Ion. *Dalton Trans.* **2016**, 45 (24), 9962–9969. <https://doi.org/10.1039/C6DT00422A>.
- (60) Swidan, A.; Binder, J. F.; Onge, B. J. St.; Suter, R.; Burford, N.; Macdonald, C. L. B. 2,6-Bis(Benzimidazol-2-Yl)Pyridines as More Electron-Rich and Sterically Accessible Alternatives to 2,6-Bis(Imino)Pyridine for Group 13 Coordination Chemistry. *Dalton Trans.* **2019**, 48 (4), 1284–1291. <https://doi.org/10.1039/C8DT04276D>.
- (61) Allen, F. H.; Kennard, O.; Watson, D. G.; Brammer, L.; Orpen, A. G.; Taylor, R. Tables of Bond Lengths Determined by X-Ray and Neutron Diffraction. Part 1. Bond Lengths in Organic Compounds. *J. Chem. Soc., Perkin Trans. 2* **1987**, No. 12, S1–S19. <https://doi.org/10.1039/P298700000S1>.
- (62) Jiang, W.; Gorden, J. D.; Goldsmith, C. R. A Homogeneous Gallium(III) Compound Selectively Catalyzes the Epoxidation of Alkenes. *Inorg. Chem.* **2012**, 51 (5), 2725–2727. <https://doi.org/10.1021/ic300159a>.
- (63) Cole, B. E.; Wolbach, J. P.; Dougherty, W. G.; Piro, N. A.; Kassel, W. S.; Graves, C. R. Synthesis and Characterization of Aluminum- $\alpha$ -Diimine Complexes over Multiple Redox States. *Inorg. Chem.* **2014**, 53 (7), 3899–3906. <https://doi.org/10.1021/ic5003989>.
- (64) Baker, R. J.; Farley, R. D.; Jones, C.; Mills, D. P.; Kloth, M.; Murphy, D. M. An EPR and ENDOR Investigation of a Series of Diazabutadiene-Group 13 Complexes. *Chem. Eur. J.* **2005**, 11 (10), 2972–2982. <https://doi.org/10.1002/chem.200401103>.
- (65) Scott, J.; Gambarotta, S.; Korobkov, I.; Knijnenburg, Q.; de Bruin, B.; Budzelaar, P. H. M. Formation of a Paramagnetic Al Complex and Extrusion of Fe during the Reaction of (Diiminepyridine)Fe with  $AlR_3$  (R = Me, Et). *J. Am. Chem. Soc.* **2005**, 127 (49), 17204–17206. <https://doi.org/10.1021/ja056135s>.
- (66) Flamini, A.; Poli, N. Intermolecular Interaction of Tris-Bipyridyl Metal Complexes,  $M(Bpy)_3$  (M = Al, V, Fe), with Tetracyanoethylene. *Inorganica Chimica Acta* **1988**, 150 (2), 149–151. [https://doi.org/10.1016/S0020-1693\(00\)90585-1](https://doi.org/10.1016/S0020-1693(00)90585-1).
- (67) Thompson, E. J.; Berben, L. A. Electrocatalytic Hydrogen Production by an Aluminum(III) Complex: Ligand-Based Proton and Electron Transfer. *Angew. Chem.* **2015**, 127 (40), 11808–11812. <https://doi.org/10.1002/ange.201503935>.
- (68) Yoon, S.; Kim, S. H.; Heo, J.; Kim, Y. Dimeric Aluminum Methyl Complex Bridged by 2-Oxy-2-Methyl-1-(Phenylamino)Propane: Synthesis, Structure, and Use in Ring Opening Polymerization of Lactide. *Inorganic Chemistry Communications* **2013**, 29, 157–159. <https://doi.org/10.1016/j.inoche.2012.12.025>.
- (69) Altaf, C. T.; Wang, H.; Keram, M.; Yang, Y.; Ma, H. Aluminum Methyl and Isopropoxide Complexes with Ketiminate Ligands: Synthesis, Structural

- Characterization and Ring-Opening Polymerization of Cyclic Esters. *Polyhedron* **2014**, *81*, 11–20. <https://doi.org/10.1016/j.poly.2014.05.055>.
- (70) Kan, C.; Ge, J.; Ma, H. Aluminum Methyl, Alkoxide and  $\alpha$ -Alkoxy Ester Complexes Supported by 6,6'-Dimethylbiphenyl-Bridged Salen Ligands: Synthesis, Characterization and Catalysis for Rac-Lactide Polymerization. *Dalton Trans.* **2016**, *45* (15), 6682–6695. <https://doi.org/10.1039/C5DT04633E>.
- (71) Ikpo, N.; Barbon, S. M.; Drover, M. W.; Dawe, L. N.; Kerton, F. M. Aluminum Methyl and Chloro Complexes Bearing Monoanionic Aminophenolate Ligands: Synthesis, Characterization, and Use in Polymerizations. *Organometallics* **2012**, *31* (23), 8145–8158. <https://doi.org/10.1021/om300757u>.
- (72) Stoll, S.; Schweiger, A. *EasySpin, a Comprehensive Software Package for Spectral Simulation and Analysis in EPR*; 2006.
- (73) Hinchliffe, A.; Mair, F. S.; McInnes, E. J. L.; Pritchard, R. G.; Warren, J. E. Light Group 13 Chloride Diazadiene Complexes: Consequences of Varying Substituent Bulk. *Dalton Trans.* **2008**, No. 2, 222–233. <https://doi.org/10.1039/B712911D>.
- (74) Zhao, Y.; Liu, Y.; Yang, L.; Yu, J.-G.; Li, S.; Wu, B.; Yang, X.-J. Mechanistic Insight into the N–N Bond-Cleavage of Azo-Compounds That Was Induced by an Al–Al-Bonded Compound [L<sub>2</sub>–Al(III)–Al(III)L<sub>2</sub>–]. *Chem. Eur. J.* **2012**, *18* (19), 6022–6030. <https://doi.org/10.1002/chem.201103607>.
- (75) Rufino-Felipe, E.; Lopez, N.; Vengoechea-Gómez, F. A.; Guerrero-Ramírez, L.-G.; Muñoz-Hernández, M.-Á. Ring-Opening Polymerization of Rac -Lactide Catalyzed by Al(III) and Zn(II) Complexes Incorporating Schiff Base Ligands Derived from Pyrrole-2-Carboxaldehyde: FULL PAPER. *Appl Organometal Chem* **2018**, *32* (6), e4315. <https://doi.org/10.1002/aoc.4315>.
- (76) Stienen, C.; Gondzik, S.; Gehlhaar, A.; Haack, R.; Wölper, C.; Jansen, G.; Schulz, S. (MeZn)<sub>2</sub> ( $\mu$ - $\eta^2$ : $\eta^2$ -N<sub>6</sub>Ph<sub>2</sub>): A Powerful Starting Reagent for the Synthesis of Metal Hexazene Complexes. *Organometallics* **2016**, *35* (7), 1022–1029. <https://doi.org/10.1021/acs.organomet.6b00116>.
- (77) Sherbow, T. J.; Fettinger, J. C.; Berben, L. A. Control of Ligand pK<sub>a</sub> Values Tunes the Electrocatalytic Dihydrogen Evolution Mechanism in a Redox-Active Aluminum(III) Complex. *Inorg. Chem.* **2017**, *56* (15), 8651–8660. <https://doi.org/10.1021/acs.inorgchem.7b00230>.
- (78) Schwarz, A. D.; Chu, Z.; Mountford, P. Sulfonamide-Supported Aluminum Catalysts for the Ring-Opening Polymerization of Rac -Lactide. *Organometallics* **2010**, *29* (5), 1246–1260. <https://doi.org/10.1021/om901070g>.
- (79) Myers, T. W.; Berben, L. A. Aluminum–Ligand Cooperative N–H Bond Activation and an Example of Dehydrogenative Coupling. *J. Am. Chem. Soc.* **2013**, *135* (27), 9988–9990. <https://doi.org/10.1021/ja4032874>.
- (80) Abdalla, J. A. B.; Tirfoin, R. C.; Niu, H.; Aldridge, S. A Zwitterionic Hydrocarbon-Soluble Boremium Ion Based on a  $\beta$ -Diketiminato Backbone. *Chem. Commun.* **2017**, *53* (44), 5981–5984. <https://doi.org/10.1039/C7CC03121A>.

- (81) Zhao, Y.; Liu, Y.; Wu, B.; Yang, X.-J. Reactions of  $\alpha$ -Diimine-Aluminum Complexes with Sodium Alkynides: Versatile Structures of Aluminum  $\sigma$ -Alkynide Complexes. *Dalton Trans.* **2015**, 44 (30), 13671–13680. <https://doi.org/10.1039/C5DT01693B>.
- (82) Zhao, Y.; Liu, Y.; Lei, Y.; Wu, B.; Yang, X.-J. Activation of Alkynes by an  $\alpha$ -Diimine-Stabilized Al–Al-Bonded Compound: Insertion into the Al–Al Bond or Cycloaddition to AlN<sub>2</sub>C<sub>2</sub> Rings. *Chem. Commun.* **2013**, 49 (40), 4546. <https://doi.org/10.1039/c3cc41756e>.
- (83) Sokolov, V. G.; Koptseva, T. S.; Rumyantsev, R. V.; Yang, X.-J.; Zhao, Y.; Fedushkin, I. L. Reactivity of Aluminum Complexes of Redox-Active Ligand toward N-Heterocyclic Carbene and Its Thione. *Organometallics* **2020**, 39 (1), 66–73. <https://doi.org/10.1021/acs.organomet.9b00611>.
- (84) Snyder, C. J.; Zavalij, P.; Bowen, K.; Schnöckel, H.; Eichhorn, B. Synthesis, Structure, and Properties of a Dialumane Supported by Pyrazolate Ligands. *Dalton Trans.* **2015**, 44 (7), 2956–2958. <https://doi.org/10.1039/C4DT03533J>.
- (85) Kretsch, J.; Kreyenschmidt, A.; Schillmöller, T.; Herbst-Irmer, R.; Stalke, D. Mixed Low-Valent Alanes from the Bis(4-Methyl-Benzoxazol-2-Yl)Methanide Ligand. *Inorg. Chem.* **2020**, 59 (18), 13690–13699. <https://doi.org/10.1021/acs.inorgchem.0c02066>.
- (86) Koptseva, T. S.; Sokolov, V. G.; Ketkov, S. Y.; Rychagova, E. A.; Cherkasov, A. V.; Skatova, A. A.; Fedushkin, I. L. Reversible Addition of Carbon Dioxide to Main Group Metal Complexes at Temperatures about 0 °C. *Chemistry – A European Journal* **2021**, 27 (18), 5745–5753. <https://doi.org/10.1002/chem.202004991>.
- (87) Thompson, E. J.; Myers, T. W.; Berben, L. A. Synthesis of Square-Planar Aluminum(III) Complexes. *Angew. Chem. Int. Ed.* **2014**, 53 (51), 14132–14134. <https://doi.org/10.1002/anie.201407098>.
- (88) Nikiforov, G. B.; Roesky, H. W.; Noltemeyer, M.; Schmidt, H.-G. Reactivity of Ti(Bipy)<sub>3</sub> and Preparation of the Li(THF)<sub>4</sub>[Al(Bipy)<sub>2</sub>] Complex with the Dinegative Bipy Ligand. *Polyhedron* **2004**, 23 (4), 561–566. <https://doi.org/10.1016/j.poly.2003.10.008>.
- (89) Anker, M. D.; Schwamm, R. J.; Coles, M. P. Synthesis and Reactivity of a Terminal Aluminium–Imide Bond. *Chem. Commun.* **2020**, 56 (15), 2288–2291. <https://doi.org/10.1039/C9CC09214E>.
- (90) Gaussian 16, Revision C.01, Frisch, M. J.; Trucks, G. W.; Schlegel, H.B.; Scuseria, G. E.; Robb, M. A.; Cheeseman, J. R.; Scalmani, G.; Barone, V.; Petersson, G. A.; Nakatsuji, H.; Li, X.; Caricato, M.; Marenich, A. V.; Bloino, J.; Janesko, B. G.; Gomperts, R.; Mennucci, B.; Hratchian, H. P.; Ortiz, J. V.; Izmaylov, A. F.; Sonnenberg, J. L.; Williams-Young, D.; Ding, F.; Lipparini, F.; Egidi, F.; Goings, J.; Peng, B.; Petrone, A.; Henderson, T.; Ranasinghe, D.; Zakrzewski, V. G.; Gao, J.; Rega, N.; Zheng, G.; Liang, W.; Hada, M.; Ehara, M.; Toyota, K.; Fukuda, R.; Hasegawa, J.; Ishida, M.; Nakajima, T.; Honda, Y.; Kitao, O.; Nakai, H.; Vreven, T.; Throssell, K.; Montgomery, J. A., Jr.; Peralta, J. E.; Ogliaro, F.; Bearpark, M. J.; Heyd, J. J.; Brothers, E. N.; Kudin, K. N.; Staroverov, V. N.; Keith, T. A.; Kobayashi,

- R.; Normand, J.; Raghavachari, K.; Rendell, A. P.; Burant, J. C.; Iyengar, S. S.; Tomasi, J.; Cossi, M.; Millam, J. M.; Klene, M.; Adamo, C.; Cammi, R.; Ochterski, J. W.; Martin, R. L.; Morokuma, K.; Farkas, O.; Foresman, J. B.; Fox, D. J. Gaussian, Inc., Wallingford CT, **2016**.
- (91) Becke, A. D. *J. Chem. Phys.* **1993**, *98*, 5648-52.
- (92) Hay, P. J.; Wadt, W. R. *J. Chem. Phys.* **1985**, *82*, 299-310.
- (93) Hay, P. J.; Wadt, W. R. *J. Chem. Phys.* **1985**, *82*, 270-83.
- (94) Wadt, W. R.; Hay, P. J. *J. Chem. Phys.* **1985**, *82*, 284-98.
- (95) Wiitala, K. W.; Hoye, T. R.; Cramer, C. J. *J. Chem. Theory. Comput.* **2006**, *2*, 1085.
- (96) Easton, R. E.; Giesen, D. J.; Welch, C.J.; Truhlar, D. G. *Theor. Chem. Acc.* **1996**, *93*, 281-301.
- (97) Hickman, A. J.; Sanford, M. S. Catalyst Control of Site Selectivity in the PdII/IV-Catalyzed Direct Arylation of Naphthalene. *ACS Catal.* **2011**, *1* (3), 170–174.
- (98) Boglia, A.; Leone, G.; Masi, F.; Ricci, G.; Sommazzi, A. Bis-imine complex of lanthanides, catalytic system comprising said bis-imine complex and process for the (co)polymerization of conjugated dienes. U.S. Patent 20140228206, August 14, **2014**.
- (99) Thomson, R. K.; Scott, B. L.; Morris, D. E.; Kiplinger, J. L. *C. R. Chim.* **2010**, *13*, 790-802.
- (100) APEX3 2016. 1-0: Bruker-AXS, Madison, Wisconsin, USA (**2016**).
- (101) APEX2 2014.11-0: Bruker-AXS, Madison, Wisconsin, USA (**2014**).
- (102) SAINT v8.34A: Bruker-AXS, Madison, Wisconsin, USA (**2014**).
- (103) SADABS v2014/5: Krause, L., Herbst-Irmer, R., Sheldrick, G.M. & Stalke, D., *J. Appl. Cryst.*, *48*, 3-10 (**2015**).
- (104) SHELXT v2014/4: Sheldrick, G.M., *Acta Cryst.*, *A*, *71*, 3-8 (**2015**).
- (105) SHELXS-97: Sheldrick, G.M., *Acta Cryst.*, *A64*, 112-122 (**2008**).
- (106) SHELXL-2017/1: Sheldrick, G.M., *Acta Cryst.*, *A71*, 3-8 (**2015**).
- (107) CELL\_NOW v**2008/4**
- (108) TWINABS v**2012/1**
- (109) CrysAlisPro 1.171.40.53: Rigaku Oxford Diffraction, Rigaku Corporation, Oxford, UK. (**2019**).
- (110) SCALE3 ABSPACK v1.0.7: an Oxford Diffraction program; Oxford Diffraction Ltd: Abingdon, UK, **2005**.
- (111) SHELXL-2018/3: Sheldrick, G.M., *Acta Cryst.*, *A*, *71*, 3-8 (**2015**).

## 5. Supplementary Information

### 5.1 Methods

#### **5.1.1 Physical measurements**

All NMR spectra were recorded at ambient temperature using a Bruker 400 MHz spectrometer (399.78 MHz for  $^1\text{H}$ , 100.52 MHz for  $^{13}\text{C}$ , and 161.83 MHz for  $^{31}\text{P}$ ). Chemical shifts were referenced to residual solvent. s = singlet, bs = broad singlet, d = doublet, q = quartet, td = triplet of doublets, m = multiplet, bm = broad multiplet, at = apparent triplet. CHN analysis was performed at the Midwest Microlab. Electrochemical measurements were done in a glovebox under a dinitrogen environment using a CHI Potentiostat/Galvanostat. A glassy carbon working electrode, a platinum wire auxiliary electrode, and a silver wire plated with AgCl as a quasi-reference electrode were utilized. Potentials were reported versus ferrocene, which was added as an internal standard for calibration at the end of each run. Solutions employed during these studies were ~5 mM in analyte and 100 mM in  $[n\text{-Pr}_4\text{N}][\text{BAR}^{\text{F}}]$  ( $(\text{BAR}^{\text{F}})^{-} = \text{B}(3,5\text{-CF}_3)_2\text{-C}_6\text{H}_3)_4^{-}$ ) in ~5 mL of dichloromethane (for **1–6**). Data was collected in a positive-feedback IR compensation mode at 100  $\text{mV s}^{-1}$ . EPR spectra were collected on 1 mM solutions in 50:50 toluene:DCM using a X-band CW EPR spectrometer (microwave frequency 9.389 GHz, power 2.130 mW, temperature 298 K, modulation amplitude 0.1 mT). Fitting of EPR spectra was performed in MATLAB using the garlic function of the EasySpin package.<sup>72</sup>

### 5.1.2 Computational details

All structure optimizations were performed with Gaussian 16<sup>90</sup> using the B3LYP hybrid DFT method<sup>91</sup> and the LANL2DZ basis set.<sup>92-94</sup> Geometry optimization of the  $[\text{Al}(\text{L}_{\text{Ph}})_2\text{I}_2]^+$  cation was performed using the crystal structure geometry as the initial starting point. Molecular orbitals are rendered at an isovalue of  $\pm 0.06$  a.u. NMR modelling for the  $[\text{Al}(\text{L}_{\text{Ph}})_2\text{I}_2]^+$  cation was done using GIAO calculations with the WP04 functional<sup>95</sup> and the MidiX<sup>96</sup> basis set. NMR modelling for the  $[\text{Al}(\text{L}_{\text{Ph}})_2(\text{NCMe})_2]^{3+}$  cation was done using GIAO calculations with the WP04 functional<sup>95</sup> and the aug-cc-pVDZ basis set.

Atom colors: aluminum: orange; nitrogen: blue; carbon: gray; hydrogen: black; iodine: purple; oxygen: red; chlorine: green; boron: pink. MO colors:  $\alpha$ -orbital: red;  $\beta$ -orbital: green.

### 5.1.3 Preparation of compounds

All reactions and manipulations were performed under a dinitrogen atmosphere in a Vacuum Atmospheres, Inc. NextGen drybox equipped with both oxygen and moisture purifier systems. Glassware was dried overnight at 150 °C before use.  $\text{CDCl}_3$  and  $\text{CD}_3\text{CN}$  were degassed and stored over 4 Å molecular sieves prior to use. Acetonitrile, DCM, DME, ether, hexane, pentane, THF, and toluene were sparged for 20 min with dry argon and dried using a commercial two-column solvent purification system comprising of two columns packed with neutral alumina (for acetonitrile, DCM, DME, ether, and THF) or Q5 reactant then neutral alumina (for hexanes, pentane, and toluene).  $\text{L}_{\text{Ar}}$  ligand<sup>97</sup>,  $\text{PhDAB}$  ligand<sup>98</sup>, and [*n*-

$\text{Pr}_4\text{N}][\text{BAr}^{\text{F}}]$  electrolyte<sup>99</sup> were prepared according to literature procedures. All other reagents were purchased from commercial sources and used as received.

*General Synthesis of  $[\text{Al}(\text{L}_{\text{Ar}})_2\text{I}_2]\cdot\text{I}$  (1–4):*

$\text{AlI}_3$  (0.204 g, 0.50 mmol) was dissolved in 25 mL diethyl ether in a 125 mL flask equipped with a magnetic stir bar. To this stirring solution was added  $\text{L}_{\text{Ar}}$  (1.00 mmol) dissolved in sufficient diethyl ether to give a homogenous solution. The resulting reaction was let to stir for 12 h at room temperature, after which the product was collected as a powder by filtration over a medium porosity frit. The powder was washed with diethyl ether (~20 mL) and dried in vacuo.

*Characterization Data for  $[\text{Al}(\text{L}_{\text{Ph}})_2\text{I}_2]\cdot\text{I}$  (1):*

Yield: 0.407 g, 0.462 mmol (93%) of a pale-orange powder.

$^1\text{H}$  NMR ( $\text{CDCl}_3$ ):  $\delta$  8.18 (t,  $J = 7.3$  Hz, 2H), 8.04 (d,  $J = 7.3$  Hz, 2H), 7.64 (m, 4H), 7.54 (d,  $J = 7.4$  Hz, 2H), 7.37 (m, 4H), 7.27 (m, 2H), 7.14 (t,  $J = 7.3$  Hz, 2H), 4.79 (d,  $J = 7.6$  Hz, 2H), 2.74 (s, 6H,  $\text{CH}_3\text{C}=\text{N}$ ), 2.38 (s, 6H,  $\text{CH}_3\text{C}=\text{N}$ ).

$^{13}\text{C}\{^1\text{H}\}$  NMR ( $\text{CDCl}_3$ ):  $\delta$  171.8 (C=N), 171.5 (C=N), 143.3, 142.2, 132.6, 131.1, 129.4 (b, two overlapping signals), 128.9, 128.3, 125.8, 125.7, 122.0, 121.7, 22.8 ( $\text{H}_3\text{CC}=\text{N}$ ), 22.1 ( $\text{H}_3\text{CC}=\text{N}$ ).

Anal. Calcd for  $\text{C}_{32}\text{H}_{32}\text{AlI}_3\text{N}_4$ : C, 43.66; H, 3.66; N, 6.36. Found: C, 43.43; H, 3.66; N, 6.24.

*Characterization Data for  $[\text{Al}(\text{L}_{\text{ToI}})_2\text{I}_2]\cdot\text{I}$  (2):*

Yield: 0.391 g, 0.418 mmol (84%) of an orange powder.

$^1\text{H}$  NMR ( $\text{CDCl}_3$ ):  $\delta$  7.86 (d,  $J = 7.2$  Hz, 4H), 7.35 (s, 4H), 7.12 (m,  $J = 8.2$  Hz, 4H), 6.90 (d,  $J = 7.2$  Hz, 2H), 4.72 (d,  $J = 6.9$  Hz, 2H), 2.66 (s, 6H,  $\text{CH}_3\text{C}=\text{N}$ ), 2.50 (s, 6H,  $\text{CH}_3\text{C}=\text{N}$ ), 2.31 (s, 6H,  $\text{CH}_3\text{C}_6\text{H}_4-\text{N}$ ), 2.31 (s, 6H,  $\text{CH}_3\text{C}_6\text{H}_4-\text{N}$ ).

$^{13}\text{C}\{^1\text{H}\}$  NMR ( $\text{CDCl}_3$ ):  $\delta$  171.7 (C=N), 171.2 (C=N), 140.8, 139.7, 139.6, 138.9, 128.7, 125.6, 125.5, 121.9, 121.6, 22.6 ( $\text{H}_3\text{CC}=\text{N}$ ), 21.9 ( $\text{H}_3\text{CC}=\text{N}$ ), 21.2 ( $\text{H}_3\text{CC}_6\text{H}_4-\text{N}$ ), 21.2 ( $\text{H}_3\text{CC}_6\text{H}_4-\text{N}$ ).

Anal. Calcd for  $\text{C}_{36}\text{H}_{40}\text{Al}_3\text{N}_4$ : C, 46.17; H, 4.31; N, 5.98. Found: C, 45.55; H, 4.48; N, 5.63.

*Characterization Data for  $[\text{Al}(\text{L}_{\text{tBu}})_2\text{I}_2]\cdot\text{I}$  (3):*

Yield: 0.480 g, 0.434 mmol (87%) of an orange powder.

$^1\text{H}$  NMR ( $\text{CDCl}_3$ ):  $\delta$  8.09 (d,  $J = 7.5$  Hz, 2H), 7.89 (s, 2H), 7.62 (d,  $J = 7.5$  Hz, 2H), 7.42 (s, 2H), 7.34 (s, 2H), 7.16 (m,  $J = 7.0$  Hz, 2H), 7.02 (s, 2H), 4.65 (s, 2H), 2.69 (s, 6H,  $\text{CH}_3\text{C}=\text{N}$ ), 2.30 (s, 6H,  $\text{CH}_3\text{C}=\text{N}$ ), 1.46 (s, 18H,  $\text{CH}_3\text{C}(\text{CH}_3)_2\text{C}_6\text{H}_4-\text{N}$ ), 1.28 (s, 18H,  $\text{CH}_3\text{C}(\text{CH}_3)_2\text{C}_6\text{H}_4-\text{N}$ ).

$^{13}\text{C}\{^1\text{H}\}$  NMR ( $\text{CDCl}_3$ ):  $\delta$  171.2 (C=N), 171.0 (C=N), 153.0, 152.0, 140.8, 139.6, 128.8, 128.0, 125.4, 125.3, 121.5, 121.4, 35.2 ( $(\text{CH})_3\text{CC}_6\text{H}_4-\text{N}$ ), 34.7 ( $(\text{CH})_3\text{CC}_6\text{H}_4-\text{N}$ ), 31.5 ( $\text{C}(\text{CH})_3\text{C}_6\text{H}_4-\text{N}$ ), 31.3 ( $\text{C}(\text{CH})_3\text{C}_6\text{H}_4-\text{N}$ ), 22.5 ( $\text{H}_3\text{CC}=\text{N}$ ), 21.8 ( $\text{H}_3\text{CC}=\text{N}$ ).

Anal. Calcd for  $\text{C}_{48}\text{H}_{64}\text{Al}_3\text{N}_4$ : C, 52.19; H, 5.84; N, 5.07. Found: C, 51.86; H, 6.08; N, 4.96.



*General Synthesis of [Al(L<sub>Ar</sub>)<sub>2</sub>(NCMe)<sub>2</sub>] $\cdot$ 3I (4–6):*

[Al(L<sub>Ar</sub>)<sub>2</sub>I<sub>2</sub>] $\cdot$ I (0.050 g) was weighed into a 25 mL vial and acetonitrile (~1.5 mL) was added. The resulting deep purple solution was let to stand for 24 h at room temperature. The supernatant was decanted and the remaining crystals were washed with cold acetonitrile (3 x 1 mL), after which the crystals were dried in vacuo and collected.

*Characterization Data for [Al(L<sub>Tol</sub>)<sub>2</sub>(NCMe)<sub>2</sub>] $\cdot$ 3I (5):*

Yield: 0.042 g, 0.041 mmol (77%) of a purple crystal.

<sup>1</sup>H NMR (CD<sub>3</sub>CN):  $\delta$  7.54 (m,  $J$  = 8.3 Hz, 5.5 Hz, 6H), 7.32 (d,  $J$  = 7.2 Hz, 2H), 7.20 (d,  $J$  = 2.4 Hz, 2H), 7.18 (d,  $J$  = 2.4 Hz, 2H), 7.07 (d,  $J$  = 8.2 Hz, 2H), 6.67 (dd,  $J$  = 2.4 Hz, 8.1 Hz, 2H), 4.87 (dd,  $J$  = 2.4 Hz, 8.2 Hz, 2H), 2.79 (s, 6H, CH<sub>3</sub>C=N), 2.49 (s, 6H, CH<sub>3</sub>C=N), 2.48 (s, 6H, CH<sub>3</sub>C<sub>6</sub>H<sub>4</sub>-N), 2.31 (s, 6H, CH<sub>3</sub>C<sub>6</sub>H<sub>4</sub>-N).

<sup>13</sup>C{<sup>1</sup>H} NMR (CD<sub>3</sub>CN):  $\delta$  178.6 (C=N), 178.5 (C=N), 141.0, 140.0, 139.9, 139.8, 132.3, 132.0, 130.8, 130.5, 122.1, 121.6, 121.3, 121.2, 23.2 (H<sub>3</sub>CC<sub>6</sub>H<sub>4</sub>-N), 23.2 (H<sub>3</sub>CC<sub>6</sub>H<sub>4</sub>-N), 20.8 (H<sub>3</sub>CC=N), 20.6 (H<sub>3</sub>CC=N).

Anal. Calcd for C<sub>40</sub>H<sub>46</sub>AlI<sub>3</sub>N<sub>6</sub>: C, 47.17; H, 4.55; N, 8.25. Found: C, 46.18; H, 4.41; N, 7.17.

*Characterization Data for [Al(L<sub>tBu</sub>)<sub>2</sub>(NCMe)<sub>2</sub>] $\cdot$ 3I (6):*

Yield: 0.046 g, 0.039 mmol (86%) of a purple crystal.

$^1\text{H}$  NMR ( $\text{CD}_3\text{CN}$ ):  $\delta$  7.86 (dd,  $J = 2.2$  Hz, 8.4 Hz, 2H), 7.79 (dd,  $J = 2.1$  Hz, 8.4 Hz, 2H), 7.60 (dd,  $J = 2.4$  Hz, 8.4 Hz, 2H), 7.56 (dd,  $J = 2.2$  Hz, 8.4 Hz, 2H), 7.24 (dd,  $J = 1.5$  Hz, 8.6 Hz, 4H), 6.76 (m,  $J = 2.5$  Hz, 8.4 Hz, 2H), 4.76 (m,  $J = 2.4$  Hz, 8.4 Hz, 2H), 2.85 (s, 6H,  $\text{CH}_3\text{C}=\text{N}$ ), 2.52 (s, 6H,  $\text{CH}_3\text{C}=\text{N}$ ), 1.44 (s, 18H,  $(\text{CH}_3)_3\text{CC}_6\text{H}_4-\text{N}$ ), 1.28 (s, 18H,  $(\text{CH}_3)_3\text{CC}_6\text{H}_4-\text{N}$ ).

$^{13}\text{C}\{^1\text{H}\}$  NMR ( $\text{CD}_3\text{CN}$ ):  $\delta$  178.6 (C=N), 178.4 (C=N), 154.1, 152.8, 139.9, 139.9, 129.1, 128.3, 127.4, 126.8, 121.6, 121.6, 121.0, 120.9, 35.4 ( $(\text{CH}_3)_3\text{CC}_6\text{H}_4-\text{N}$ ), 35.0 ( $(\text{CH}_3)_3\text{CC}_6\text{H}_4-\text{N}$ ), 31.0 ( $(\text{CH}_3)_3\text{CC}_6\text{H}_4-\text{N}$ ), 30.8 ( $(\text{CH}_3)_3\text{CC}_6\text{H}_4-\text{N}$ ), 23.2 ( $\text{H}_3\text{CC}=\text{N}$ ), 23.1 ( $\text{H}_3\text{CC}=\text{N}$ ).

*Synthesis of  $[\text{Al}(\text{L}_{\text{Ph}})_2(\text{POEt}_3)_2] \cdot 3\text{I}$  (7):*

$[\text{Al}(\text{L}_{\text{Ph}})_2\text{I}_2] \cdot \text{I}$  (0.100 g, 0.114 mmol) was weighed into a 25 mL vial equipped with a mechanical stirrer and dichloromethane (~1.5 mL) was added. In a separate vial,  $\text{POEt}_3$  (0.13 g, 0.038 mmol) was weighed and dissolved in dichloromethane (~1.5 mL). The  $\text{POEt}_3$  solution was added via pipette to the stirring  $[\text{Al}(\text{L}_{\text{Ph}})_2\text{I}_2] \cdot \text{I}$  solution. The resulting deep blue solution was let to stir for 24 h at room temperature. The solution was filtered over a Celite-padded frit and solvents were removed to give a blue powder.

*Synthesis of  $[\text{Al}(\text{L}_{\text{Ph}})_2(\text{NCMe})_2] \cdot \text{BPh}_4 \cdot 2\text{I}$  (8):*

$[\text{Al}(\text{L}_{\text{Ph}})_2\text{I}_2] \cdot \text{I}$  (0.100 g, 0.114 mmol) was weighed into a 25 mL vial equipped with a mechanical stirrer and acetonitrile (~1.5 mL) was added. In a separate vial,  $\text{NaBPh}_4$  (0.13 g, 0.038 mmol) was weighed and dissolved in acetonitrile (~1.5 mL).

The NaBPh<sub>4</sub> solution was added via pipette to the stirring [Al(L<sub>Ph</sub>)<sub>2</sub>I<sub>2</sub>]<sup>+</sup>I solution. The resulting deep purple solution was let to stir for 24 h at room temperature. Crystals suitable for X-ray diffraction were obtained from an acetonitrile/toluene slow evaporation at -25 °C.

*Synthesis of Al(L<sub>Mes</sub><sup>-</sup>)Me<sub>2</sub> (9):*

L<sub>Mes</sub> (0.250 g, 0.780 mmol) was weighed into a 25 mL vial and dissolved in diethyl ether (~1.5 mL). Sodium metal (0.020 g, 0.870 mmol) was added to a 125 mL flask equipped with a mechanical stirrer and the L<sub>Mes</sub> solution was transferred by pipette. The resulting yellow solution was let to stir for 4 h at room temperature. The solution progressed from yellow to deep red concomitant with ligand reduction. 1 M ClAlMe<sub>2</sub> (0.78 mL, 0.780 mmol) solution was added to the stirring reaction matrix by syringe. The resulting light-orange solution was let to stir for 24 h at room temperature. The solution was then filtered over a Celite-padded frit. Solvents were removed to give an orange powder in 58% yield (0.158 g, 0.45 mmol). Al(L<sub>Mes</sub><sup>-</sup>)<sub>2</sub>Me<sub>2</sub> crystals suitable for X-ray diffraction were obtained by cooling a saturated hexane solution at -25 °C.

*Synthesis of [AlMe<sub>2</sub>]<sub>2</sub>(μ-L<sub>HMes</sub><sup>-</sup>-L<sub>HMes</sub><sup>-</sup>) (10):*

L<sub>HMes</sub> (0.250 g, 0.855 mmol) was weighed into a 25 mL vial and dissolved in diethyl ether (~1.5 mL). Sodium metal (0.022 g, 0.940 mmol) was added to a 125 mL flask equipped with a mechanical stirrer and the L<sub>HMes</sub> solution was transferred by pipette. The resulting yellow solution was let to stir for 4 h at room temperature.

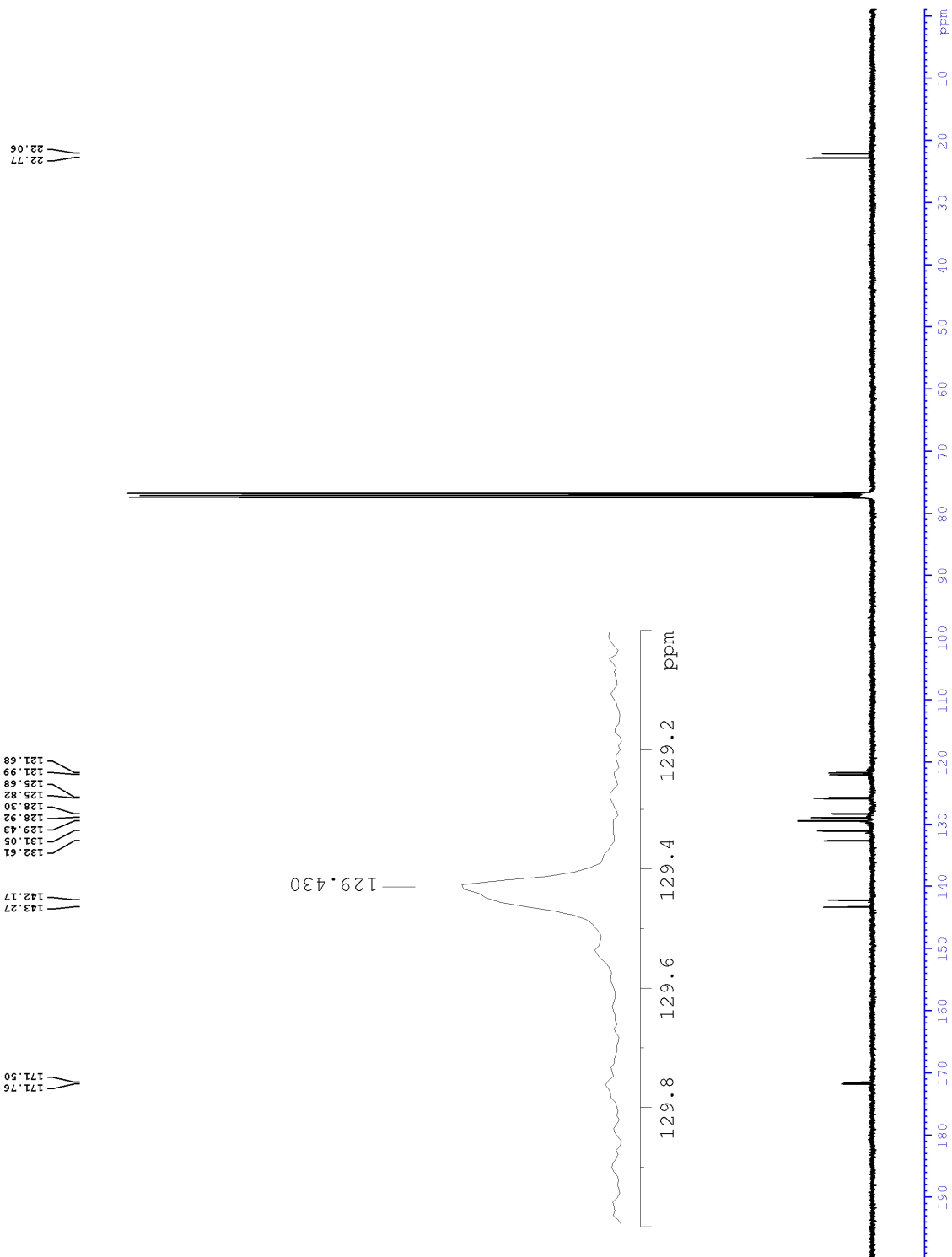
The solution progressed from yellow to deep red concomitant with ligand reduction. 1 M ClAlMe<sub>2</sub> (0.86 mL, 0.855 mmol) solution was added to the stirring reaction matrix by syringe. The resulting reddish-brown solution was let to stir for 24 h at room temperature. The solution was filtered over a Celite-padded frit and solvents were removed to give a brown powder, the totality of which was taken up into hot hexane. [Al(L<sub>HMe</sub>s<sup>-</sup>)<sub>2</sub>Me<sub>2</sub>]<sub>2</sub> crystals suitable for X-ray diffraction were obtained by cooling a saturated hexane solution at -25 °C.

*Synthesis of [(L<sub>Mes</sub><sup>2-</sup>)(THF)Al–Al(THF)(L<sub>Mes</sub><sup>2-</sup>)] (11):*

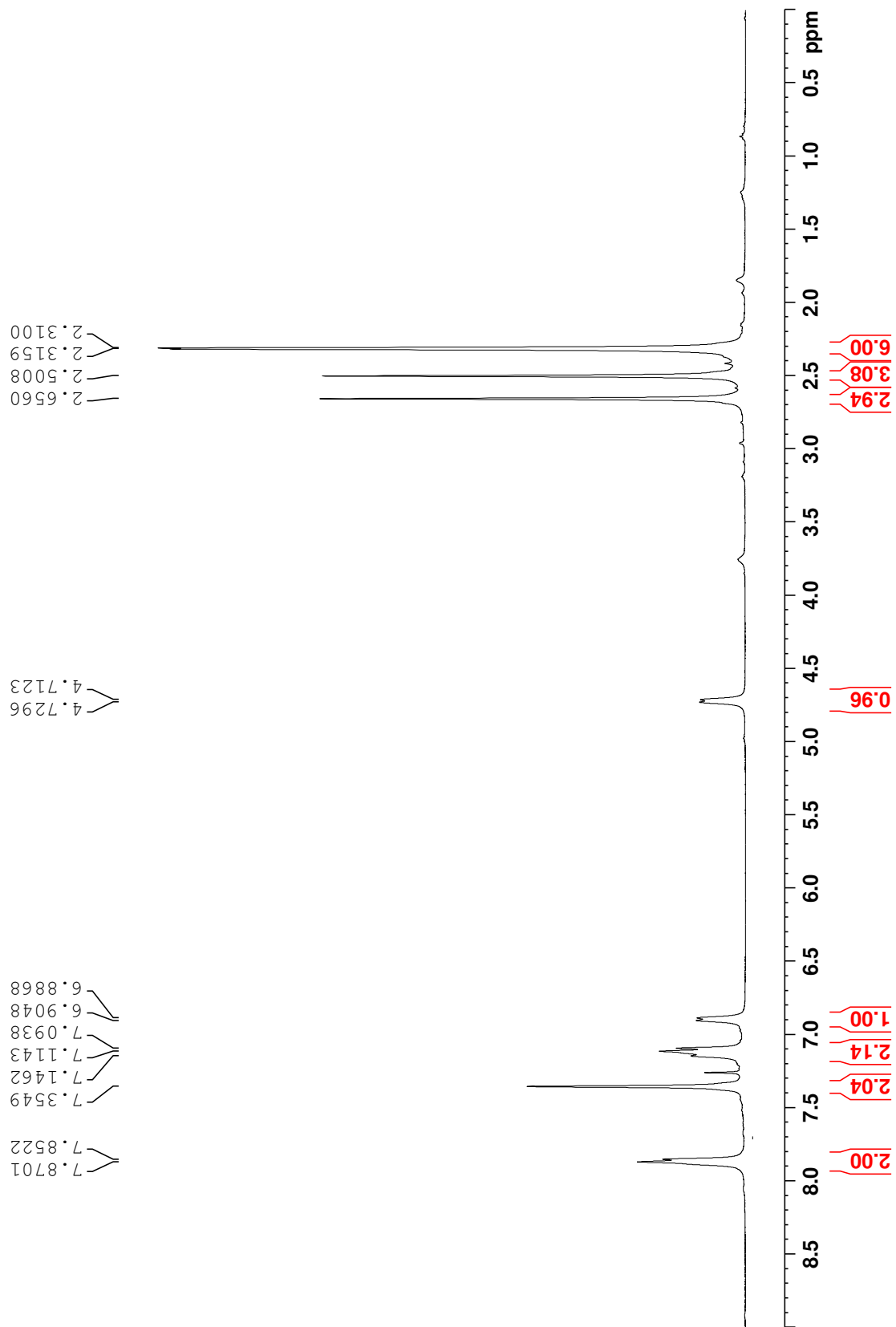
AlCl<sub>3</sub> (0.104 g, 0.780 mmol) was weighed into a 125 mL flask equipped with a mechanical stirrer and THF (~20 mL) was added. In a separate vial, L<sub>Mes</sub> (0.250 g, 0.780 mmol) was weighed and dissolved in THF (~1.5 mL). The L<sub>Mes</sub> solution was added via pipette to the stirring AlCl<sub>3</sub> solution. KC<sub>8</sub> (0.327 g, 2.419 mmol) was added to the yellow solution as a bronze powder. A color change from yellow to green was observed, at which point the formation of graphite powder turned the solution black. This black solution was let to stir for 24 h at room temperature. The solution was filtered over a Celite-padded frit and solvents were removed to give a yellow powder in 77% yield (0.504 g, 0.600 mmol). [(L<sub>Mes</sub><sup>2-</sup>)(THF)Al–Al(THF)(L<sub>Mes</sub><sup>2-</sup>)] crystals suitable for X-ray diffraction were obtained from a THF/toluene slow evaporation at -25 °C.

## 5.2 Spectra

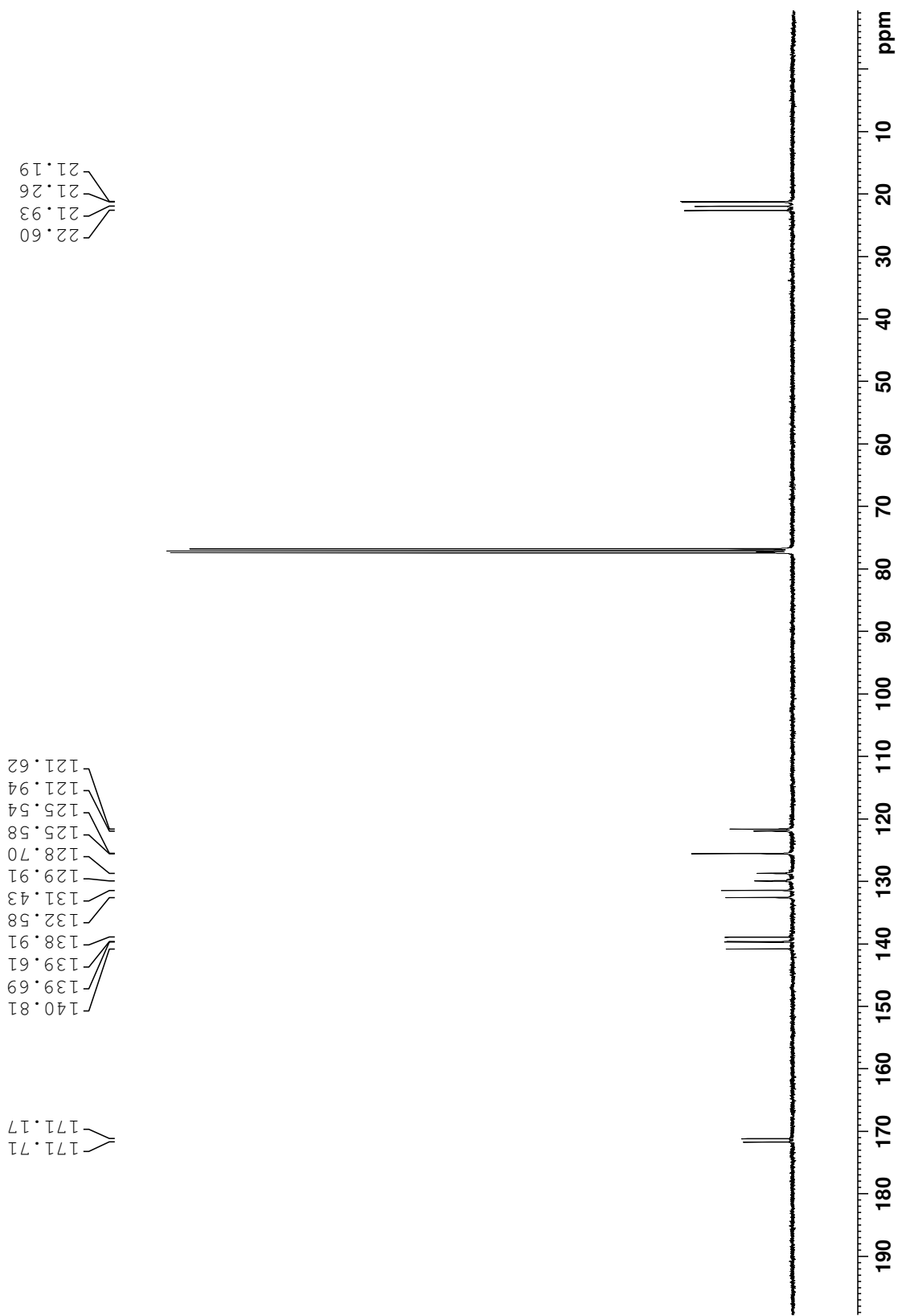
FIGURE S1. $^{13}\text{C}$ NMR SPECTRUM OF $[\text{Al}(\text{L}_{\text{PH}})_2\text{I}_2]\cdot\text{I}$ (1) IN $\text{CDCl}_3$ AT 25 °C. ....	S10
FIGURE S2. $^1\text{H}$ NMR SPECTRUM OF $[\text{Al}(\text{L}_{\text{TOl}})_2\text{I}_2]\cdot\text{I}$ (2) IN $\text{CDCl}_3$ AT 25 °C. ....	S11
FIGURE S3. $^{13}\text{C}$ NMR SPECTRUM OF $[\text{Al}(\text{L}_{\text{TOl}})_2\text{I}_2]\cdot\text{I}$ (2) IN $\text{CDCl}_3$ AT 25 °C. ....	S12
FIGURE S4. $^1\text{H}$ NMR SPECTRUM OF $[\text{Al}(\text{L}_{\text{TBU}})_2\text{I}_2]\cdot\text{I}$ (3) IN $\text{CDCl}_3$ AT 25 °C. ....	S13
FIGURE S5. $^{13}\text{C}$ NMR SPECTRUM OF $[\text{Al}(\text{L}_{\text{TBU}})_2\text{I}_2]\cdot\text{I}$ (3) IN $\text{CDCl}_3$ AT 25 °C. ....	S14
FIGURE S6. $^1\text{H}$ NMR SPECTRUM OF $[\text{Al}(\text{L}_{\text{PH}})_2(\text{NCME})_2]\cdot 3\text{I}$ (4) IN $\text{CDCl}_3$ AT 25 °C. ....	S15
FIGURE S7. SIMULATED $^1\text{H}$ NMR SPECTRUM OF $[\text{Al}(\text{L}_{\text{PH}})_2(\text{NCME})_2]\cdot 3\text{I}$ (4) IN $\text{CDCl}_3$ . ....	S16
FIGURE S8. $^{13}\text{C}$ NMR SPECTRUM OF $[\text{Al}(\text{L}_{\text{PH}})_2(\text{NCME})_2]\cdot 3\text{I}$ (4) IN $\text{CDCl}_3$ AT 25 °C. ....	S17
FIGURE S9. $^1\text{H}$ NMR SPECTRUM OF $[\text{Al}(\text{L}_{\text{TOl}})_2(\text{NCME})_2]\cdot 3\text{I}$ (5) IN $\text{CDCl}_3$ AT 25 °C. ....	S18
FIGURE S10. $^{13}\text{C}$ NMR SPECTRUM OF $[\text{Al}(\text{L}_{\text{TOl}})_2(\text{NCME})_2]\cdot 3\text{I}$ (5) IN $\text{CDCl}_3$ AT 25 °C. ....	S19
FIGURE S11. $^1\text{H}$ NMR SPECTRUM OF $[\text{Al}(\text{L}_{\text{TBU}})_2(\text{NCME})_2]\cdot 3\text{I}$ (6) IN $\text{CDCl}_3$ AT 25 °C. ....	S20
FIGURE S12. $^{13}\text{C}$ NMR SPECTRUM OF $[\text{Al}(\text{L}_{\text{TBU}})_2(\text{NCME})_2]\cdot 3\text{I}$ (6) IN $\text{CDCl}_3$ AT 25 °C. ....	S21
FIGURE S13. $^1\text{H}$ NMR SPECTRUM OF $[\text{Al}(\text{L}_{\text{PH}})_2(\text{P}(\text{OET})_3)_2]\cdot 3\text{I}$ (7) IN $\text{CDCl}_3$ AT 25 °C. ....	S22
FIGURE S14. $^{31}\text{P}$ NMR SPECTRUM OF $[\text{Al}(\text{L}_{\text{PH}})_2(\text{P}(\text{OET})_3)_2]\cdot 3\text{I}$ (7) IN $\text{CDCl}_3$ AT 25 °C. ....	S23
FIGURE S15. $^1\text{H}$ NMR SPECTRUM OF $\text{Al}(\text{L}_{\text{MES}}^-)\text{ME}_2$ (9) IN $\text{C}_6\text{D}_6$ AT 25 °C. ....	S24
FIGURE S16. $^1\text{H}$ NMR SPECTRUM OF $[(\text{L}_{\text{MES}}^{2-})(\text{THF})\text{Al}-\text{Al}(\text{THF})(\text{L}_{\text{MES}}^{2-})]$ (11) IN $\text{C}_6\text{D}_6$ AT 25 °C. ....	S25



**Figure S1.**  $^{13}\text{C}$  NMR spectrum of  $[\text{Al}(\text{LPhI})_2\text{I}_2] \cdot \text{I}$  (1) in  $\text{CDCl}_3$  at  $25^\circ\text{C}$ .

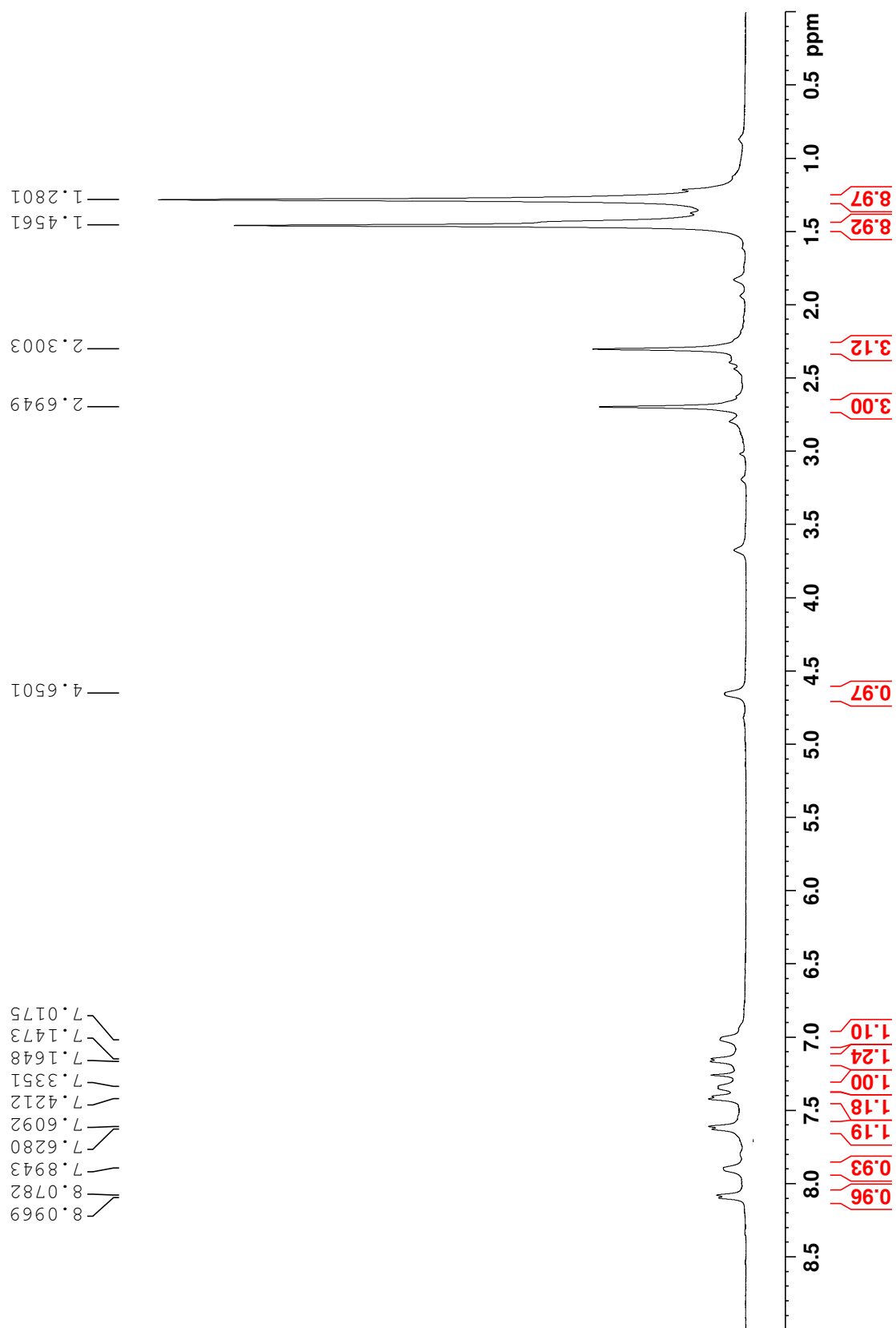


**Figure S2.**  $^1\text{H}$  NMR spectrum of  $[\text{Al}(\text{L}_{\text{Tol}})_2]_2 \cdot \text{I}$  (2) in  $\text{CDCl}_3$  at  $25^\circ\text{C}$ .

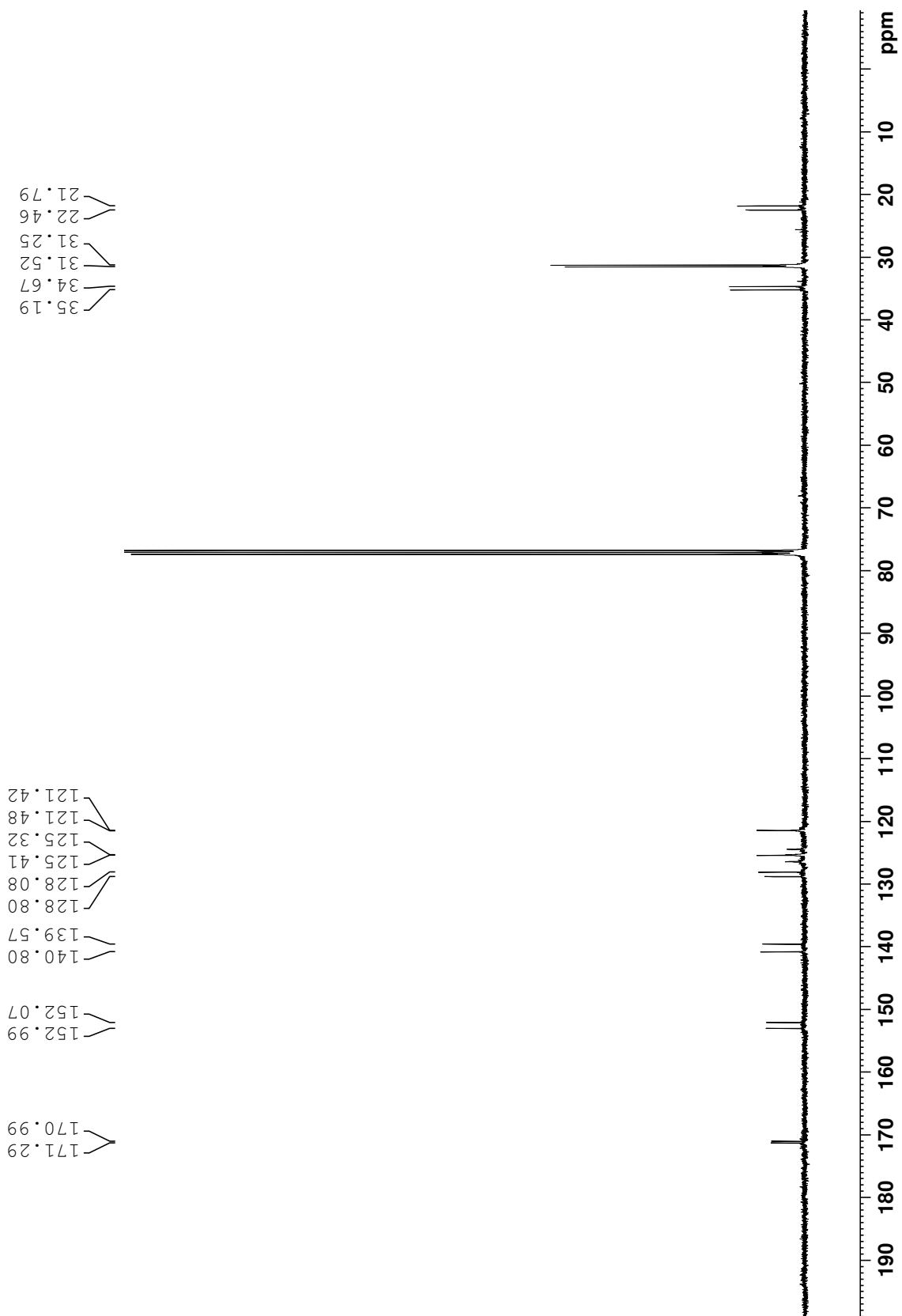


**Figure S3.**  $^{13}\text{C}$  NMR spectrum of  $[\text{Al}(\text{L}_{\text{Tol}})_2\text{I}_2]\cdot\text{I}$  (2) in  $\text{CDCl}_3$  at  $25^\circ\text{C}$ .



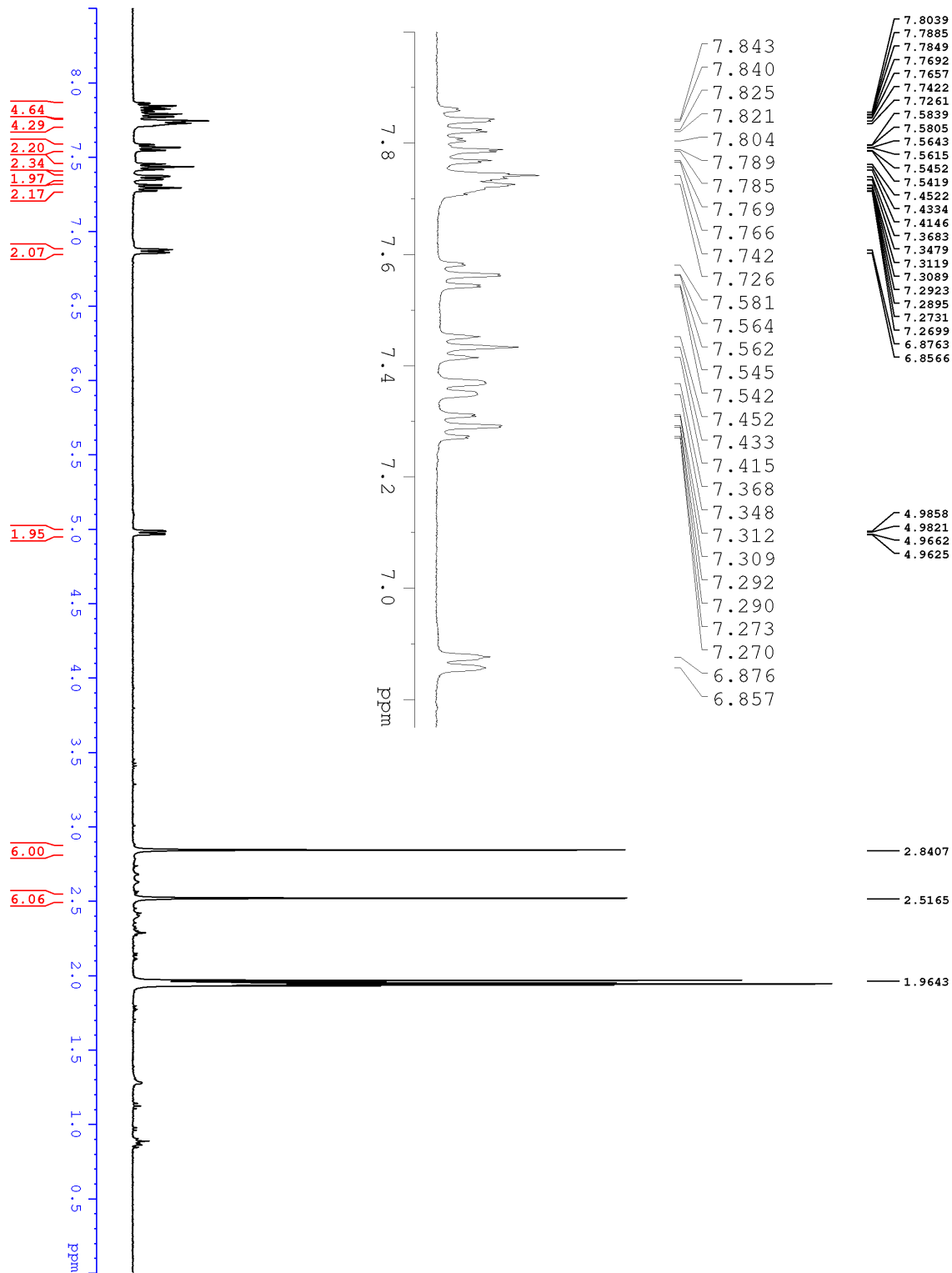


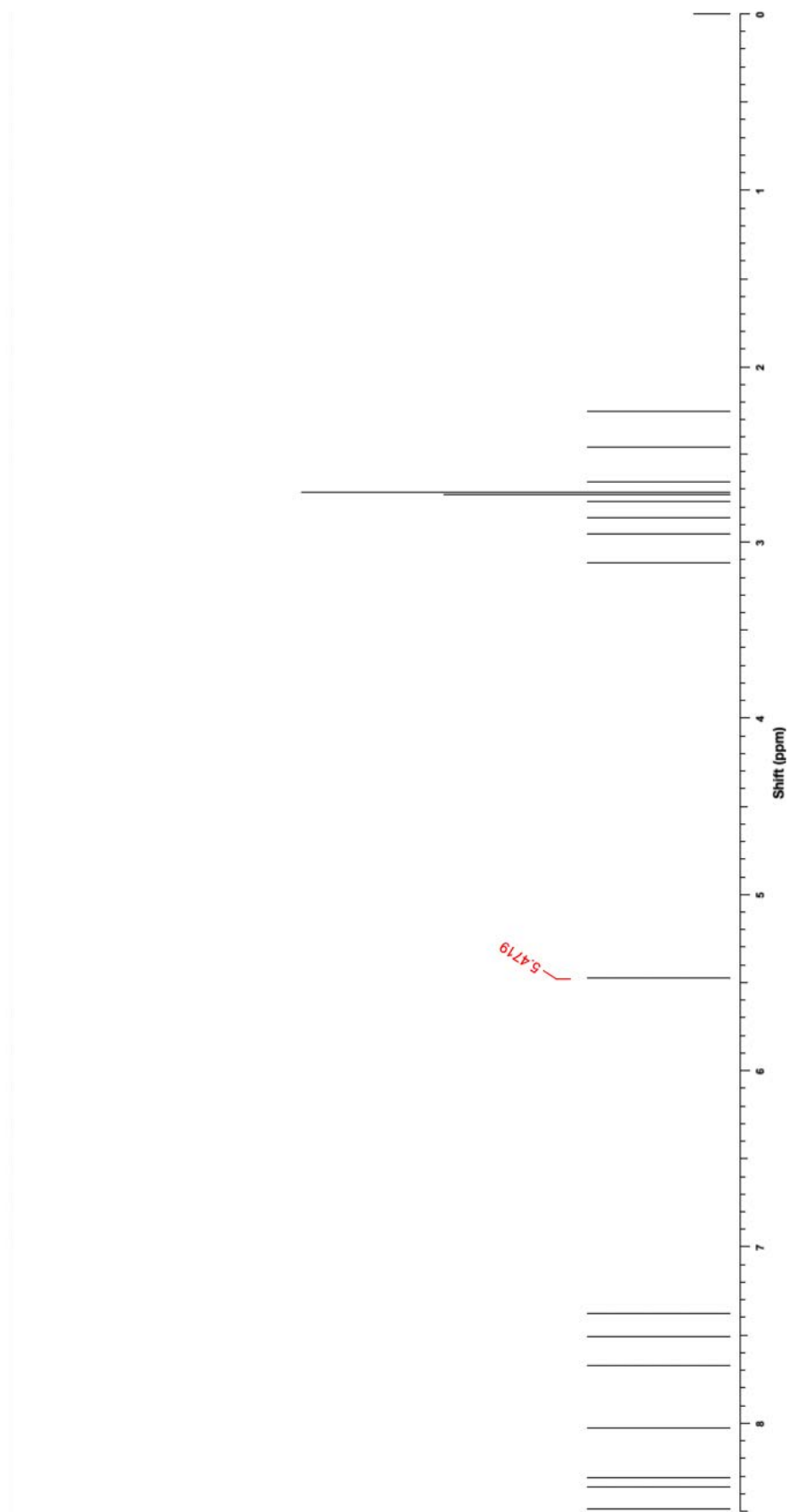
**Figure S4.**  $^1\text{H}$  NMR spectrum of  $[\text{Al}(\text{L}_{\text{tBu}})_2\text{I}_2] \cdot \text{I}$  (**3**) in  $\text{CDCl}_3$  at  $25^\circ\text{C}$ .



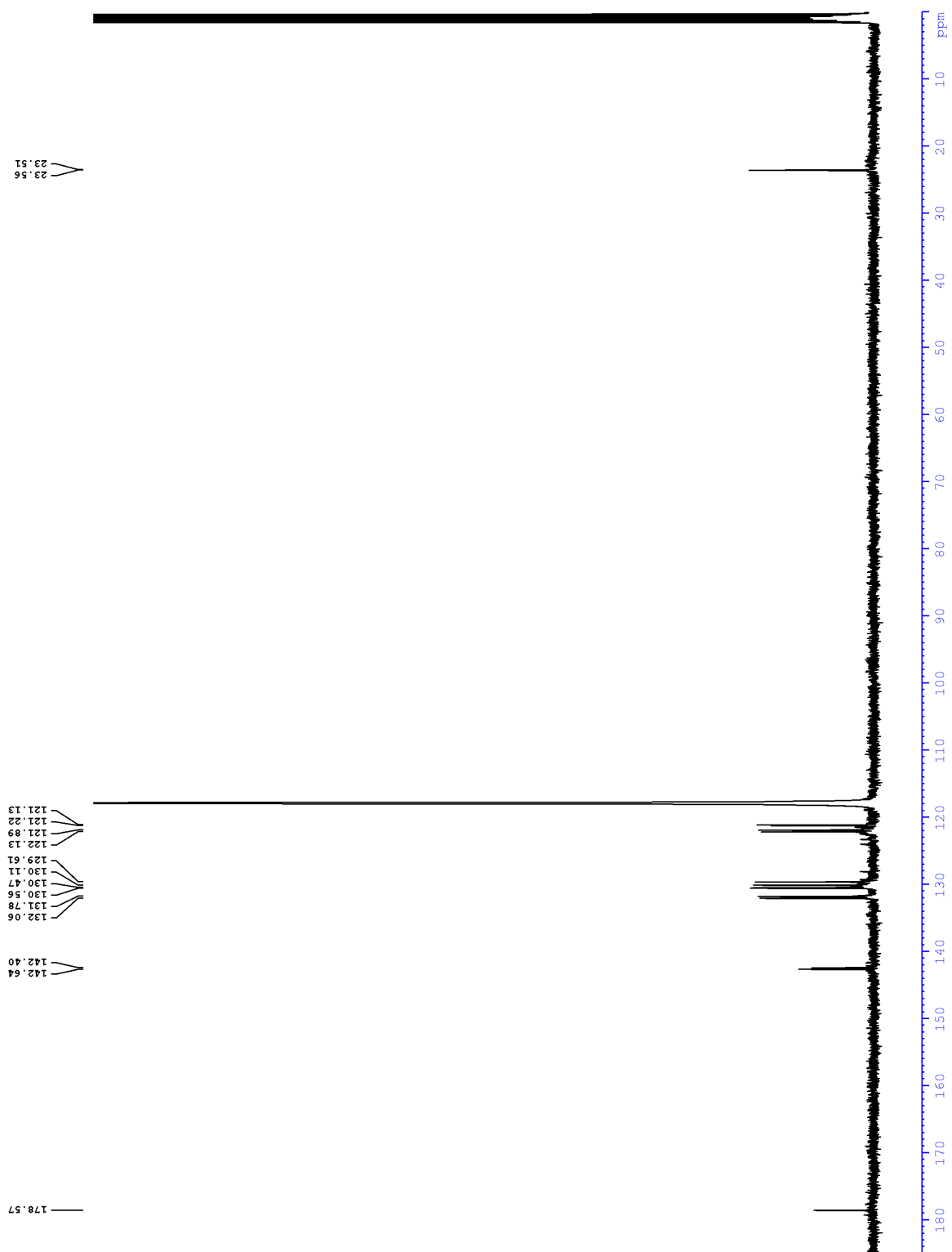
**Figure S5.**  $^{13}\text{C}$  NMR spectrum of  $[\text{Al}(\text{L}_{t\text{Bu}})_2]_2 \cdot \text{I}$  (3) in  $\text{CDCl}_3$  at  $25^\circ\text{C}$ .

Figure S6.  $^1\text{H}$  NMR spectrum of  $[\text{Al}(\text{L}^{\text{Ph}})_2(\text{NMe}_2)_2] \cdot 31$  (**4**) in  $\text{CDCl}_3$  at 25 °C. Previously reported by Wilson et. al.<sup>18</sup>





**Figure S7.** Simulated  $^1\text{H}$  NMR spectrum of  $[\text{Al}(\text{L}_{\text{Ph}})_2(\text{NCMe})_2] \cdot 3\text{I}$  (**4**) in  $\text{CDCl}_3$ .



**Figure S8.**  $^{13}\text{C}$  NMR spectrum of  $[\text{Al}(\text{L}_{\text{Ph}})_2(\text{NCMe})_2] \cdot 3\text{I}$  (4) in  $\text{CDCl}_3$  at  $25^\circ\text{C}$ . Previously reported by Wilson et. al.<sup>18</sup>

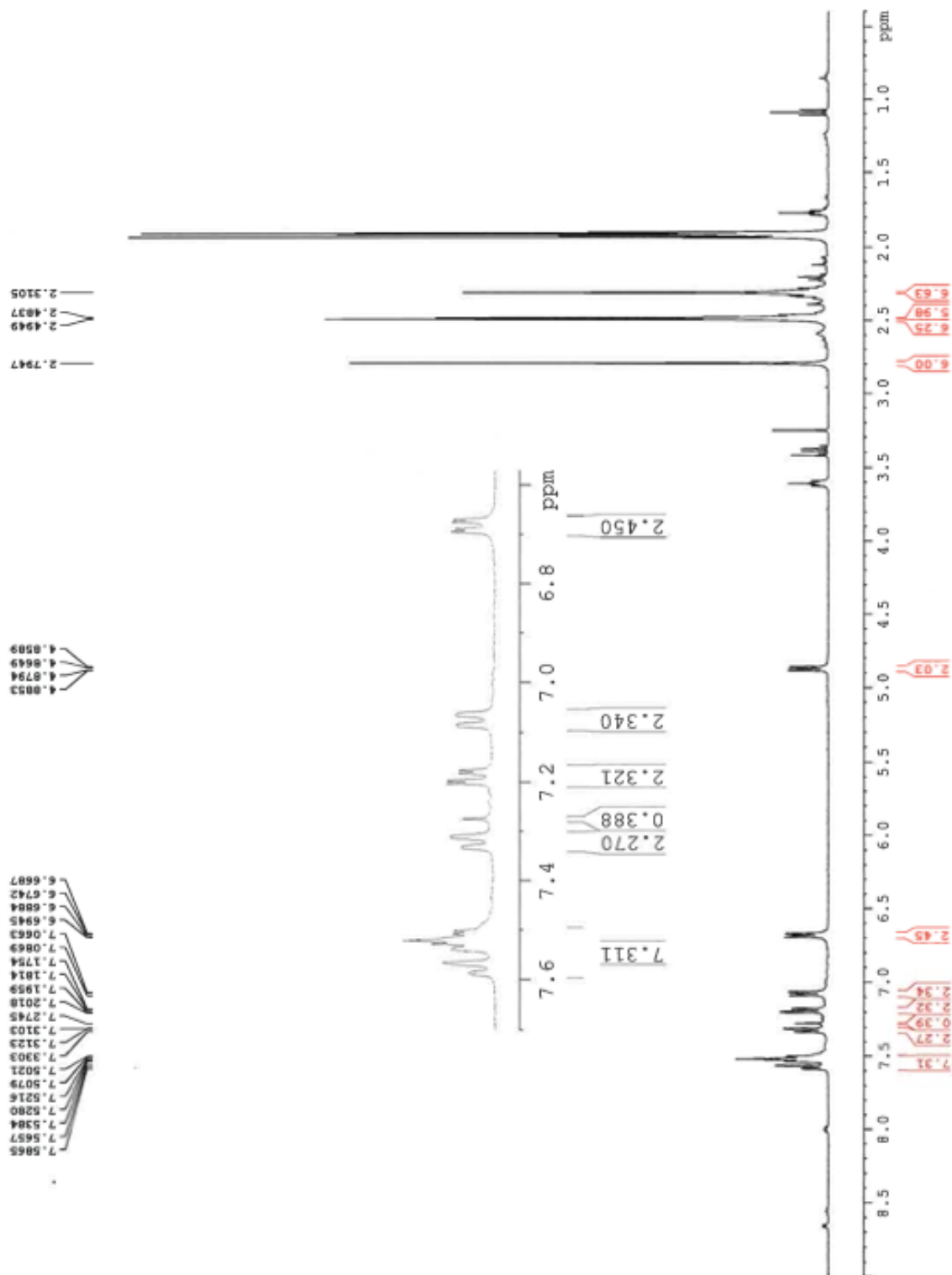


**Figure S9.** <sup>1</sup>H NMR spectrum of [Al(L<sub>Tol</sub>)<sub>2</sub>(NCMe)<sub>2</sub>]•3I (5) in CDCl<sub>3</sub> at 25 °C.

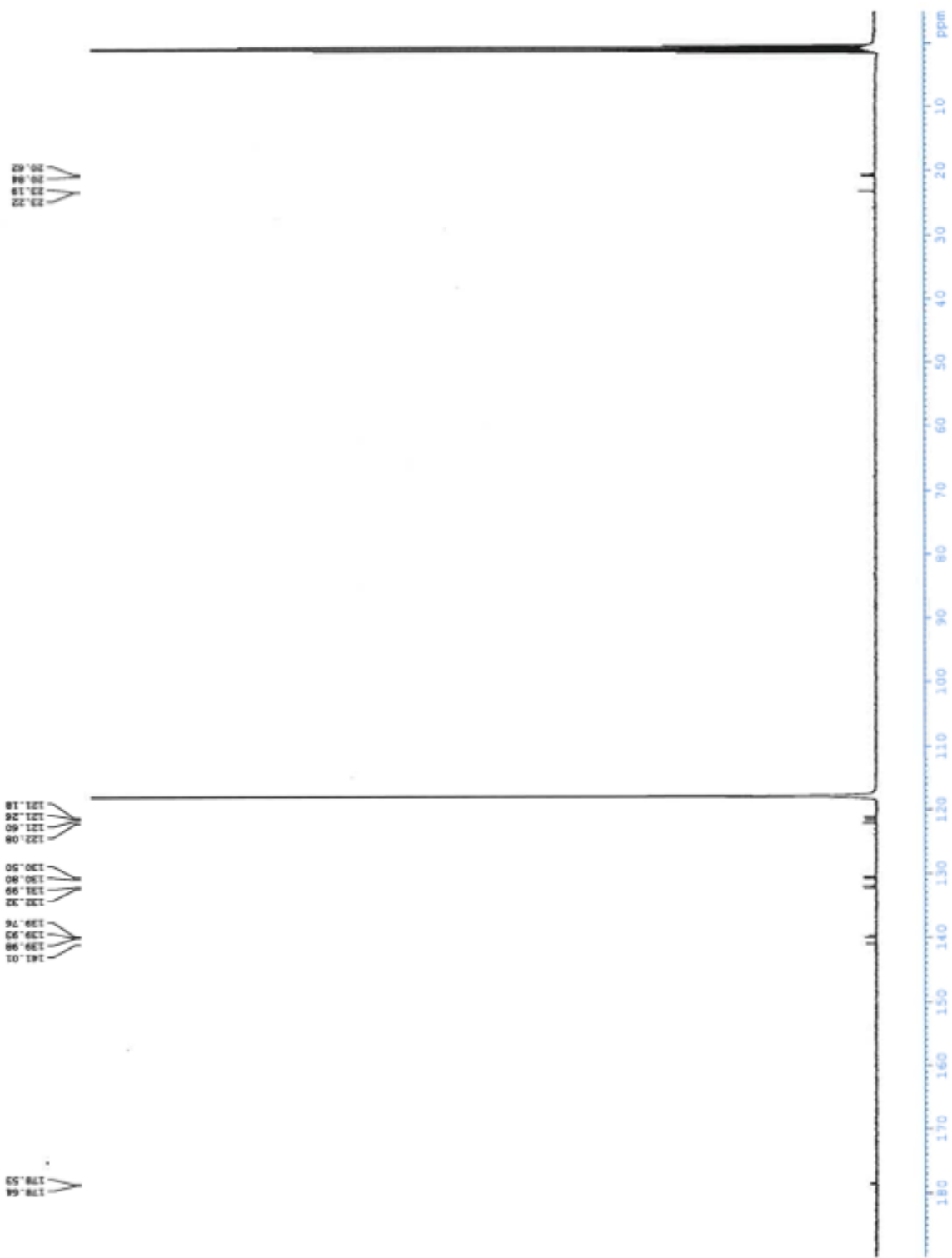


**Figure S10.**  $^{13}\text{C}$  NMR spectrum of  $[\text{Al}(\text{L}_{\text{Tol}})_2(\text{NCMe})_2]\cdot 3\text{I}$  (**5**) in  $\text{CDCl}_3$  at  $25\text{ }^\circ\text{C}$ .

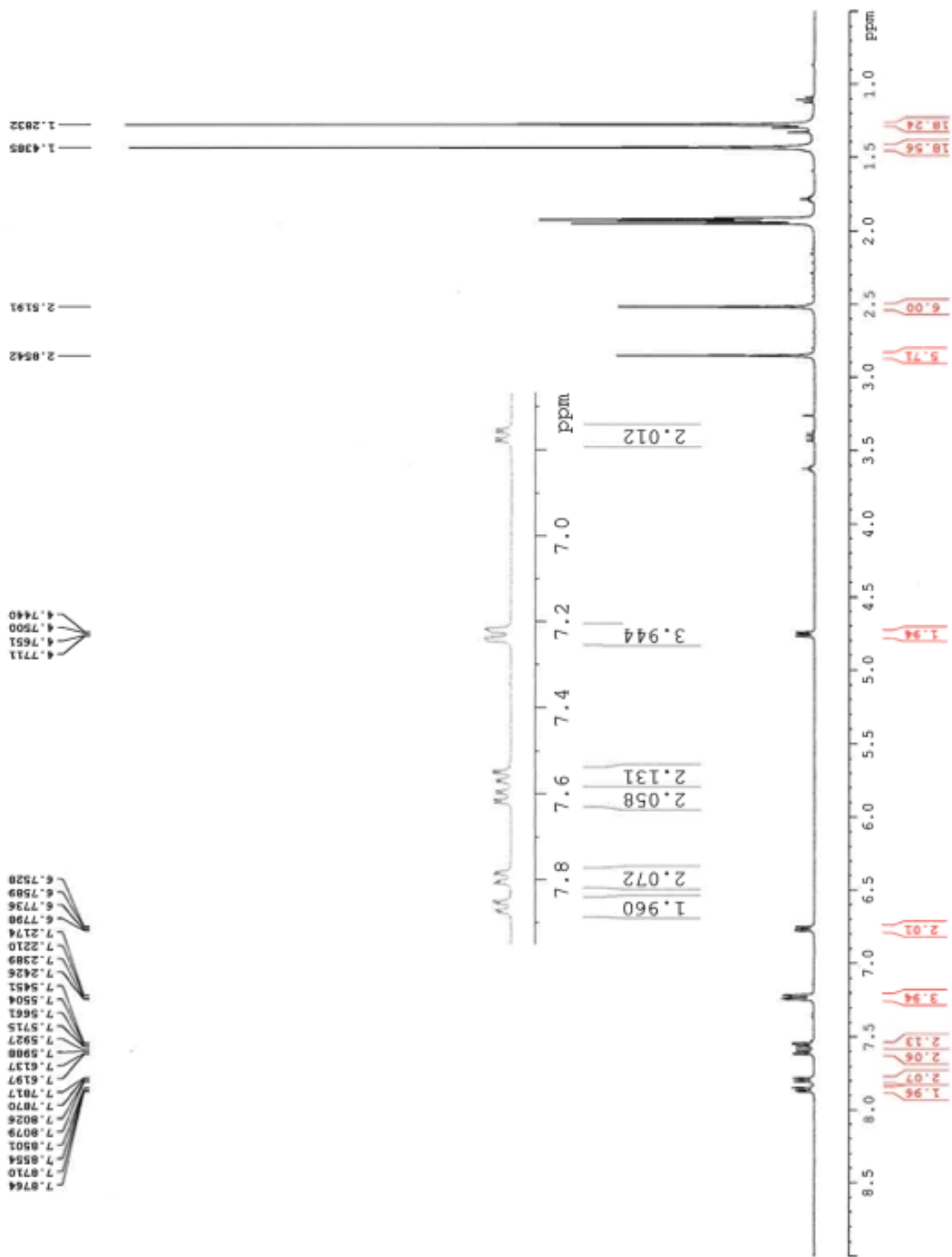


**Figure S11.**  $^1\text{H}$  NMR spectrum of  $[\text{Al}(\text{L}_{t\text{Bu}})_2(\text{NCMe})_2] \cdot 3\text{I}$  (**6**) in  $\text{CDCl}_3$  at  $25\text{ }^\circ\text{C}$ .



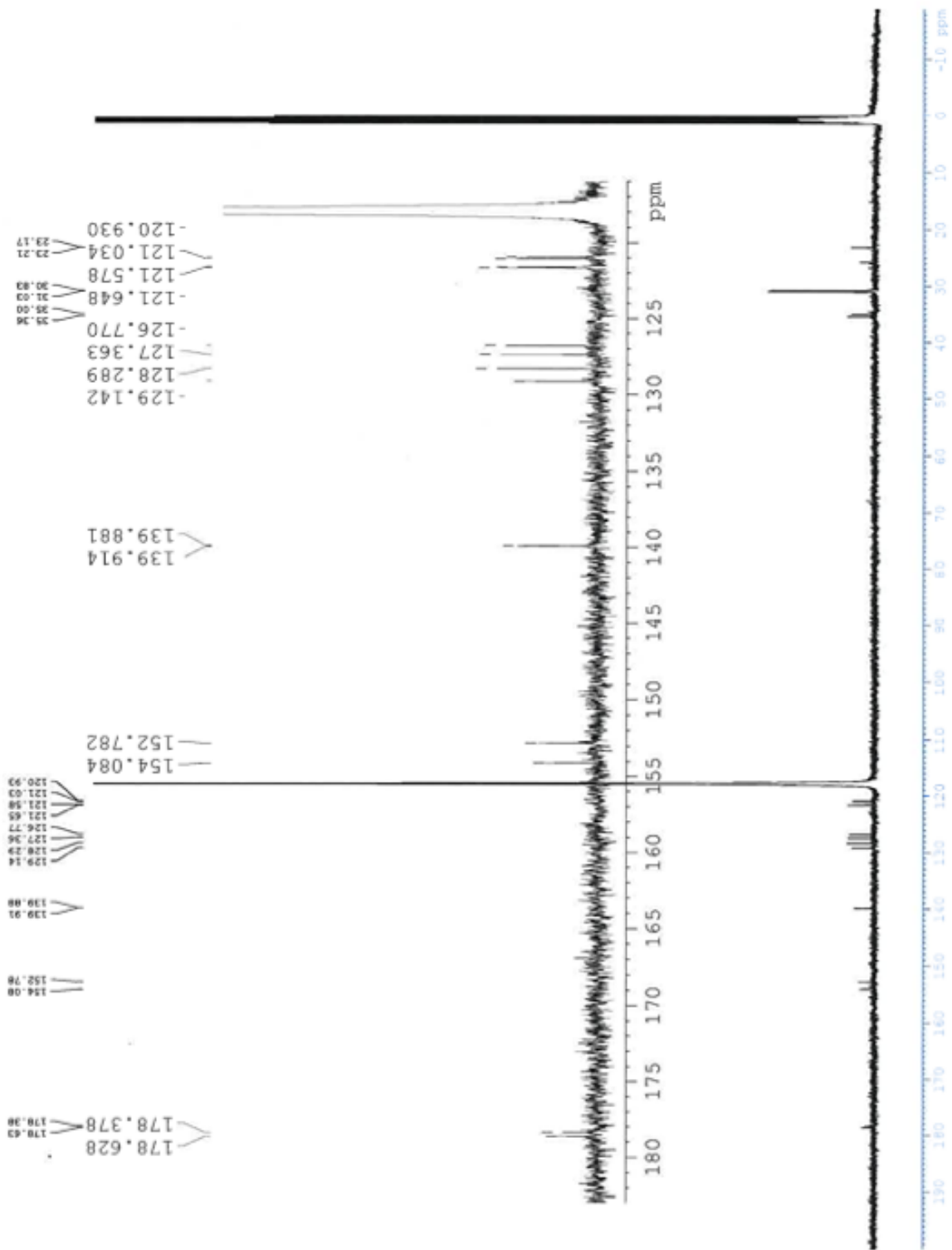


**Figure S12.**  $^{13}\text{C}$  NMR spectrum of  $[\text{Al}(\text{L}_{t\text{Bu}})_2(\text{NCMe})_2] \cdot 3\text{I}$  (**6**) in  $\text{CDCl}_3$  at  $25^\circ\text{C}$ .

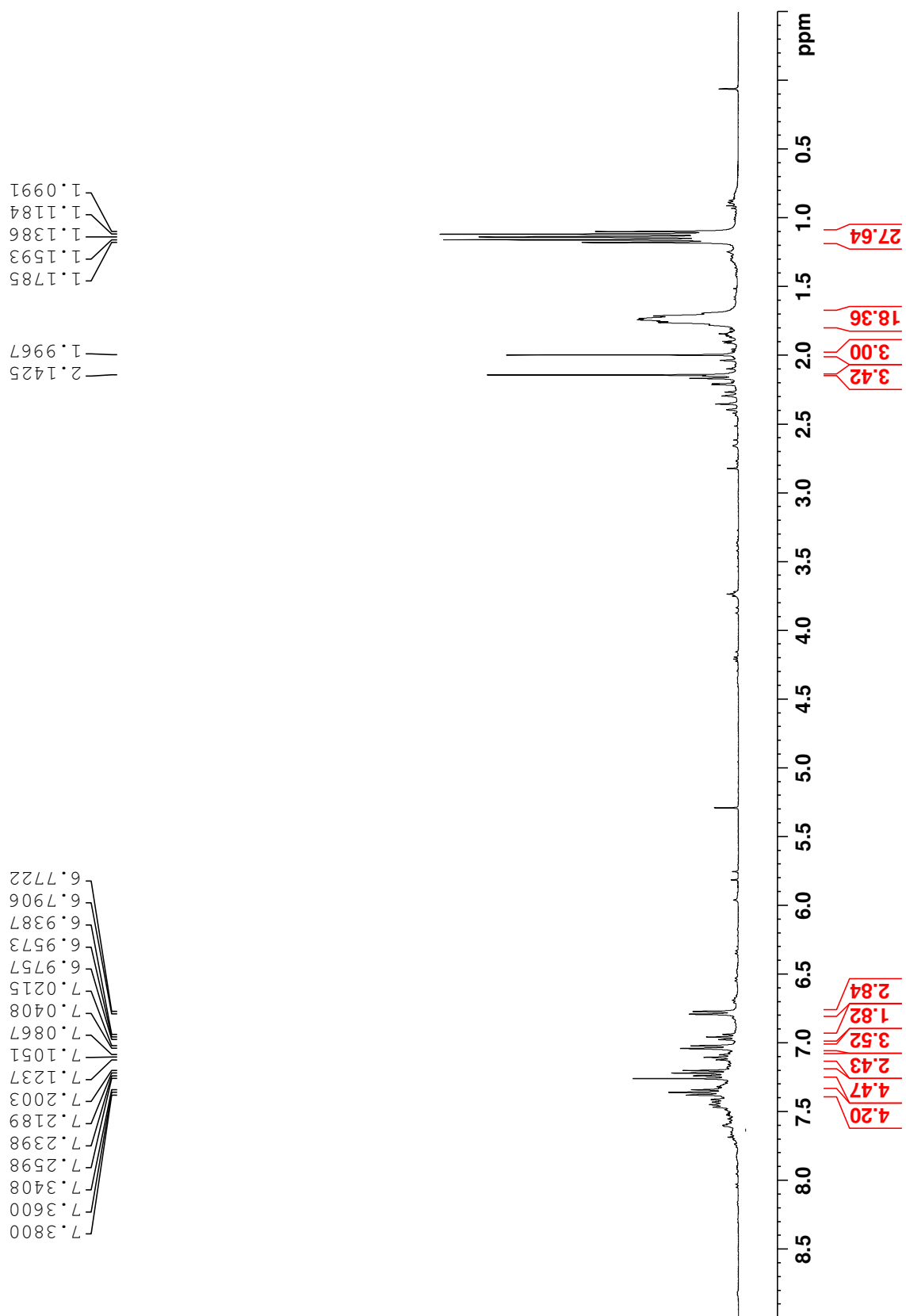


**Figure S13.**  $^1\text{H}$  NMR spectrum of  $[\text{Al}(\text{L}_{\text{Ph}})_2(\text{P}(\text{OEt})_3)_2] \cdot 3\text{I}$  (7) in  $\text{CDCl}_3$  at  $25^\circ\text{C}$ .

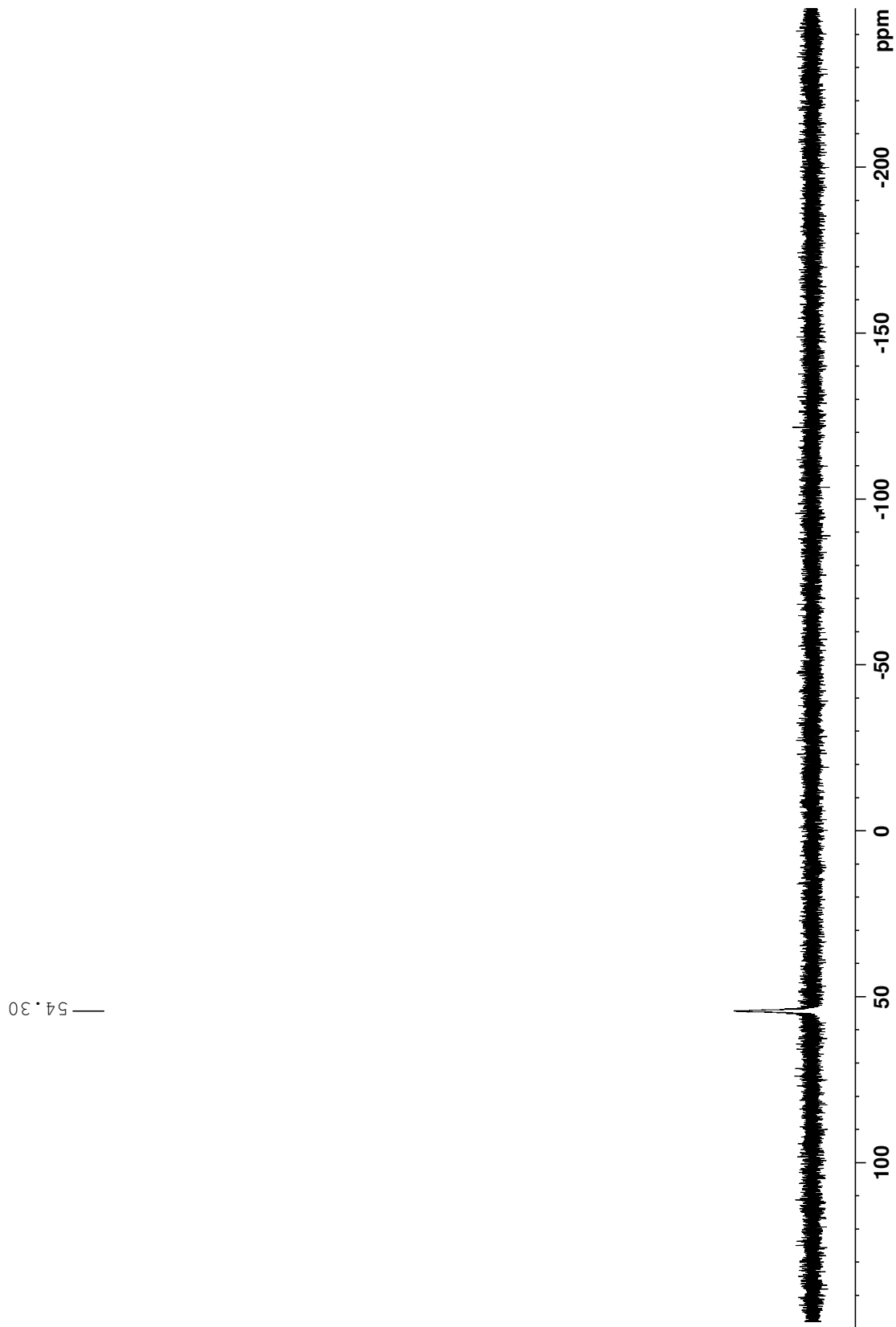


**Figure S14.**  $^{31}\text{P}$  NMR spectrum of  $[\text{Al}(\text{L}_{\text{Ph}})_2(\text{P}(\text{OEt})_3)_2] \cdot 3\text{I}$  (7) in  $\text{CDCl}_3$  at 25 °C.

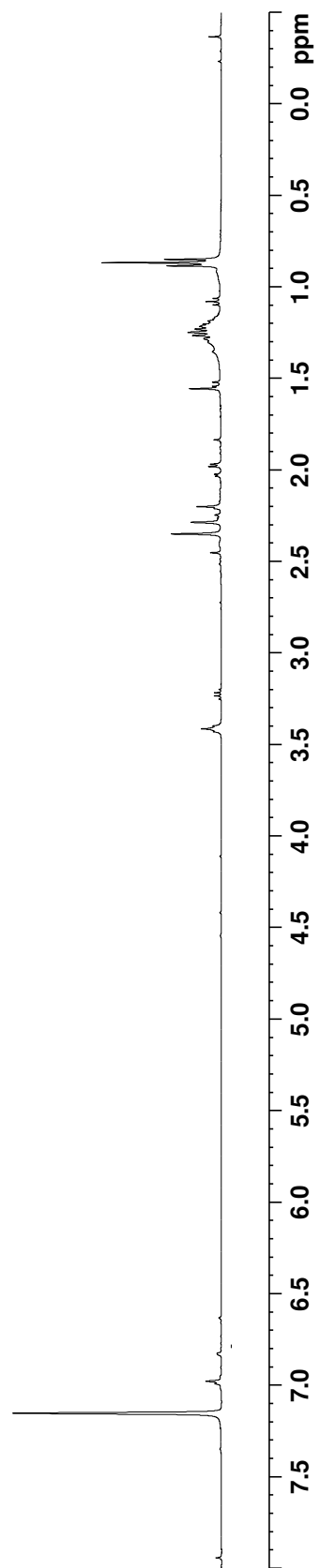


**Figure S15.**  $^1\text{H}$  NMR spectrum of  $\text{Al}(\text{LMes}^-)\text{Me}_2$  (**9**) in  $\text{C}_6\text{D}_6$  at 25 °C.

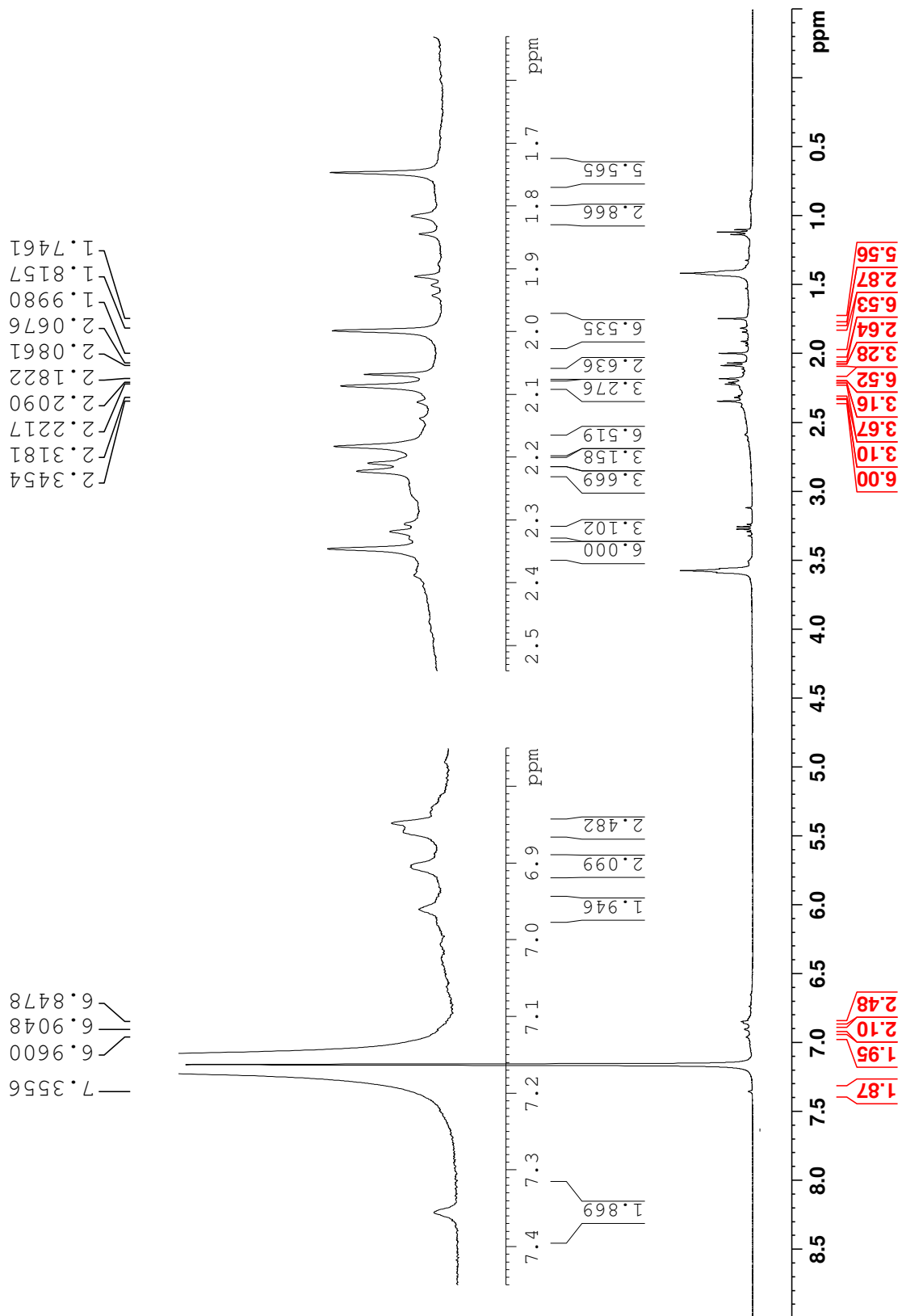


**Figure S16.**  $^1\text{H}$  NMR spectrum of  $[(\text{L}_{\text{Mes}}^{2-})(\text{THF})\text{Al}-\text{Al}(\text{THF})(\text{L}_{\text{Mes}}^{2-})]$  (11) in  $\text{C}_6\text{D}_6$  at  $25\text{ }^\circ\text{C}$ .

### 5.3 X-ray structure determination

X-ray diffraction data for **1–3**, and **6** were collected on either a Bruker D8QUEST<sup>100</sup> CMOS area detector (**1** and **2**), a Bruker APEXII<sup>101</sup> CCD area detector (**3** and **6**), both of which employ graphite-monochromated Mo-K $\alpha$  radiation ( $\lambda = 0.71073 \text{ \AA}$ ) at 100K. The rotation frames for these samples were integrated using SAINT<sup>102</sup>, producing a list of unaveraged  $F^2$  and  $\sigma(F^2)$  values for which the intensity values were corrected for Lorentz and polarization effects and for absorption using SADABS<sup>103</sup>. The structures were then solved by direct methods - ShelXT<sup>104</sup> in the case of **1** and **2** and direct methods - ShelXS-97<sup>105</sup> in the case of **3** and **6**. All structures were then refined by full-matrix least squares based on  $F^2$  using SHELXL-2017<sup>106</sup>. All non-hydrogen atoms were refined anisotropically and hydrogen atoms were refined using a riding model.

X-ray diffraction data for **5** was collected on a Bruker APEXII<sup>101</sup> CCD area detector employing graphite-monochromated Mo-K $\alpha$  radiation ( $\lambda = 0.71073 \text{ \AA}$ ) at 100K. The crystal grew as a non-merohedral twin, and the program CELL\_NOW<sup>107</sup> was used to index the diffraction images and determine the twinning mechanism. The crystal was twinned by a rotation of  $180^\circ$  about the 010 reciprocal direction. The rotation frame for this sample was integrated using SAINT<sup>102</sup>, producing a list of unaveraged  $F^2$  and  $\sigma(F^2)$  values for which the intensity values were corrected for Lorentz and polarization effects and for absorption using TWINABS<sup>108</sup>. The structure was then solved by direct methods - ShelXT<sup>104</sup>. The structure was then refined by full-matrix least squares based on  $F^2$  using SHELXL-2017<sup>106</sup>. All non-

hydrogen atoms were refined anisotropically and hydrogen atoms were refined using a riding model.

X-ray diffraction data for **8** was collection on a Rigaku XtaLAB Synergy-S diffractometer equipped with an HPC area detector (HyPix-6000HE) and employing confocal multilayer optic-monochromated Mo-K $\alpha$  radiation ( $\lambda = 0.71073$  Å) at 100K. The rotation frames for this sample were integrated using CrysAlisPro<sup>109</sup>, producing a list of unaveraged  $F^2$  and  $\sigma(F^2)$  values for which the intensity values were corrected for Lorentz and polarization effects and for absorption using SCALE3 ABSPACK<sup>110</sup>. The structure was then solved by direct methods - ShelXT<sup>101</sup> and refined by full-matrix least squares based on  $F^2$  using SHELXL-2018<sup>111</sup>. All non-hydrogen atoms were refined anisotropically and hydrogen atoms were refined using a riding model.

X-ray diffraction data for **9** was collected on a Bruker APEXII<sup>101</sup> CCD area detector employing graphite-monochromated Mo-K $\alpha$  radiation ( $\lambda = 0.71073$  Å) at 100K. The rotation frames for this sample were integrated using SAINT<sup>102</sup>, producing a list of unaveraged  $F^2$  and  $\sigma(F^2)$  values for which the intensity values were corrected for Lorentz and polarization effects and for absorption using SADABS<sup>103</sup>. The structure was then solved by direct methods - ShelXS-97<sup>105</sup>. The structure was then refined by full-matrix least squares based on  $F^2$  using SHELXL-2017<sup>106</sup>. All non-hydrogen atoms were refined anisotropically and hydrogen atoms were refined using a riding model.

X-ray diffraction data for **10** was collected on a Bruker D8QUEST<sup>100</sup> CMOS area detector employing graphite-monochromated Mo-K $\alpha$  radiation ( $\lambda = 0.71073$

Å) at 100K. The rotation frames for these samples were integrated using SAINT<sup>102</sup>, producing a list of unaveraged  $F^2$  and  $\sigma(F^2)$  values for which the intensity values were corrected for Lorentz and polarization effects and for absorption using SADABS<sup>103</sup>. The structures were then solved by direct methods - ShelXT<sup>104</sup>. All structures were then refined by full-matrix least squares based on  $F^2$  using SHELXL-2018<sup>111</sup>. All non-hydrogen atoms were refined anisotropically and hydrogen atoms were refined using a riding model.

X-ray diffraction data for **11** was collected on a Bruker D8QUEST<sup>100</sup> CMOS area detector employing graphite-monochromated Mo-K $\alpha$  radiation ( $\lambda = 0.71073$  Å) at 100K. The rotation frames for these samples were integrated using SAINT<sup>102</sup>, producing a list of unaveraged  $F^2$  and  $\sigma(F^2)$  values for which the intensity values were corrected for Lorentz and polarization effects and for absorption using SADABS<sup>103</sup>. The structures were then solved by direct methods - ShelXT<sup>104</sup>. All structures were then refined by full-matrix least squares based on  $F^2$  using SHELXL-2018<sup>111</sup>. All non-hydrogen atoms were refined anisotropically and hydrogen atoms were refined using a riding model.



**Table S1.** Summary of Structure Determination of [Al(L<sub>Ph</sub>)<sub>2</sub>I<sub>2</sub>]**·I (1)**:

Empirical formula	C <sub>32</sub> H <sub>32</sub> AlI <sub>3</sub> N <sub>4</sub>
Formula weight	880.32 g/mol
Temperature	100 K
Wavelength	0.71073 Å
Crystal system	monoclinic
Space group	P2 <sub>1</sub> /n
Cell constants:	
a	15.7424(11) Å
b	10.1222(7) Å
c	23.0345(16) Å
β	100.184(2)°
Volume	3612.7(4) Å <sup>3</sup>
Z	4
Density (calculated)	1.775 g/cm <sup>3</sup>
Absorption coefficient	2.796 mm <sup>-1</sup>
F(000)	1864.0
Crystal size	0.33 x 0.09 x 0.04 mm <sup>3</sup>
2θ range for data collection	5.822 to 55.156°
Index ranges	-20 ≤ h ≤ 20, -13 ≤ k ≤ 13, -29 ≤ l ≤ 29
Reflections collected	126252
Independent reflections	8343 [R(int) = 0.0836]
Max. and min. transmission	0.7456 and 0.5445
Data / restraints / parameters	8343 / 0 / 392
Goodness-of-fit on F <sup>2</sup>	1.212
Final R indices [I ≥ 2σ (I)]	R <sub>1</sub> = 0.0638, wR <sub>2</sub> = 0.1502
R indices (all data)	R <sub>1</sub> = 0.0776, wR <sub>2</sub> = 0.1585
Largest diff. peak and hole	3.09 and -1.98 eÅ <sup>-3</sup>

**Table S2.** Summary of Structure Determination of  $[\text{Al}(\text{L}_{\text{Tot}})_2\text{I}_2]\cdot\text{I}$  (**2**):

Empirical formula	$\text{C}_{36}\text{H}_{40}\text{AlI}_3\text{N}_4$
Formula weight	936.42 g/mol
Temperature	100 K
Wavelength	0.71073 Å
Crystal system	monoclinic
Space group	$\text{P}2_1/\text{n}$
Cell constants:	
a	16.8972(6) Å
b	13.6452(5) Å
c	23.6248(9) Å
$\beta$	97.9400(10)°
Volume	5394.8(3) Å <sup>3</sup>
Z	4
Density (calculated)	1.676 g/cm <sup>3</sup>
Absorption coefficient	2.282 mm <sup>-1</sup>
F(000)	2664.0
Crystal size	0.17 x 0.13 x 0.11 mm <sup>3</sup>
2 $\theta$ range for data collection	5.772 to 55.082°
Index ranges	-21 ≤ h ≤ 21, -17 ≤ k ≤ 17, -30 ≤ l ≤ 30
Reflections collected	89797
Independent reflections	12411 [R(int) = 0.0807]
Max. and min. transmission	0.7456 and 0.6569
Data / restraints / parameters	12411 / 144 / 633
Goodness-of-fit on F <sup>2</sup>	1.143
Final R indices [I ≥ 2σ (I)]	R <sub>1</sub> = 0.0520, wR <sub>2</sub> = 0.0802
R indices (all data)	R <sub>1</sub> = 0.0781, wR <sub>2</sub> = 0.0890
Largest diff. peak and hole	0.97 and -1.50 eÅ <sup>-3</sup>

**Table S3.** Summary of Structure Determination of [Al(L<sub>t</sub>Bu)<sub>2</sub>I<sub>2</sub>]**·**I (**3**):

Empirical formula	C <sub>48</sub> H <sub>64</sub> AlI <sub>3</sub> N <sub>4</sub>
Formula weight	1104.74 g/mol
Temperature	100 K
Wavelength	0.71073 Å
Crystal system	monoclinic
Space group	P2 <sub>1</sub> /n
Cell constants:	
a	17.0949(17) Å
b	9.8555(10) Å
c	35.321(4) Å
β	101.433(6)°
Volume	5832.7(10) Å <sup>3</sup>
Z	4
Density (calculated)	1.451 g/cm <sup>3</sup>
Absorption coefficient	1.840 mm <sup>-1</sup>
F(000)	2544.0
Crystal size	0.14 x 0.11 x 0.05
2θ range for data collection	2.482 to 55.272°
Index ranges	-22 ≤ h ≤ 22, -12 ≤ k ≤ 12, -45 ≤ l ≤ 45
Reflections collected	89870
Independent reflections	13461 [R(int) = 0.0712]
Max. and min. transmission	0.7456 and 0.6449
Data / restraints / parameters	13461 / 18 / 575
Goodness-of-fit on F <sup>2</sup>	1.307
Final R indices [I ≥ 2σ (I)]	R <sub>1</sub> = 0.0979, wR <sub>2</sub> = 0.2162
R indices (all data)	R <sub>1</sub> = 0.1178, wR <sub>2</sub> = 0.2286
Largest diff. peak and hole	4.63 and -3.14 eÅ <sup>-3</sup>

**Table S4.** Summary of Structure Determination of [Al(L<sub>Tol</sub>)<sub>2</sub>(NCMe)<sub>2</sub>]•3I (**6**):

Empirical formula	C <sub>40</sub> H <sub>46</sub> AlI <sub>3</sub> N <sub>6</sub>
Formula weight	1018.53 g/mol
Temperature	100 K
Wavelength	0.71073 Å
Crystal system	triclinic
Space group	P
Cell constants:	
a	10.5938(10) Å
b	11.1597(10) Å
c	20.496(2) Å
α	94.088(2)°
β	91.264(2)°
γ	115.774(2)°
Volume	2172.7(4) Å <sup>3</sup>
Z	2
Density (calculated)	1.557 g/cm <sup>3</sup>
Absorption coefficient	2.212 mm <sup>-1</sup>
F(000)	1000.0
Crystal size	0.12 x 0.09 x 0.04
2θ range for data collection	3.992 to 55.102°
Index ranges	-13 ≤ h ≤ 13, -14 ≤ k ≤ 14, 0 ≤ l ≤ 26
Reflections collected	64670
Independent reflections	9768 [R(int) = 0.0412]
Max. and min. transmission	0.7456 and 0.6854
Data / restraints / parameters	9768 / 0 / 462
Goodness-of-fit on F <sup>2</sup>	1.056
Final R indices [I ≥ 2σ (I)]	R <sub>1</sub> = 0.0351, wR <sub>2</sub> = 0.0818
R indices (all data)	R <sub>1</sub> = 0.0496, wR <sub>2</sub> = 0.0885
Largest diff. peak and hole	1.24 and -1.35 eÅ <sup>-3</sup>

**Table S5.** Summary of Structure Determination of [Al(L<sub>t</sub>Bu)<sub>2</sub>(NCMe)<sub>2</sub>]<sub>3</sub>I (7):

Empirical formula	C <sub>52</sub> H <sub>70</sub> AlI <sub>3</sub> N <sub>6</sub>
Formula weight	1186.84 g/mol
Temperature	100 K
Wavelength	0.71073 Å
Crystal system	monoclinic
Space group	Cc
Cell constants:	
a	16.4854(16) Å
b	18.1248(17) Å
c	20.0270(18) Å
β	102.936(5)°
Volume	5832.1(10) Å <sup>3</sup>
Z	4
Density (calculated)	1.398 g/cm <sup>3</sup>
Absorption coefficient	1.661 mm <sup>-1</sup>
F(000)	2472.0
Crystal size	0.16 x 0.06 x 0.05 mm <sup>3</sup>
2θ range for data collection	3.3888 to 55.024°
Index ranges	-21 ≤ h ≤ 21, -23 ≤ k ≤ 23, -25 ≤ l ≤ 25
Reflections collected	46722
Independent reflections	13339[R(int) = 0.0271]
Max. and min. transmission	0.7456 and 0.6550
Data / restraints / parameters	13339 / 2 / 605
Goodness-of-fit on F <sup>2</sup>	1.052
Final R indices [I ≥ 2σ (I)]	R <sub>1</sub> = 0.0415, wR <sub>2</sub> = 0.1106
R indices (all data)	R <sub>1</sub> = 0.0446, wR <sub>2</sub> = 0.1126
Largest diff. peak and hole	4.55 and -1.38 eÅ <sup>-3</sup>

**Table S6.** Summary of Structure Determination of [Al(L<sub>Ph</sub>)<sub>2</sub>(NCMe)<sub>2</sub>]•BPh<sub>4</sub>•2I (**8**):

Empirical formula	C <sub>60</sub> H <sub>58</sub> AlBI <sub>2</sub> N <sub>6</sub>
Formula weight	1154.74 g/mol
Temperature	100 K
Wavelength	0.71073 Å
Crystal system	monoclinic
Space group	Pc
Cell constants:	
a	15.8431(3) Å
b	20.3375(3) Å
c	19.5744(3) Å
β	110.552(2)°
Volume	5905.63(18) Å <sup>3</sup>
Z	4
Density (calculated)	1.391 g/cm <sup>3</sup>
Absorption coefficient	1.126 mm <sup>-1</sup>
F(000)	2512.0
Crystal size	0.31 x 0.24 x 0.09 mm <sup>3</sup>
2θ range for data collection	4.328 to 56.56°
Index ranges	-20 ≤ h ≤ 20, -26 ≤ k ≤ 27, -26 ≤ l ≤ 25
Reflections collected	99100
Independent reflections	27962[R(int) = 0.0382]
Max. and min. transmission	1.0000 and 0.6068
Data / restraints / parameters	27962 / 29 / 1379
Goodness-of-fit on F <sup>2</sup>	1.041
Final R indices [I ≥ 2σ (I)]	R <sub>1</sub> = 0.0302, wR <sub>2</sub> = 0.0681
R indices (all data)	R <sub>1</sub> = 0.0353, wR <sub>2</sub> = 0.0706
Largest diff. peak and hole	0.44 and -0.72 eÅ <sup>-3</sup>

**Table S7.** Summary of Structure Determination of Al(L<sub>Mes</sub><sup>-</sup>)Me<sub>2</sub> (**9**):

Empirical formula	C <sub>24</sub> H <sub>34</sub> N <sub>2</sub> Al
Formula weight	377.51 g/mol
Temperature	100 K
Wavelength	0.71073 Å
Crystal system	orthorhombic
Space group	Pnma
Cell constants:	
a	23.5077(12) Å
b	12.1639(6) Å
c	7.9018(4) Å
Volume	2259.5(2) Å <sup>3</sup>
Z	4
Density (calculated)	1.110 g/cm <sup>3</sup>
Absorption coefficient	0.100 mm <sup>-1</sup>
F(000)	820.0
Crystal size	0.35 x 0.12 x 0.1 mm <sup>3</sup>
2θ range for data collection	4.82 to 55.008°
Index ranges	-29 ≤ h ≤ 30, -15 ≤ k ≤ 14, -10 ≤ l ≤ 10
Reflections collected	37641
Independent reflections	2714[R(int) = 0.0291]
Max. and min. transmission	1.0000 and 0.6068
Data / restraints / parameters	2714 / 0 / 149
Goodness-of-fit on F <sup>2</sup>	1.078
Final R indices [I ≥ 2σ (I)]	R <sub>1</sub> = 0.0392, wR <sub>2</sub> = 0.1123
R indices (all data)	R <sub>1</sub> = 0.0439, wR <sub>2</sub> = 0.1165
Largest diff. peak and hole	0.44 and -0.27 eÅ <sup>-3</sup>

**Table S8.** Summary of Structure Determination of [Al(L<sub>HMe</sub>s<sup>-</sup>)Me<sub>2</sub>]<sub>2</sub> (**10**):

Empirical formula	C <sub>44</sub> H <sub>60</sub> Al <sub>2</sub> N <sub>4</sub>
Formula weight	698.92 g/mol
Temperature	100 K
Wavelength	0.71073 Å
Crystal system	triclinic
Space group	Pwith
Cell constants:	
a	8.1742(3) Å
b	11.0230(4) Å
c	11.7467(4) Å
α	96.2460(10)°
β	105.0240(10)°
γ	97.7320(10)°
Volume	1001.47(6) Å <sup>3</sup>
Z	1
Density (calculated)	1.159 g/cm <sup>3</sup>
Absorption coefficient	0.108 mm <sup>-1</sup>
F(000)	378.0
Crystal size	0.26 x 0.14 x 0.08 mm <sup>3</sup>
2θ range for data collection	6.456 to 55.102°
Index ranges	-10 ≤ h ≤ 10, -14 ≤ k ≤ 14, -15 ≤ l ≤ 15
Reflections collected	19793
Independent reflections	4602[R(int) = 0.0419]
Max. and min. transmission	0.7456 and 0.7033
Data / restraints / parameters	4602 / 0 / 234
Goodness-of-fit on F <sup>2</sup>	1.039
Final R indices [I ≥ 2σ (I)]	R <sub>1</sub> = 0.0426, wR <sub>2</sub> = 0.0981
R indices (all data)	R <sub>1</sub> = 0.0560, wR <sub>2</sub> = 0.1044
Largest diff. peak and hole	0.31 and -0.25 eÅ <sup>-3</sup>



**Table S9.** Summary of Structure Determination of  $[\text{Al}(\text{L}_{\text{Mes}}^{2-})(\text{THF})_2]$  (**11**):

Empirical formula	$\text{C}_{52}\text{H}_{72}\text{Al}_2\text{N}_4\text{O}_2$
Formula weight	839.09 g/mol
Temperature	100 K
Wavelength	0.71073 Å
Crystal system	monoclinic
Space group	$\text{P}2_1/\text{n}$
Cell constants:	
a	12.5753(4) Å
b	15.7929(5) Å
c	12.6024(4) Å
$\beta$	106.6250(10)°
Volume	2398.22(13) Å <sup>3</sup>
Z	2
Density (calculated)	1.162 g/cm <sup>3</sup>
Absorption coefficient	0.104 mm <sup>-1</sup>
F(000)	908.0
Crystal size	0.39 x 0.34 x 0.14 mm <sup>3</sup>
2 $\theta$ range for data collection	6 to 55.088°
Index ranges	$-16 \leq h \leq 16$ , $-20 \leq k \leq 20$ , $-15 \leq l \leq 16$
Reflections collected	47341
Independent reflections	5536[R(int) = 0.0585]
Max. and min. transmission	0.7456 and 0.6963
Data / restraints / parameters	5536 / 0 / 279
Goodness-of-fit on $F^2$	1.015
Final R indices [ $I \geq 2\sigma(I)$ ]	$R_1 = 0.0438$ , $wR_2 = 0.1011$
R indices (all data)	$R_1 = 0.0586$ , $wR_2 = 0.1095$
Largest diff. peak and hole	1.06 and -0.28 eÅ <sup>-3</sup>

## 5.4 Computational data

**Table S10.** Optimized coordinates for **1**.

Atom	X	Y	Z
I	5.58973	5.95633	4.80292
Al	3.23476	6.48398	5.95908
C	3.69309	3.73926	6.55521
C	2.65819	3.70863	5.49067
C	1.59517	8.72817	4.91352
C	0.77804	7.83182	5.79993
C	1.04293	10.00141	4.24608
H	0.24388	9.7394	3.58444
H	0.67852	10.66918	4.99853
H	1.8227	10.48031	3.69153
C	-0.67529	8.3079	5.98105
H	-1.17472	8.29697	5.03482
H	-1.18267	7.65456	6.65972
H	-0.67824	9.30296	6.37444
C	4.16364	2.39659	7.14464
H	3.33037	1.88755	7.58217
H	4.58212	1.79268	6.36677
H	4.90538	2.57664	7.89451
C	2.19087	2.35663	4.92031
H	1.66457	1.81309	5.67693
H	1.54208	2.52635	4.08655
H	3.04128	1.79106	4.60117
C	4.72215	5.02037	7.80614
C	6.10976	4.90344	7.72612
C	4.11358	5.27886	9.03465
C	6.88907	5.04467	8.87469
H	6.58952	4.70003	6.75782
C	4.8926	5.4196	10.18306
H	3.01951	5.37142	9.09736
C	6.28077	5.3021	10.10307
H	7.98296	4.95166	8.8114
H	4.4132	5.62264	11.15169
H	6.89491	5.41281	11.00853
C	1.59181	4.95725	4.23849
C	0.29095	5.41697	4.44335
C	2.01276	4.60327	2.95634

C	-0.58933	5.52251	3.36611
H	-0.04081	5.69631	5.45382
C	1.1326	4.7083	1.87939
H	3.03862	4.24122	2.79506
C	-0.16897	5.16773	2.08445
H	-1.61508	5.88425	3.52806
H	1.46384	4.42869	0.86875
H	-0.86295	5.25029	1.23541
C	3.51119	8.75151	4.15176
C	4.37356	9.76744	4.56379
C	3.54217	8.30313	2.831
C	5.26689	10.3354	3.65503
H	4.34943	10.12066	5.60484
C	4.43493	8.87124	1.92228
H	2.8624	7.50182	2.50652
C	5.2973	9.88795	2.33439
H	5.9461	11.13685	3.97998
H	4.45913	8.51857	0.88097
H	6.00098	10.33602	1.61788
C	0.77589	6.28772	7.16656
C	0.08547	5.10953	6.88242
C	0.77861	6.79889	8.46468
C	-0.60264	4.44244	7.8963
H	0.08355	4.70639	5.85937
C	0.09029	6.13227	9.47827
H	1.32341	7.72764	8.68851
C	-0.60084	4.95385	9.19387
H	-1.1475	3.51401	7.6718
H	0.09162	6.53528	10.50144
H	-1.14372	4.42843	9.99294
N	2.80716	8.30363	4.86792
N	1.31843	6.81352	6.36762
N	2.28579	4.87418	5.08738
N	4.10779	4.90927	6.90096

---

**Table S11.** Optimized coordinates for **4**.

<b>Atom</b>	<b>X</b>	<b>Y</b>	<b>Z</b>
Al	0	-0.17924	0.00001
C	1.53848	0.89453	2.22299
C	0.25157	1.66368	2.23498
C	-1.53849	0.89459	-2.22295
C	-0.25157	1.66375	-2.23491
C	-2.52496	1.10444	-3.34211
H	-3.09874	2.02977	-3.19595
H	-2.00312	1.19327	-4.30063
H	-3.23536	0.27919	-3.40312
C	0.00972	2.65464	-3.33818
H	-0.88275	3.25153	-3.5507
H	0.83797	3.32212	-3.09688
H	0.26988	2.12192	-4.26448
C	2.52497	1.10436	3.34214
H	3.09875	2.02969	3.19598
H	2.00314	1.19318	4.30067
H	3.23537	0.27911	3.40314
C	-0.00973	2.65453	3.33828
H	0.88273	3.25143	3.55081
H	-0.838	3.32201	3.09701
H	-0.26988	2.12178	4.26457
C	2.8747	-0.78708	1.15506
C	2.81311	-2.1855	1.31026
C	4.10383	-0.14374	0.89824
C	3.99687	-2.93758	1.21801
H	1.86499	-2.67235	1.50794
C	5.27627	-0.90904	0.78833
H	4.14036	0.93333	0.76182
C	5.22749	-2.30731	0.95292
H	3.95158	-4.01531	1.34495
H	6.22128	-0.416	0.57705
H	6.13608	-2.89765	0.87238
C	-1.90803	2.00352	1.25628
C	-2.0844	3.16629	0.47847
C	-2.96924	1.48244	2.02031
C	-3.3344	3.8133	0.47125
H	-1.254	3.57613	-0.0903
C	-4.21453	2.13853	2.00623

H	-2.82426	0.57455	2.59722
C	-4.40206	3.30229	1.23605
H	-3.46786	4.71938	-0.11399
H	-5.03264	1.73853	2.59863
H	-5.36278	3.80944	1.2375
C	-2.8747	-0.78706	-1.15507
C	-2.81311	-2.18547	-1.31031
C	-4.10384	-0.14372	-0.89825
C	-3.99687	-2.93755	-1.21808
H	-1.86499	-2.67232	-1.50799
C	-5.27628	-0.90902	-0.78836
H	-4.14037	0.93335	-0.7618
C	-5.2275	-2.30729	-0.95299
H	-3.95158	-4.01529	-1.34505
H	-6.22129	-0.41599	-0.57707
H	-6.13608	-2.89764	-0.87247
C	1.90803	2.00355	-1.25623
C	2.08441	3.16633	-0.47844
C	2.96923	1.48246	-2.02027
C	3.33442	3.81333	-0.47123
H	1.25403	3.57618	0.09033
C	4.21453	2.13854	-2.00621
H	2.82425	0.57456	-2.59717
C	4.40207	3.30231	-1.23604
H	3.46789	4.71942	0.114
H	5.03262	1.73853	-2.59861
H	5.3628	3.80945	-1.2375
N	-1.65856	0.00945	-1.25913
N	0.60381	1.35304	-1.28958
N	-0.60381	1.353	1.28963
N	1.65856	0.00942	1.25915
N	-0.76372	-1.43943	1.3075
N	0.76372	-1.4394	-1.30752
C	-1.76392	-3.08983	3.01986
H	-1.28062	-4.03965	2.92409
H	-2.81197	-3.2028	2.83619
H	-1.61398	-2.71152	4.00945
C	1.76391	-3.08976	-3.01992
H	2.57046	-3.62798	-2.56748
H	2.12805	-2.54738	-3.86734

H	1.00804	-3.77839	-3.33512
C	-1.20179	-2.16228	2.05749
C	1.20179	-2.16223	-2.05753

---

**Table S12.** Optimized coordinates for **9**.

<b>Atom</b>	<b>X</b>	<b>Y</b>	<b>Z</b>
Al	14.6178	3.041	2.9644
N	16.5033	3.041	3.2619
N	14.5031	3.041	4.8975
C	16.8266	3.041	4.5823
C	15.7041	3.041	5.4815
C	17.5767	3.041	2.308
C	18.104	4.2572	1.8485
C	19.1567	4.2312	0.9327
H	19.5086	5.0537	0.6133
C	19.706	3.041	0.4733
C	17.5744	5.5744	2.355
H	18.0869	6.3078	1.9553
H	17.6619	5.6082	3.3305
H	16.6301	5.6633	2.1084
C	13.3143	3.041	5.717
C	12.7525	4.2613	6.1124
C	11.6154	4.2351	6.9257
H	11.2196	5.0565	7.1924
C	11.0481	3.041	7.355
C	13.3747	5.575	5.7251
H	12.7753	6.3077	5.9786
H	13.522	5.5938	4.7564
H	14.2321	5.6794	6.188
C	18.104	1.8247	1.8485
C	19.1567	1.8507	0.9327
H	19.5086	1.0283	0.6133
C	17.5744	0.5076	2.355
H	18.0869	-0.2259	1.9553
H	17.6619	0.4737	3.3305
H	16.6301	0.4187	2.1084
C	12.7525	1.8207	6.1124
C	11.6154	1.8468	6.9257
H	11.2196	1.0255	7.1924
C	13.3747	0.507	5.7251
H	12.7753	-0.2258	5.9786
H	13.522	0.4882	4.7564
H	14.2321	0.4026	6.188
C	9.84759	3.041	8.31956

H	10.20138	3.0342	9.32935
H	9.25731	3.91803	8.15434
H	9.24994	2.17077	8.14516
C	13.89844	4.73279	2.12728
H	14.17556	4.76535	1.0943
H	12.83181	4.74654	2.21101
H	14.3069	5.58262	2.6331
C	13.89844	1.34921	2.12728
H	12.83182	1.33538	2.21116
H	14.17542	1.31673	1.09426
H	14.30703	0.49938	2.63299
C	15.88126	3.041	7.01128
H	15.74286	4.0335	7.38635
H	15.15819	2.38831	7.45407
H	16.86584	2.70118	7.2563
C	18.28229	3.041	5.08487
H	18.6984	2.06165	4.97253
H	18.85673	3.74024	4.51393
H	18.30315	3.32111	6.11734
C	20.90693	3.041	-0.49074
H	21.81655	3.03177	0.07264
H	20.86432	2.172	-1.11358
H	20.87432	3.91923	-1.10111

---



**Table S13.** Optimized coordinates for **10**.

<b>Atom</b>	<b>X</b>	<b>Y</b>	<b>Z</b>
Al	4.3159	1.8682	6.1234
N	2.9842	1.2694	7.4938
N	3.3347	0.7805	4.974
C	2.2313	0.332	7.0604
H	1.6024	-0.0923	7.6321
C	2.368	-0.0813	5.6203
H	1.4833	0.0318	5.168
C	2.8953	1.7178	8.8702
C	3.5451	0.9967	9.8795
C	3.5093	1.5281	11.169
H	3.9531	1.0628	11.8681
C	2.8473	2.7123	11.4689
C	2.1911	3.3786	10.4421
H	1.7246	4.1829	10.6377
C	2.1972	2.8997	9.1309
C	4.2138	-0.3239	9.6124
H	4.7382	-0.5891	10.3968
H	4.8066	-0.239	8.8367
H	3.5324	-1.0042	9.4299
C	2.8452	3.2511	12.8796
H	2.1472	3.933	12.9679
H	3.7184	3.6498	13.0782
H	2.6696	2.5201	13.5082
C	1.4239	3.6125	8.0513
H	0.6912	3.0398	7.7419
H	2.0207	3.8135	7.3004
H	1.0568	4.4476	8.4094
C	3.126	1.1393	3.6137
C	4.1967	0.9767	2.7061
C	4.0306	1.3188	1.3669
H	4.7462	1.1686	0.7606
C	2.8468	1.8746	0.8899
C	1.8282	2.0931	1.806
H	1.0221	2.4947	1.5039
C	1.9398	1.7467	3.1546
C	5.5435	0.4908	3.1881
H	6.1309	0.3396	2.4184
H	5.4305	-0.3478	3.6825

H	5.9428	1.1654	3.7762
C	2.7066	2.2723	-0.5615
H	2.9249	1.5063	-1.1326
H	3.3197	3.0113	-0.7582
H	1.7854	2.5572	-0.7349
C	0.814	2.1169	4.0847
H	1.1808	2.3702	4.9574
H	0.2138	1.3496	4.193
H	0.3143	2.8716	3.7089
C	4.2181	3.7725	5.6507
H	4.8155	3.9524	4.8947
H	4.4927	4.3143	6.4198
H	3.2984	4.0006	5.4019
C	6.0872	1.2444	6.7863
H	6.1561	0.2738	6.6703
H	6.1773	1.4672	7.7364
H	6.7999	1.6855	6.2784
N	2.145	-2.9726	3.7228
N	1.7945	-2.4836	6.2426
C	2.8978	-2.0352	4.1562
H	3.5268	-1.6109	3.5845
C	2.7612	-1.6219	5.5963
H	3.6459	-1.735	6.0486
C	2.2338	-3.421	2.3464
C	1.584	-2.6999	1.3371
C	1.6199	-3.2313	0.0476
H	1.176	-2.766	-0.6515
C	2.2819	-4.4155	-0.2523
C	2.9381	-5.0818	0.7745
H	3.4046	-5.8861	0.5789
C	2.932	-4.6029	2.0857
C	0.9154	-1.3792	1.6042
H	0.391	-1.1141	0.8198
H	0.3225	-1.4641	2.3799
H	1.5968	-0.699	1.7867
C	2.284	-4.9543	-1.663
H	2.982	-5.6362	-1.7513
H	1.4108	-5.3529	-1.8616
H	2.4596	-4.2233	-2.2916
C	3.7053	-5.3157	3.1653

H	4.438	-4.743	3.4747
H	3.1085	-5.5167	3.9162
H	4.0724	-6.1508	2.8072
C	2.0031	-2.8425	7.6029
C	0.9325	-2.6799	8.5105
C	1.0986	-3.022	9.8497
H	0.3829	-2.8718	10.456
C	2.2824	-3.5777	10.3267
C	3.3009	-3.7962	9.4106
H	4.1071	-4.1979	9.7127
C	3.1894	-3.4499	8.062
C	-0.4143	-2.1939	8.0285
H	-1.0017	-2.0427	8.7982
H	-0.3013	-1.3554	7.5341
H	-0.8137	-2.8685	7.4404
C	2.4225	-3.9755	11.7781
H	2.2042	-3.2095	12.3492
H	1.8094	-4.7145	11.9748
H	3.3438	-4.2604	11.9515
C	4.3152	-3.8201	7.1318
H	3.9484	-4.0734	6.2592
H	4.9154	-3.0528	7.0236
H	4.8149	-4.5748	7.5077
Al	0.8133	-3.5714	5.0932
C	0.9111	-5.4756	5.5659
H	0.3137	-5.6556	6.3219
H	0.6365	-6.0175	4.7968
H	1.8308	-5.7037	5.8147
C	-0.958	-2.9476	4.4303
H	-1.0269	-1.977	4.5463
H	-1.0481	-3.1704	3.4802
H	-1.6707	-3.3887	4.9382

---

**Table S14.** Optimized coordinates for **11**.

<b>Atom</b>	<b>X</b>	<b>Y</b>	<b>Z</b>
Al	4.80628	7.30764	4.92434
O	5.25632	5.48448	5.38726
N	6.24313	7.7799	3.8652
N	3.78687	7.05444	3.40459
C	9.50275	10.37726	4.67724
C	8.52789	10.72805	3.75
H	8.60261	11.55946	3.29646
C	7.44424	9.89864	3.46457
C	7.33085	8.65252	4.11488
C	0.50552	8.10939	1.98274
H	0.16744	8.76075	1.3795
C	1.86858	8.10997	2.27754
C	2.39473	7.11911	3.13062
C	1.5116	6.18944	3.71596
C	0.15056	6.24961	3.41134
H	-0.4387	5.62775	3.82203
C	2.00971	5.12397	4.65314
H	2.75615	4.64507	4.23614
H	1.28447	4.49381	4.84635
H	2.31308	5.53871	5.48761
C	5.77414	4.56432	4.36564
H	6.50281	4.98812	3.84646
H	5.05548	4.28833	3.74318
C	6.29017	3.38147	5.14898
H	7.22462	3.52504	5.44272
H	6.24105	2.54855	4.61612
C	5.33705	3.33454	6.3385
H	4.47525	2.91488	6.09096
H	5.73436	2.83727	7.09678
C	5.15603	4.80035	6.6782
H	4.27226	4.95989	7.09483
H	5.86371	5.10941	7.2977
C	4.69047	6.96042	2.29664
C	4.20955	6.22897	1.07789
H	3.91028	5.33123	1.33259
H	4.94113	6.15779	0.42972
H	3.46315	6.72019	0.6754
C	5.96404	7.35461	2.53144

C	7.13814	7.16464	1.60651
H	7.65837	7.99408	1.56437
H	6.8143	6.93626	0.7102
H	7.70544	6.43998	1.94335
C	6.37911	10.38176	2.51035
H	6.46529	11.35023	2.38774
H	5.49404	10.17646	2.8776
H	6.48651	9.93225	1.64617
C	9.35878	9.16175	5.33174
H	10.00948	8.90919	5.97617
C	8.29683	8.29991	5.07873
C	8.19434	7.01334	5.85303
H	7.37303	7.01838	6.38766
H	8.96964	6.92636	6.44611
H	8.1736	6.25757	5.2295
C	2.74155	9.217	1.73759
H	3.39784	8.84101	1.11443
H	3.20894	9.65553	2.47897
H	2.18456	9.87309	1.26885
Al	4.16339	8.48526	7.15125
O	3.71335	10.30842	6.68833
N	5.1828	8.73846	8.671
C	-0.53307	5.41564	7.39835
C	0.44178	5.06485	8.32559
H	0.36706	4.23344	8.77914
C	1.52543	5.89426	8.61102
C	1.63882	7.14038	7.96071
C	8.69374	8.28029	9.83942
H	9.2074	7.63968	10.3172
C	7.35232	8.00462	9.57594
C	6.5662	8.96141	8.90291
C	7.17901	10.14945	8.45585
C	8.5329	10.36481	8.71936
H	8.93824	11.16557	8.40809
C	6.39834	11.19713	7.71118
H	5.58723	11.41928	8.21433
H	6.94836	12.00145	7.60648
H	6.15072	10.85341	6.82748
C	3.19553	11.22858	7.70995
H	2.46686	10.80478	8.22913

H	3.91419	11.50457	8.33241
C	2.6795	12.41143	6.92661
H	1.74505	12.26786	6.63287
H	2.72862	13.24435	7.45947
C	3.63262	12.45836	5.73709
H	4.49442	12.87802	5.98463
H	3.23531	12.95563	4.97882
C	3.81364	10.99255	5.39739
H	4.69741	10.83301	4.98076
H	3.10596	10.68349	4.77789
C	4.65883	9.12201	11.21059
H	4.72392	10.09488	11.11221
H	3.89932	8.90232	11.78963
H	5.48475	8.77814	11.6106
C	2.90357	8.3995	9.5152
C	1.64204	8.55417	10.32435
H	1.14175	7.71157	10.3137
H	1.87285	8.78537	11.24829
H	1.09097	9.26619	9.93736
C	2.59056	5.41114	9.56525
H	2.50438	4.44267	9.68785
H	3.47563	5.61644	9.19799
H	2.48316	5.86065	10.42942
C	-0.38911	6.63115	6.74386
H	-1.03981	6.88371	6.09942
C	0.67285	7.49299	6.99686
C	0.77533	8.77956	6.22256
H	1.59664	8.77452	5.68793
H	0.00003	8.86654	5.62948
H	0.79607	9.53533	6.84609
C	6.7873	6.65546	9.94966
H	6.09903	6.76885	10.63802
H	6.39098	6.23642	9.15735
H	7.5051	6.08531	10.29621
C	10.34228	9.64818	9.60999
H	10.89462	8.73413	9.54423
H	10.45717	10.06469	10.58888
H	10.71068	10.34067	8.88224
C	9.30665	9.45323	9.42463
C	-1.72665	4.49202	7.09189

H	-2.62497	5.07187	7.05076
H	-1.57084	4.00845	6.15019
H	-1.81343	3.75402	7.86177
C	-1.42322	7.20185	2.32692
H	-1.96116	6.87098	3.19066
H	-1.63258	6.54971	1.50487
H	-1.72561	8.19764	2.07821
C	-0.37351	7.18909	2.53395
C	10.69632	11.30088	4.98371
H	11.07463	11.70981	4.07017
H	10.37685	12.09565	5.62493
H	11.46678	10.7389	5.46896
N	2.76749	8.04585	8.21979
C	4.12671	8.8643	9.86217

---